

UNCLASSIFIED

AD NUMBER

AD831568

LIMITATION CHANGES

TO:

Approved for public release; distribution is unlimited. Document partially illegible.

FROM:

Distribution authorized to U.S. Gov't. agencies and their contractors; Critical Technology; FEB 1968. Other requests shall be referred to Air Force Technical Application Center, Washington, DC. Document partially illegible. This document contains export-controlled technical data.

AUTHORITY

usaf ltr, 25 jan 1972

THIS PAGE IS UNCLASSIFIED

AD831568



DDC
MAY 6 1968
REGISTERED
A



TEXAS INSTRUMENTS

SCIENCE SERVICES DIVISION

1400 NORTH CENTRAL EXPRESSWAY
POST OFFICE BOX 541 • DALLAS, TEXAS 75201



VELA T/7701

This document is subject to special export controls and each transmittal to foreign governments or foreign nationals may be made only with prior approval of Chief, AFTAC.

*attn: VSC
Wash. D.C. 20333*

NETWORK STUDIES - NOISE ANALYSIS
ADVANCED ARRAY RESEARCH
Special Report No. 6

Prepared by

William A. Johnson James A. Bonner

John P. Burg, Project Scientist
George D. Hair, Program Manager
Telephone: 1-214-238-3473

TEXAS INSTRUMENTS INCORPORATED
Science Services Division
P.O. Box 5621
Dallas, Texas 75222

Contract: F33657-67-C-0708-P001
Contract Date: 15 December 1966
Amount of Contract: \$625,500
Contract Expiration Date: 14 December 1967

Sponsored by

ADVANCED RESEARCH PROJECTS AGENCY
Nuclear Test Detection Office
ARPA Order No. 624
ARPA Program Code No. 7F10

Prepared for

AIR FORCE TECHNICAL APPLICATIONS CENTER
Washington, D.C. 20333

28 February 1968

science services division



ACKNOWLEDGMENT

This research was supported by the
ADVANCED RESEARCH PROJECTS AGENCY
Nuclear Test Detection Office
under Project VELA UNIFORM
and accomplished under the technical direction of the
AIR FORCE TECHNICAL APPLICATIONS CENTER
under Contract No. F33657-67-C-0708-P001



ABSTRACT

Network studies are directed toward effective utilization of a collection of seismic stations as a coherent worldwide seismic network to lower the detection threshold for seismic events and improve their classification. This report presents an analysis of ambient seismic noise seen at the network level and is directed toward characterization of the network noise field. Simultaneously recorded noise samples from two VELA stations and eight LRSM stations are investigated through analysis of power-density spectra, coherence, high-resolution frequency-wavenumber spectra, and K-line spectra. The ambient short-period network noise field is found to be highly variable with time and with geographical position. Variations in noise power are directly related to regional storm activity. Dominant noise power at most stations is trapped-mode surface-wave energy that does not exhibit useful interstation coherence.



ACRONYMS

CPO	Cumberland Plateau Seismological Observatory
LASA	Large-Aperature Seismic Array
LPC	Low-pressure center
LRSM	Long-Range Seismic Monitor
MCF	Multichannel filter
SNR	Signal-to-noise ratio
TFO	Tonto Forest Seismological Observatory



TABLE OF CONTENTS

Section	Title	Page
I	INTRODUCTION AND SUMMARY	I-1
II	NETWORK NOISE POWER SPECTRAL ANALYSIS	II-1
	A. SHORT-PERIOD NOISE POWER SPECTRA	II-1
	B. LONG-PERIOD SPECTRAL ANALYSIS	II-11
	C. BROADBAND SPECTRAL ESTIMATES	II-17
III	ANALYSIS OF NETWORK NOISE FIELD USING HIGH-RESOLUTION FREQUENCY-WAVENUMBER SPECTRA	III-1
	A. DESCRIPTION OF EXPERIMENT	III-1
	B. RESULTS AND CONCLUSIONS	III-3
	C. PRESENTATION OF STATION NOISE SPECTRA	III-6
IV	BODYWAVE NOISE STUDIES	IV-1
	A. MULTICHANNEL-FILTER AND STRAIGHT-SUM TECHNIQUES	IV-2
	B. ANALYSIS OF K-LINE WAVENUMBER SPECTRA FROM LRSM DATA	IV-9
	1. Description of K-Line Spectra	IV-9
	2. Presentation and Analysis of K-Line Wavenumber Spectra	IV-10
	C. ANALYSIS OF BODYWAVE NOISE POWER DENSITY	IV-24
V	REFERENCES	V-1

APPENDIX

DESCRIPTIONS OF WORLDWIDE NETWORK AND DATA LIBRARY

TABLE

Table	Title	Page
III-1	Storm-Generated Coherent Energy	III-4



LIST OF ILLUSTRATIONS

Figure	Description	Page
II-1	Short-Period Vertical-Component Power Spectra at ADIS	II-3
II-2	Short-Period Vertical-Component Power Spectra at CPO	II-3
II-3	Short-Period Vertical-Component Power Spectra at GGGR	II-4
II-4	Short-Period Vertical-Component Power Spectra at OONW	II-4
II-5	Short-Period Vertical-Component Power Spectra at RKON	II-6
II-6	Short-Period Vertical-Component Power Spectra at DHNY	II-6
II-7	Short-Period Vertical-Component Power Spectra at NPNT	II-7
II-8	Short-Period Vertical-Component Power Spectra at LZBV	II-7
II-9	Short-Period Vertical-Component Power Spectra at TFO	II-8
II-10	Absolute Power-Density Levels Observed for Several Stations at 1.0 Hz	II-8
II-11	Comparison between Measured and Theoretical Phase Shifts Relative to Channel Z2, OONW	II-10
II-12	Long-Period Vertical-Component Power Spectra	II-12
II-13	Long-Period Interstation Coherences for 16 October 1964 and 29 January 1965 Samples	II-14
II-14	Broadband Spectral Estimates Using Absolute Long- and Short-Period Power-Density Spectra	II-16
III-1	Surface Weather Map for 16 October 1964 at 1800 GMT	III-8
III-2	Surface Weather Map for 29 January 1965 at 0600 GMT	III-9
III-3	Sea Wind-Wave Height Chart for 16 October 1964 at 1800 GMT	III-10
III-4	Sea Wind-Wave Height Chart for 29 January 1965 at 0600 GMT	III-11
III-5	High-Resolution $f-\vec{k}$ Spectra	III-12
III-6	High-Resolution $f-\vec{k}$ Spectra	III-14
III-7	High-Resolution $f-\vec{k}$ Spectra	III-16
III-8	High-Resolution $f-\vec{k}$ Spectra	III-18
III-9	High-Resolution $f-\vec{k}$ Spectra	III-20
III-10	High-Resolution $f-\vec{k}$ Spectra	III-22
III-11	High-Resolution $f-\vec{k}$ Spectra	III-24



LIST OF ILLUSTRATIONS (CONTD)

Figure	Description	Page
III-12	High-Resolution f - \vec{k} Spectra	III-26
III-13	High-Resolution f - \vec{k} Spectra	III-28
III-14	High-Resolution f - \vec{k} Spectra	III-30
III-15	High-Resolution f - \vec{k} Spectra	III-32
III-16	High-Resolution f - \vec{k} Spectra	III-34
III-17	High-Resolution f - \vec{k} Spectra	III-36
III-18	High-Resolution f - \vec{k} Spectra	III-38
III-19	High-Resolution f - \vec{k} Spectra	III-40
IV-1	Average and Straight-Sum Noise Power-Density Spectral Estimates at CPO and TFO	IV-4
IV-2	Percentage of High- and Low-Velocity Noise Components at CPO and TFO	IV-7
IV-3	Wavenumber and Integrated Spectra from Two Arms at OONW, 29 January 1965	IV-12
IV-4	Wavenumber and Integrated Spectra from Two Arms at OONW, 16 October 1964	IV-14
IV-5	Wavenumber and Integrated Spectra from Two Arms at NPNT, 29 January 1965	IV-16
IV-6	Wavenumber and Integrated Spectra from Two Arms at NPNT, 16 October 1964	IV-18
IV-7	Wavenumber and Integrated Spectra from Two Arms at GGGR, 29 January 1965	IV-20
IV-8	Wavenumber and Integrated Spectra from Two Arms at GGGR, 29 January 1965	IV-22
IV-9	Absolute Total and High-Velocity Power-Density Spectra (in db) for CPO NPNT, TFO, OONW, and GGGR	IV-25
IV-10	Comparison of Station Total and High-Velocity Power-Density Spectra for Each Noise Sample	IV-26

BLANK PAGE



SECTION I

INTRODUCTION AND SUMMARY

A partial goal of Contract F33657-67-C-0708 is an examination of methods to utilize effectively a collection of seismic stations as a coherent seismic network. A subtask of the network studies involves a comprehensive examination of broadband ambient noise as seen at the network level.

This report presents the results of the analysis of five noise samples recorded at the network stations between 12 August 1964 and 29 January 1965. The analysis determines the salient features of both short-period and long-period noise at the station level, with particular attention given to spectral analysis, spatial organization, and identification of modal content and noise sources. The structure of the network noise model is then inferred from an analysis of the combined effects of these features.

The network consists of VELA arrays TFO and CPO; LRSM arrays OONW, GGGR, NPNT, HWIS, and LZBV; and single-instrument stations ADIS, RKON, and DHNY. This study, which is restricted to vertical-component ambient noise, consists of single-sensor analysis through power spectra and modal noise analysis utilizing array-station data.

Outputs of single-sensor stations (and single seismometers selected from each array station) have been studied to determine: the distribution of station noise power as a function of frequency, time, and geographic position; the correlation between station noise levels and regional storm activity; and the seismic validity of the recorded data.

Array-station data have been studied to determine seismic propagation modes and velocities of the coherent energy, to establish the sources of this energy, and to determine, if possible, whether the stations are bodywave noise-limited.



Power spectra are computed from five short-period noise samples. Power spectra and interstation coherences also are computed from long-period data for two of the five noise samples.

Modal noise studies are conducted through the analysis of high-resolution frequency-wavenumber spectra, K-line spectra, Wiener disk-model MCF outputs, and straight-sum outputs.

Short-period data appear to be seismically valid and generally usable between 0.2 and 2.0 Hz. Above 2.0 Hz, several apparently nonseismic noise peaks appear. Generally, station array configurations have limited interpretation of the spatially organized coherent energy to frequencies between 0.2 and 1.0 Hz.

Station power densities are found to differ considerably across the network during each time period and to vary considerably from sample to sample. The bulk of seismic energy appears to be concentrated in the 0.2- to 0.5-Hz frequency band. At 1.0 Hz, station power densities vary from extremely low at TFO (-4 to -8 db) and NPNT (-3 to -5 db) to extremely high at ADIS (14 to 26 db) and GGGR (9 to 12 db) relative to $1.0 \text{ m}\mu^2/\text{Hz}$. These variations in noise power level with station and time appear to be directly related to regional meteorological disturbances and indicate a lack of both time- and space-stationarity at the network level.

Station ambient noise fields during the 16 October 1964 and 29 January 1965 time periods are dominated primarily by low-velocity surface-mode energy. The exception is TFO where bodywave-mode coherent energy is generally dominant. The coherent energy appears to be highly directional and generally related to regional storm activity, especially in the micro-seismic band (2- to 5-sec periods). Wind-generated surf action seems to be a primary source mechanism. Storm activity is usual in the northern latitudes



during the winter months, and conclusions from this study may not be applicable to other seasons. At frequencies above the microseismic band, significant contribution from apparently stationary sources also is observed, usually in the form of localized narrowband surface-mode energy which is probably culturally related.

While the more intense storm sources generate energy simultaneously observed at several stations in the network, the amplitude, frequency, and propagation mode of the observed energy vary with station. Such variation is probably related to several factors including station-to-source distances, source radiation patterns, travel-path geology differences, and the presence of strong regional sources that obscure weaker energy from distant sources. This last factor is particularly evident at the lower frequencies where array resolutions are poor. Therefore, the low-velocity coherent energy that is a major contributor to the noise field at the station level is apparently not coherent at the network level in the short-period frequency range, since it is primarily generated from regional sources. Wiener coherent processing does not appear advantageous for suppression of this noise at the network level.

Except for TFO, which previous studies show to be bodywave noise-limited,¹ the array stations do not appear to be bodywave noise-limited during the two time periods of intense storm activity. However, bodywave noise appears to form a larger proportion of the total noise power density at NPNT than at CPO, OONW, or GGGR. Measurements of bodywave noise levels across the network suggest that these levels are not uniform but vary with continent. At each station, the bodywave noise levels appear relatively inconsistent with time over the 0.2- to 1.0-Hz range.



Examination of the long-period data suggests valid seismic energy between 0.03 and 0.2 Hz. A major peak is seen around 0.15 Hz, with a lesser peak indicated between 0.05 and 0.08 Hz. Spectral levels are notably consistent at 0.04 Hz, averaging about 45 db relative to $1 \text{ m}\mu^2/\text{Hz}$. No usable coherence is observed between stations for the long-period data, but this is not surprising in view of the regional character of the noise field already reported for the short-period data; however, differences in tape speeds for the recorded data result in slightly different digitization rates at each station, and the coherence measurements certainly are affected. Low-level coherence (significantly above the level expected for random noise) seen for certain stations around 0.25 Hz may possibly be seismic.

Broadband spectral estimates formed by joining the absolute short-period and long-period power spectra appear generally reasonable and indicate a power peak in the spectral range between 0.1 and 0.3 Hz. Power levels above 0.2 Hz appear to decay logarithmically.

Due to the preponderance of surface-mode energy at the network stations, the extent to which the bodywave component of the noise field is coherent across the network is not established. With sufficient preprocessing to reduce the low-velocity component significantly at the station level, useful coherence could conceivably be found for an essentially body-wave noise-limited network. In this case, Wiener coherent processing would prove useful for suppressing highly directional energy from bodywave sources.

Conclusions, it should be emphasized, are drawn from examination of a very limited quantity of data; results cannot be generalized for year-round network operation without further analysis using data samples representative of all seasons. Also, the insufficient number of network stations available precluded comprehensive coverage. Continued evaluation with an expanded network of quality array stations and an ensemble of noise samples representing year-round network operation is recommended.



SECTION II

NETWORK NOISE POWER SPECTRAL ANALYSIS

A. SHORT-PERIOD NOISE POWER SPECTRA

Power-density spectra are computed using available noise samples at each station. Single vertical-component short-period seismometers are used to represent each station. These spectra are then used to interpret data validity as a function of frequency, the time- and space-stationarity of network noise, location of spectral peaks, and general distribution of power as a function of frequency.

Data gate lengths vary from 370 sec to 1400 sec, with data quality a determining factor. Trace areas containing spikes or other obviously nonseismic disturbances have been avoided. Autocorrelations are computed for ± 10 sec. The correlations are Parzen-smoothed,² yielding a frequency resolution of approximately 0.1 Hz in the resulting power spectra.

Figures II-1 through II-9 present station power spectra (corrected only at 1.0 Hz) for the various network stations. Available spectra at each station are overlaid, facilitating comparison of spectral variation with time. The power variation in the microseismic band with season shows general agreement with previous work.³ Station noise levels appear to vary primarily as a function of regional storm activity, and a general rise in noise power is evident across the network during the winter months. Since the network consists of northern-hemisphere stations only, this rise is indicative of increased storm activity in the northern hemisphere during the winter months.



Noise energy levels at ADIS appear to vary considerably with time (Figure II-1). Most notable is the considerably reduced level on 12 August 1964. The elevated level on 6 November 1964 reflects the presence of an intense low-pressure center (LPC) off the Aleutian chain. Background levels are generally higher than for stations located on the continent, suggesting that surf action may be a primary source.

Figure II-2 shows considerable energy at CPO for 0.2 Hz during 16 October 1964, indicating the presence of tropical storm Isabel along the Atlantic coast. The spectra at CPO appear generally well-equalized. Noise power appears slightly above 0 db at 1.0 Hz, agreeing well with previous work.³ There are evidences also of spectral peaks at 1.4 and 2.0 Hz; both correspond to previously reported directional surface-mode energy. High-resolution spectral analysis suggests that these peaks correspond to a common local source north-northwest of CPO.

An interesting characteristic of the spectra at GGGR is evident in Figure II-3. While microseismic power levels are generally low relative to the other stations, the 1.4- to 2.5-Hz frequency band reflects unusually high power levels with numerous peaks; whether these peaks are seismic is not established.

Figure II-4 shows the power spectra at OONW. The spectrum for 6 November 1964 indicates a much higher overall noise level up to 2.0 Hz. An intense low-pressure center was located over North Europe during this time period. The 12 August 1964 spectrum is again relatively lower across the microseismic band, indicating a lack of regional storm activity. All spectra are from compressed FM data, except the 16 October 1964 sample, which exhibits generally lower levels above 2.0 Hz.

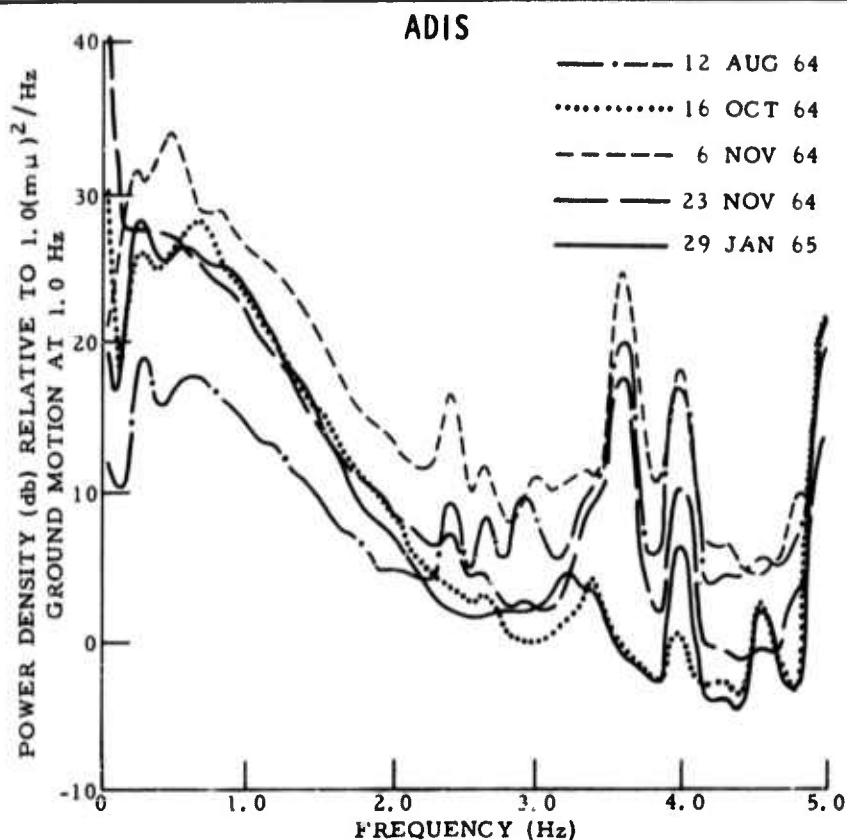


Figure II-1. Short-Period Vertical-Component Power Spectra at ADIS

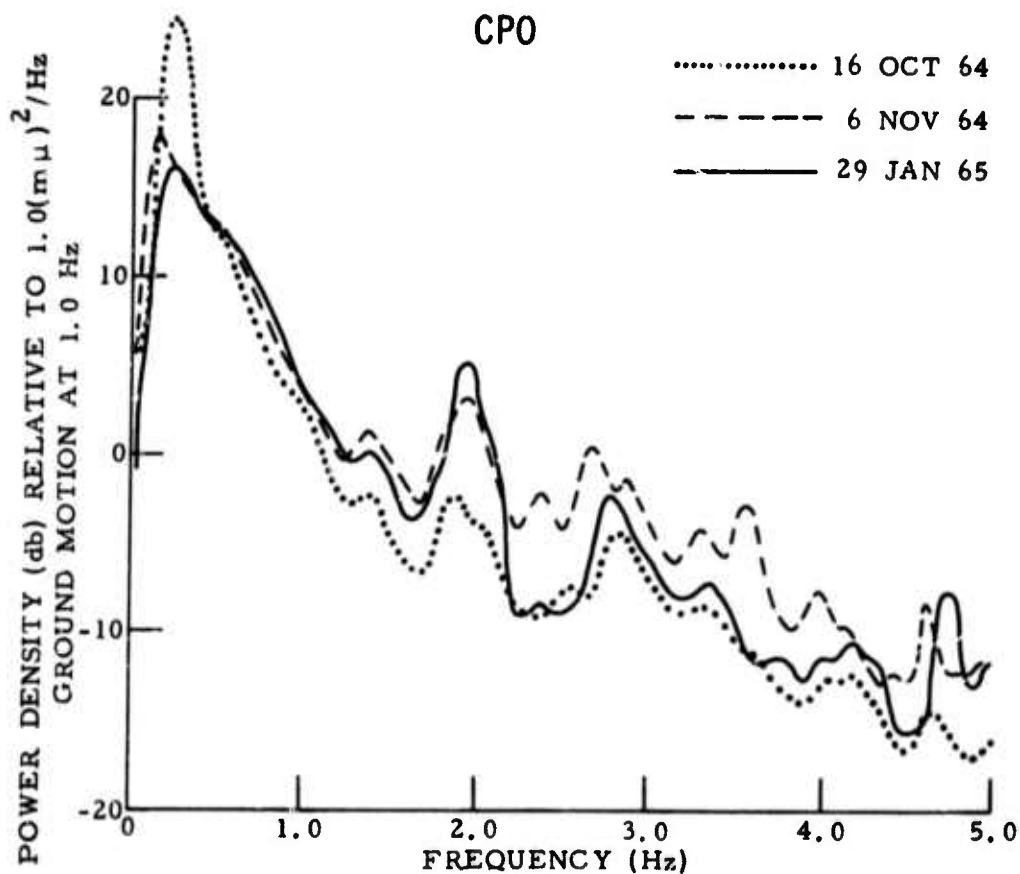


Figure II-2. Short-Period Vertical-Component Power Spectra at CPO

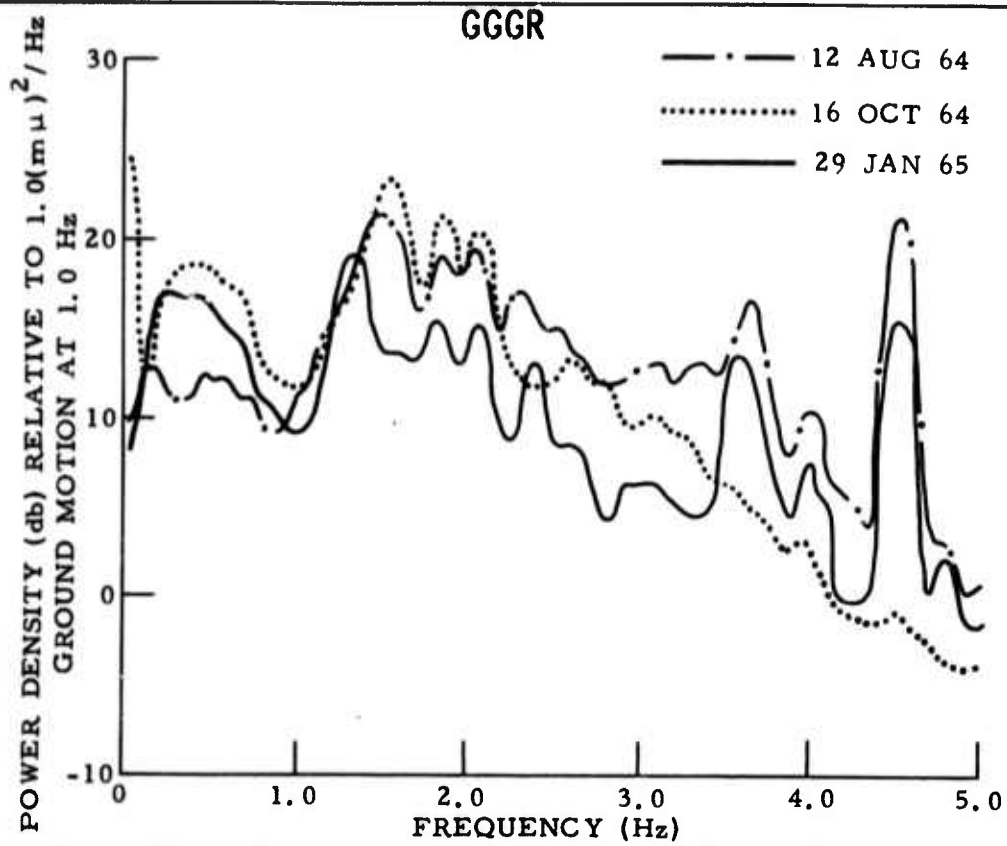


Figure II-3. Short-Period Vertical-Component Power Spectra at GGGR

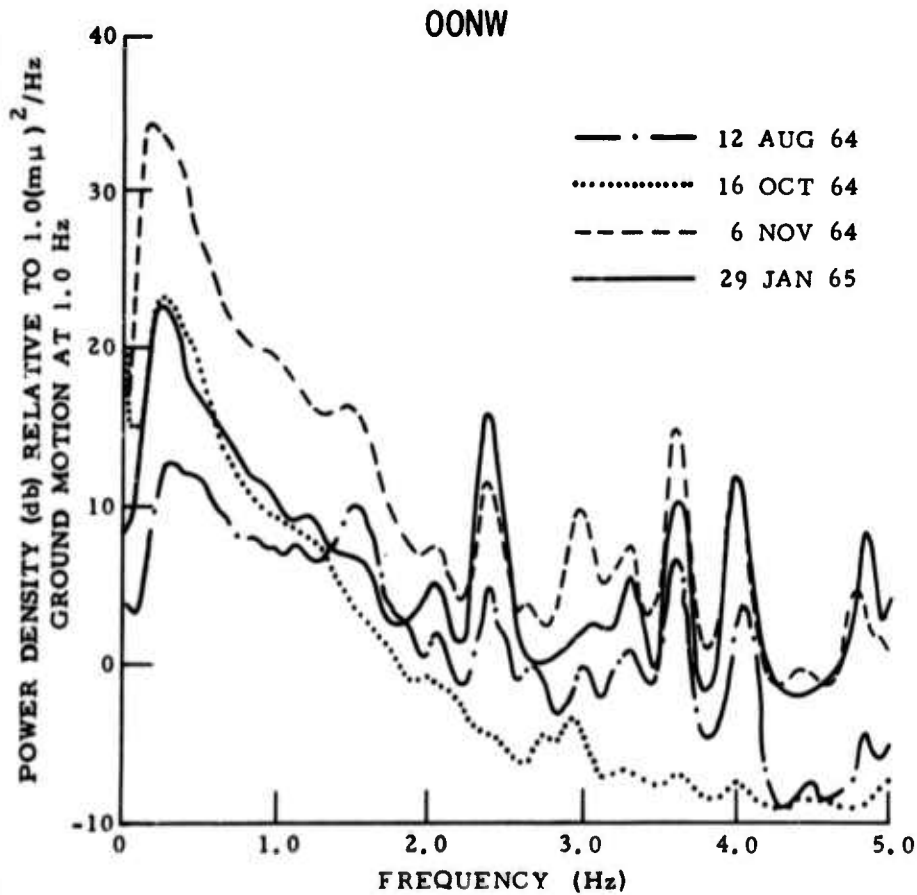


Figure II-4. Short-Period Vertical-Component Power Spectra at OONW



Figures II-5 and II-6 for RKON and DHNY, respectively, indicate generally lower microseismic energy levels on 12 August 1964. Figures II-7, II-8, and II-9 contain spectra computed for NPNT, LZBV, and TFO, respectively. The 16 October 1964 spectrum at TFO appears odd and is not believed to be seismically valid.

In general, the 16 October 1964 and 29 January 1965 samples are from noncompressed data (except OONW on 29 January 1965) and reflect lower levels above 2.0 Hz. All others are from compressed recordings and indicate numerous spectral "lines" as well as a generally higher power level at frequencies above 2.0 Hz.

Figure II-10 shows the power-density level at 1.0 Hz seen at each station for several noise samples. TFO reflects the lowest levels, followed closely by NPNT and DHNY. CPO, LZBV, RKON, and OONW appear intermediate; GGGR and ADIS indicate relatively high ambient noise levels. The 6 November 1964 sample is consistently higher in noise power across the network; other samples indicate more variance.

Calibration analysis performed on available calibration data is used, together with station-log data, to determine correction factors subsequently applied to the power spectra, yielding power density in decibels relative to $1 \text{ m}\mu^2/\text{Hz}$ at 1.0 Hz.

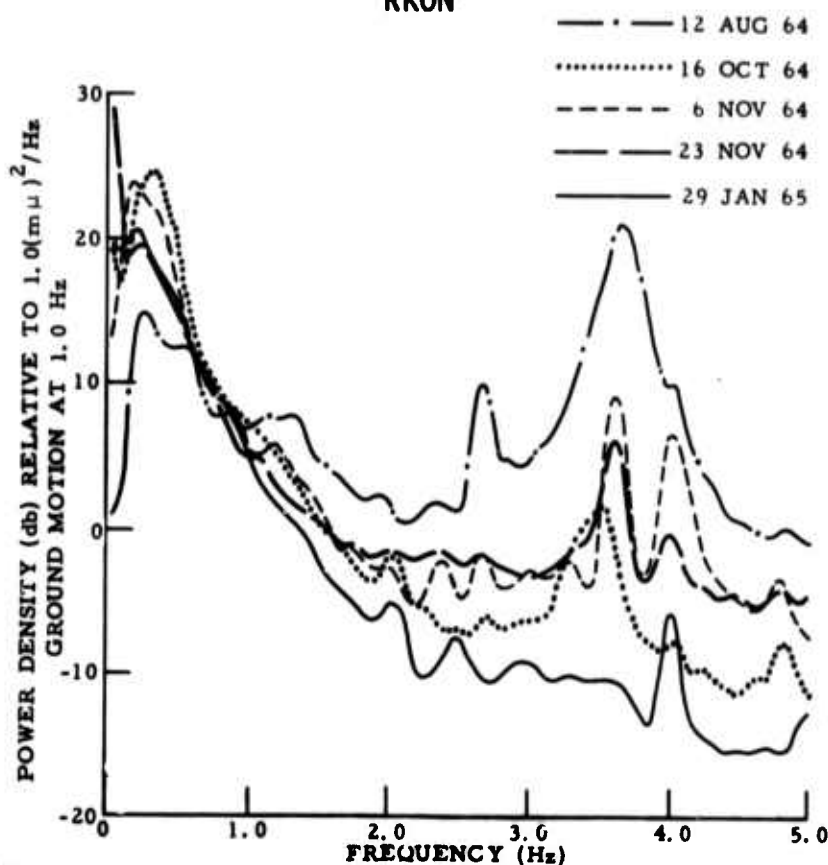
This procedure encountered several problems, however: station logs were not available for all samples, and the available ones were sometimes ambiguous; in a few instances, calibrations were not available or usable for analysis. Estimates from other days were used in several cases.

Some corrections, although consistent with available information, appear to provide questionable normalization of spectra. In general, the overall quality of the normalization through the use of calibrations is less than desired.



RKON

Figure II-5. Short-Period Vertical-Component Power Spectra at RKON



DHNY

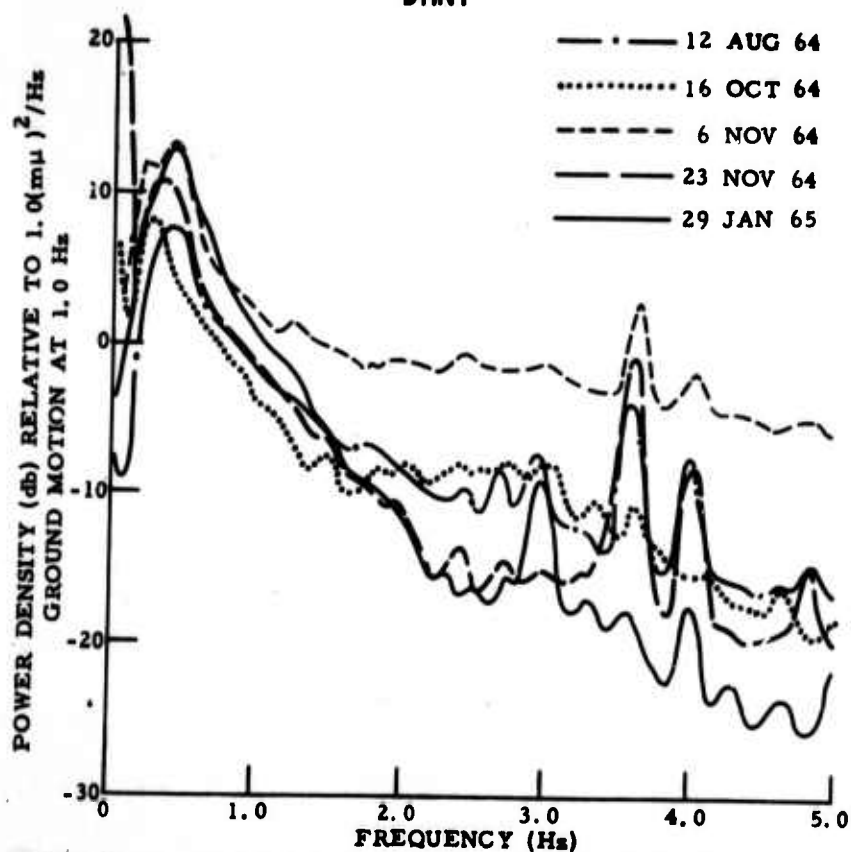


Figure II-6. Short-Period Vertical-Component Power Spectra at DHNY



NPNT

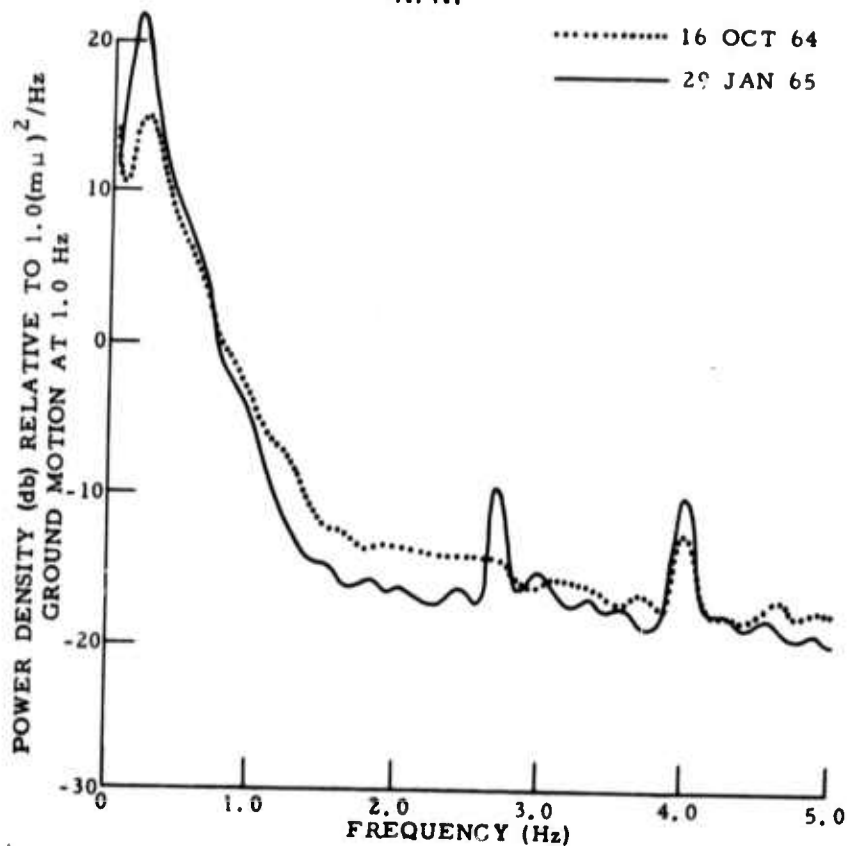
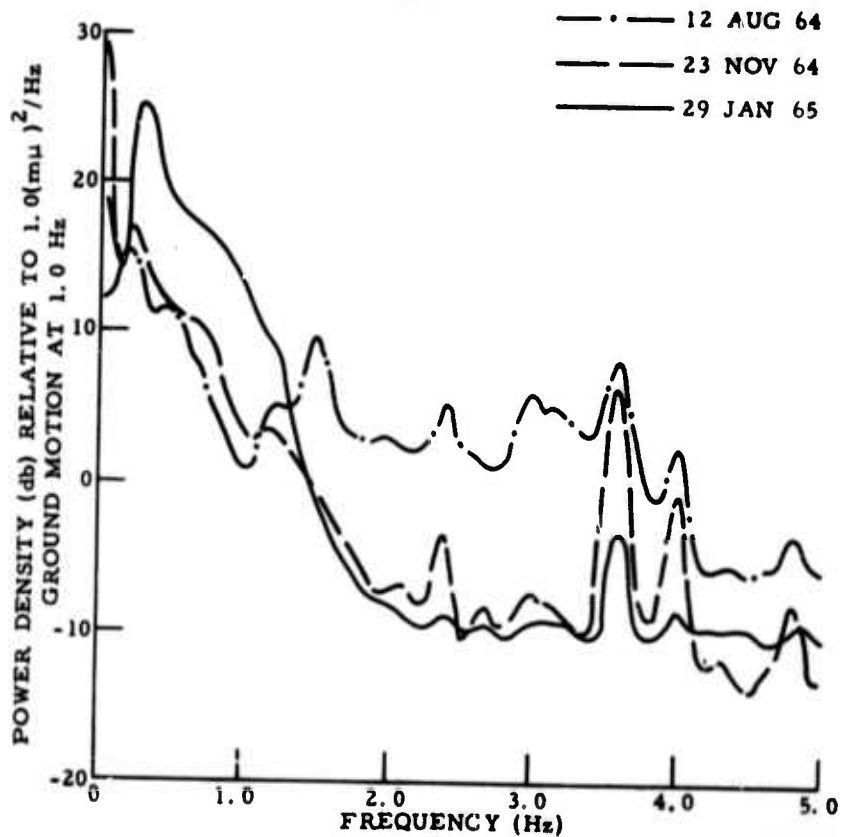


Figure II-7. Short-Period Vertical-Component Power Spectra at NPNT

LZBV

Figure II-8. Short-Period Vertical-Component Power Spectra at LZBV



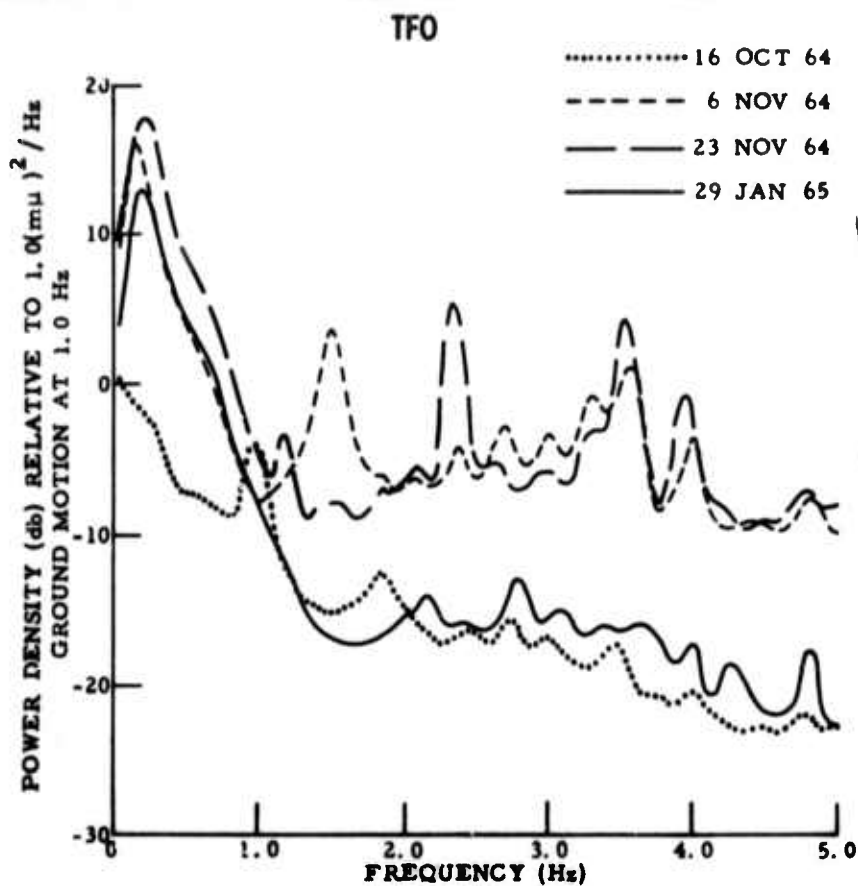


Figure II-9. Short-Period Vertical-Component Power Spectra at TFO

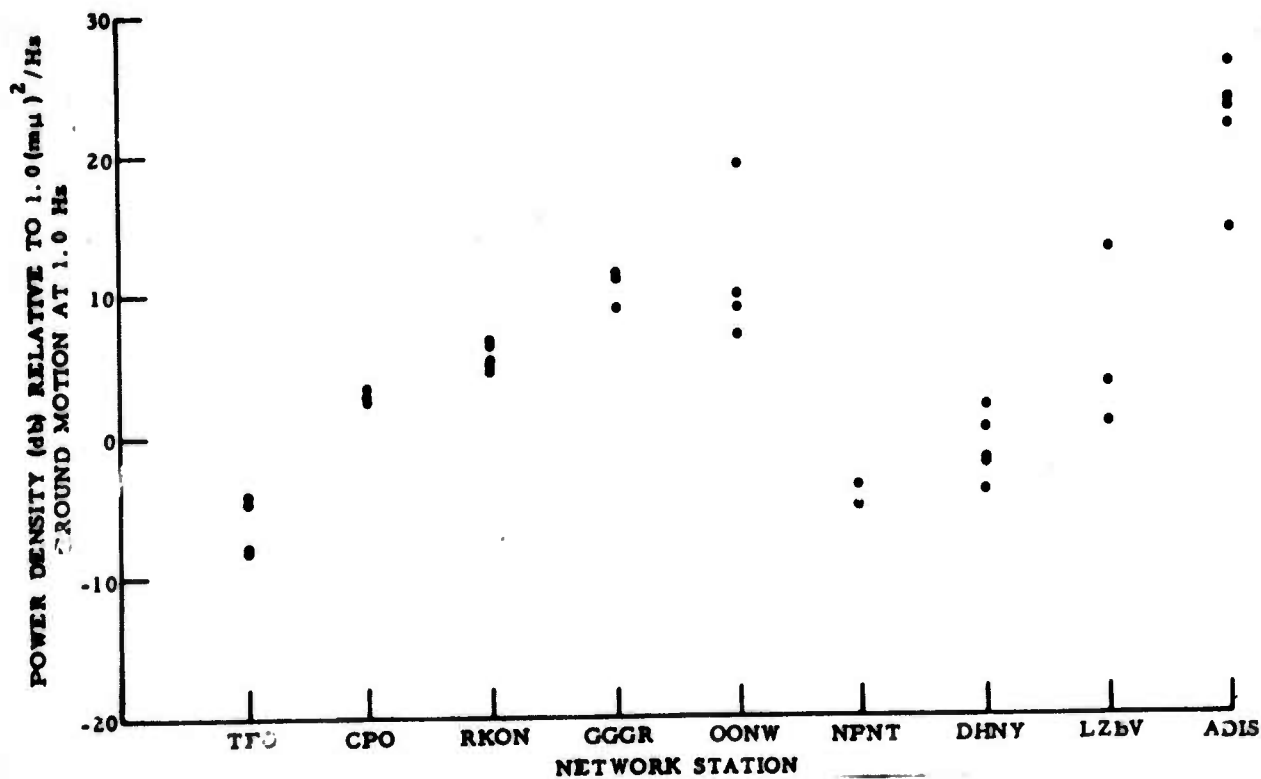


Figure II-10. Absolute Power-Density Levels Observed for Several Stations at 1.0 Hz



Several conclusions can be drawn from examination of the spectra, however. All stations except GGGR appear dominated by the 0.2- to 0.5-Hz microseismic energy. Analysis using $f\text{-}\vec{k}$ spectra (discussed in Sections III and IV) indicates that the bulk of this energy is of low velocity (surface mode); the exception is TFO. GGGR appears somewhat unique in that spectral noise power is significantly higher in the signal band, but no explanation for this elevated power level is available.

Above 2.0 Hz, the spectra rapidly break into narrowband peaks. Most of these peaks are not believed to be seismic but rather to be generated during FM recording or playback, during compression of data, or during digitization. Extremely high-velocity energy is indicated by $f\text{-}\vec{k}$ analysis for these peaks. Ideally, instrument-generated noise might be expected to exhibit infinite-velocity peaks. However, the process of digitization introduces a small but finite time delay in sampling between channels, which appears in $f\text{-}\vec{k}$ analysis as a relatively consistent phase shift across the array. This timing error is approximately 1/600 sec between adjacent channels for standard FM-to-digital tapes and 1/120 sec for compressed FM-to-digital tapes.

The strong, very narrowband peak at 3.6 Hz seen in the OONW 6 November 1964 spectrum has been analyzed through direct transforms computed for all array channels. Figure II-11 shows the phase shifts observed for each channel relative to Z2. The straight line represents theoretical phase shifts expected from compressed data, assuming a 1/120-sec delay in sampling adjacent channels containing in-phase information at 3.6 Hz. Except for Z1, which is lowest in amplitude at 3.6 Hz, there is excellent agreement between measured and theoretical phase shifts. Therefore, this timing error inherent in sampling is interpreted as the mechanism for producing the deviations from infinite velocity seen for instrumentally produced spectral peaks.

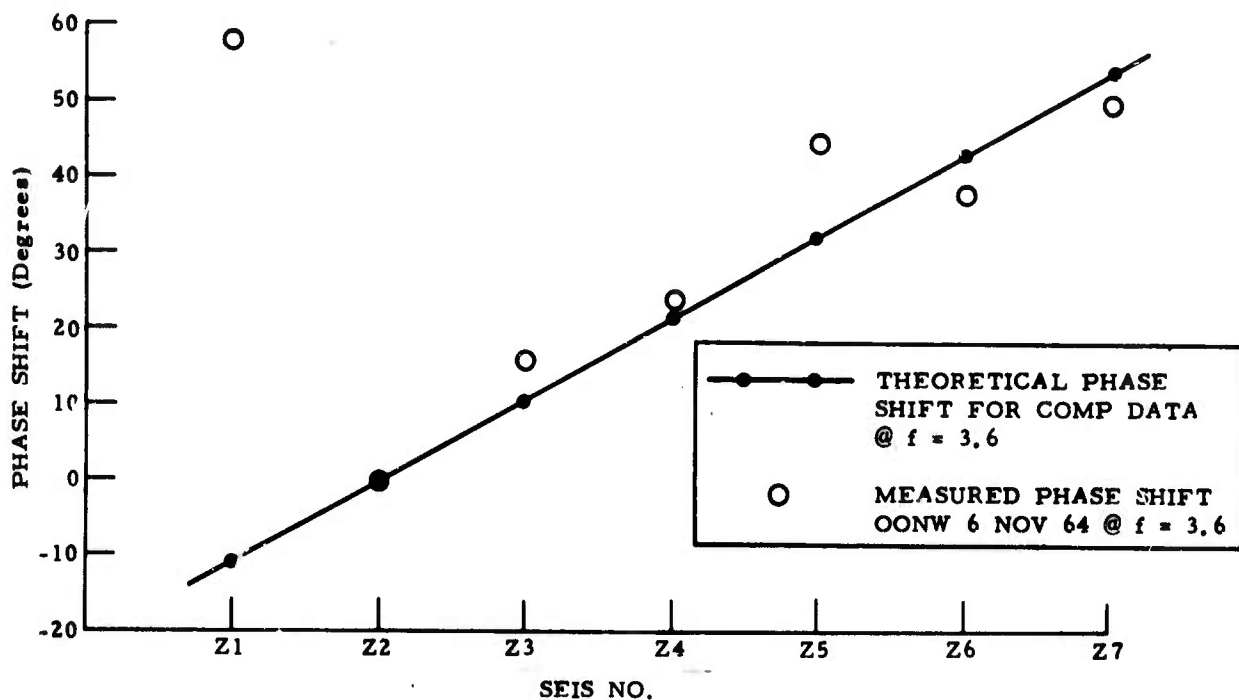


Figure II-11. Comparison between Measured and Theoretical Phase Shifts Relative to Channel Z2, OONW

The spectra generally are not believed seismically valid above 2.0 Hz. Similarly, estimates below 0.2 Hz are questionable. Therefore, the frequency range between 0.2 and 2.0 Hz appears to be generally useful for network spectral analysis.

Based on the limited amount of data analyzed, network power spectra appear neither time- nor space-stationary. The apparent dependence of station power level on regional effects suggests strongly an overall lack of coherence at the network level. Further study is indicated, using analysis of a wide range in data samples representing various seasonal and diurnal conditions. If the frequency range of valid seismic data is to be extended, higher-quality network data probably will be required.



B. LONG-PERIOD SPECTRAL ANALYSIS

Figure II-12 shows long-period power-density spectra computed from vertical-component data for 16 October 1964 and 29 January 1965. Parzen-smoothed, the correlations used in determining the spectra are computed for 100 lags (50 sec), yielding a frequency resolution of approximately 0.02 Hz. Simultaneous data gates approximately 30 min in length are used from each station.

The power spectra are shown corrected to units of absolute ground motion at 0.04 Hz for those samples where calibration information is available. Also shown in subsection C are several spectra with instrument responses removed for the broadband spectra estimates. The spectra at TFO and HWIS are shown relative to unity, since calibration information is not available for these samples.

Three major peaks characterize the power spectra for both noise samples. The sharp peak at 0.6 Hz is nonseismic and probably was introduced during FM data compression operations (or FM-to-digital conversion). However, the stronger peaks at 0.04 to 0.06 Hz and at 0.12 to 0.14 Hz do appear seismic and in close agreement to those reported at LASA.⁴ A third peak, which occurred near 0.19 to 0.21 Hz at CPO, ADIS, and HWIS on 16 October 1964, corresponds to the broad peak from 0.12 to 0.22 Hz observed at LASA. The spectra appear to contain generally valid seismic data between 0.03 and 0.2 Hz and seem to be very stationary at 0.04 Hz, with all stations reflecting levels very close to 45 db relative to $1 \mu\text{m}^2/\text{Hz}$. Larger variations are seen for the microseismic energy between 0.1 and 0.2 Hz. The rise in power below 0.03 Hz is believed related to instrument or meteorological energy rather than to seismic energy.

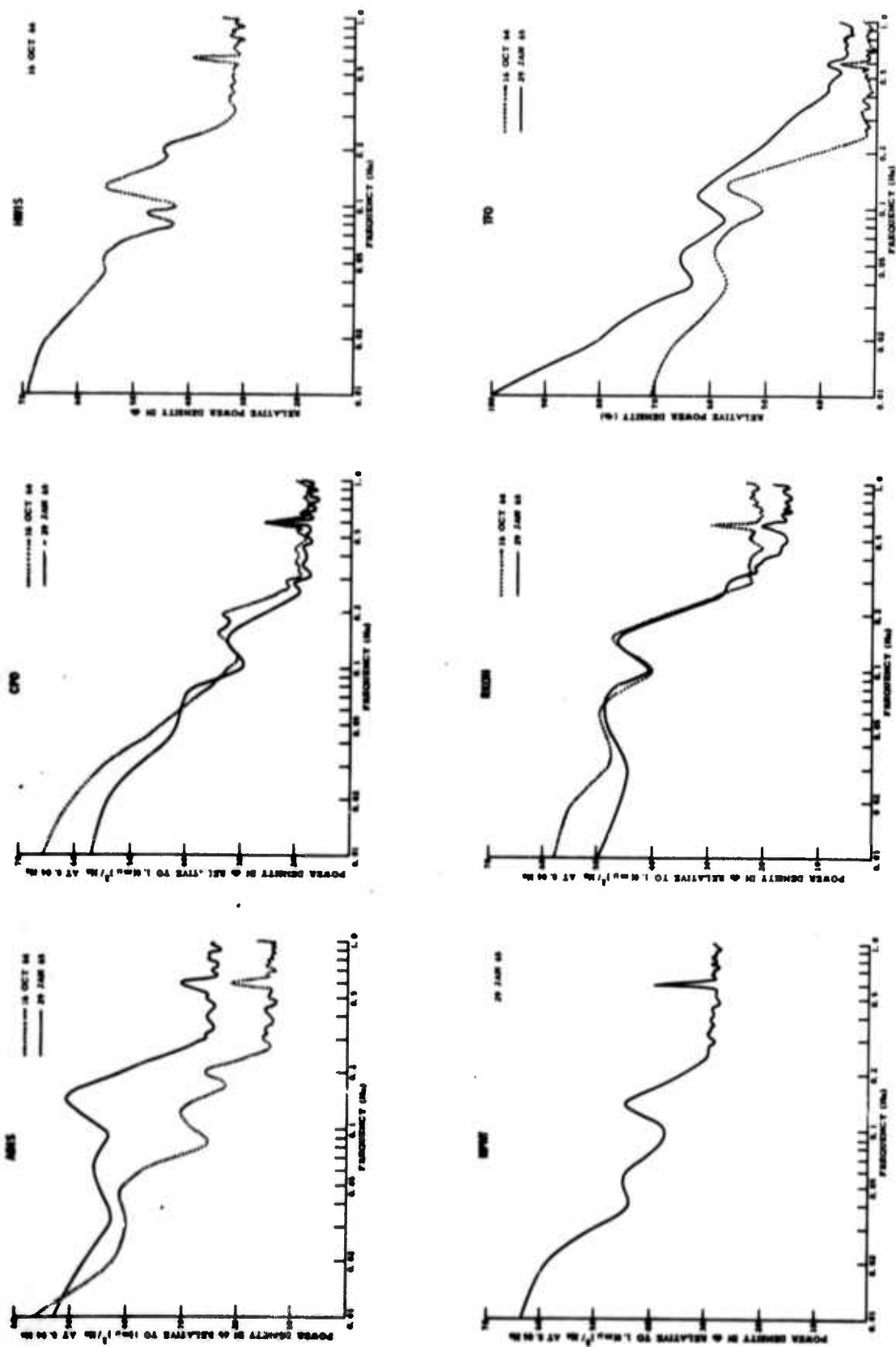


Figure II-12. Long-Period Vertical-Component Power Spectra



In general, the quality of the long-period data is low. Major portions of the recorded data are unusable because of spikes. Data digitization levels are very low, causing rather coarsely quantized samples and poor seismic-to-instrument-noise ratios. A third problem affecting coherence measurements involves apparent tape-speed differences in the station-recorded data during digitization of the FM data (or during original recording of the FM tapes). These differences result in slightly different sampling rates for each station. For example, sampling rates on 29 January 1965 vary from 7620 samples/hr at ADIS to 8100 samples/hr at CPO, based on 1 hr of station-recorded clock time; this contrasts with the "assumed" 7200 samples/hr (2 samples/sec). Total sampling-rate error is higher for the 16 October 1964 data, but station-to-station variations are smaller (e. g., 8600 samples/hr at RKON in contrast with 8500 samples/hr at CPO).

Below 0.06 Hz, observations are necessarily tentative, since data gates were only 30 min long. However, the apparently stable character of the spectra at 0.04 Hz implies a relative lack of sensitivity to regional seismic-noise activity. Additional evaluation of this behavior is indicated.

Figure II-13 shows interstation coherences computed for the stations included in the power spectral analysis. Except for highly coherent lines at 0.6 Hz and broad peaks below 0.03 Hz (all nonseismic), usable coherence is nil across the network. The sampling error described earlier certainly affects these measurements; however, in view of the dominance of regional surface-mode energy at each station in the short-period range, little coherence would be expected in the microseismic band.

Assuming that the long-period network data correspond to a weakly stationary process, an estimate of the level of coherence expected through chance correlation can be made. From tables of the distribution of coherence coefficients presented by Amos and Koopmans,⁵ this level is

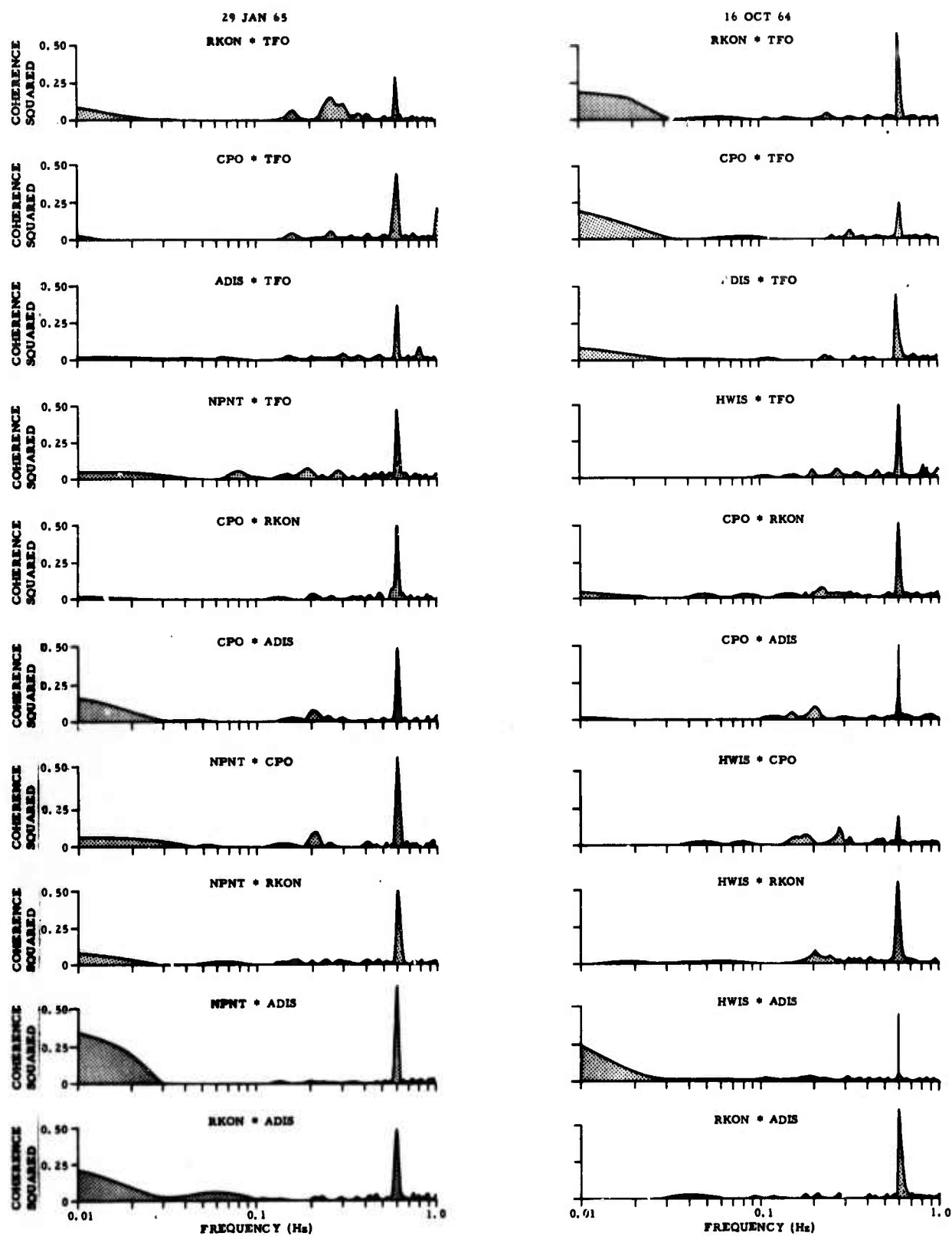


Figure II-13. Long-Period Interstation Coherences for
16 October 1964 and 29 January 1965 Samples



0.15, with a standard deviation of 0.075. The coherence curves presented in Figure II-13 actually represent coherence squared and are computed using the relation

$$\text{COH}_{ij} = \frac{\sqrt{\phi_{ij} \phi_{ij}^*}}{\sqrt{\phi_{ii} \phi_{jj}}}$$

where * denotes the complex conjugate. Since tables for the distribution of estimates for coherence squared are not as readily available, values of interest are converted to Koopmans' definition by taking the square root.

Several coherent peaks are significantly higher than the random correlation level; whether these are instrument-generated or seismic is difficult to establish. Especially interesting, however, is one peak representing 0.4 coherence (0.15 on plot of coherence squared) at 0.26 Hz between RKON and TFO. Both spectra are substantially above the background digitization levels (Figure II-12) at this frequency and both show slight evidence of a spectral peak. Also, the two stations are essentially in line with coherent energy propagating across the Canadian Shield from the intense storm located off Newfoundland. Such coherence, if seismic, is too low for practical use in array processing but certainly is academically interesting. Also, this coherence, if truly seismic, probably would be increased by the analysis of larger time samples.

In summary, the long-period spectra appear to be seismically valid, to reflect reasonably stable energy levels in the 0.03- to 0.05-Hz band where the instrument responses peak, and to indicate that microseismic energy is a significant contributor between 0.1 and 0.3 Hz. Energy levels in this latter band appear to be related to regional storm activity. No usable coherence between network stations is detected; however, due to the limited quality of the data, conclusions regarding network coherence in the long-period range cannot be drawn.

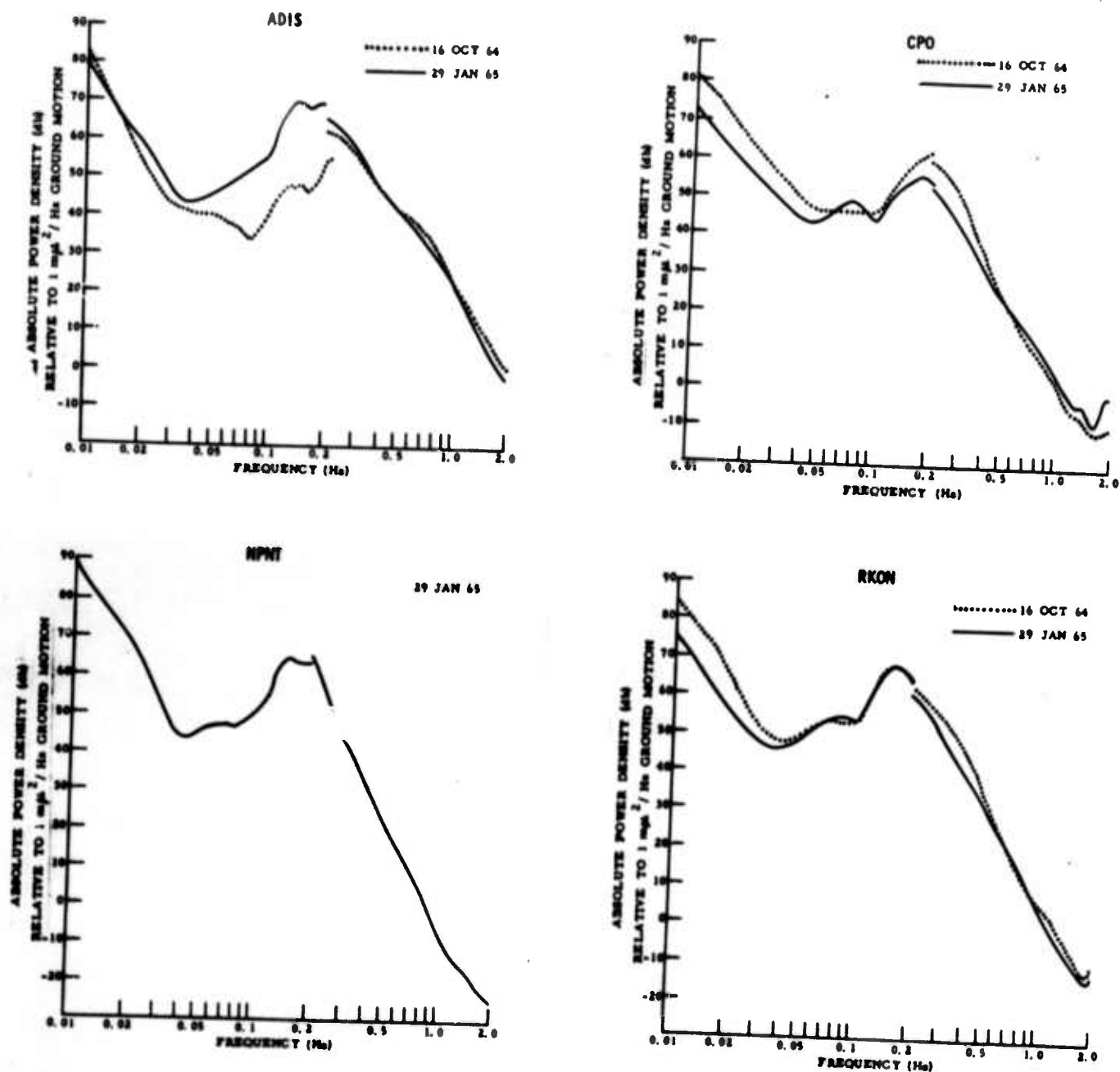


Figure II-14. Broadband Spectral Estimates Using Absolute Long- and Short-Period Power-Density Spectra



C. BROADBAND SPECTRAL ESTIMATES

Figure II-14 presents absolute power-density spectra for CPO, NPNT, ADIS, and RKON. The frequency range from 0.01 to 2.0 Hz is shown, with long-period spectral estimates used to form the curves from 0.01 to 0.2 Hz and short-period data used from 0.2 to 2.0 Hz.

The spectra join reasonably well in the 0.2-Hz vicinity and appear to provide reasonable estimates of the broadband seismic noise field. The seismic peak seen on all spectra between 0.1 and 0.3 Hz is apparently valid, although the exact level is suspect since both long-period and short-period instrument responses are low (approximately -40 db) at this point and seismic-noise-to-instrument-noise levels are poor. Below 0.03 Hz, the long-period curves are also suspect due to contamination with system noise. Noise power levels are up considerably at 0.04 Hz (45 db) relative to 1.0 Hz (-10 to +10 db) and are much stabler across the network.

BLANK PAGE



SECTION III

ANALYSIS OF NETWORK NOISE FIELD USING HIGH-RESOLUTION FREQUENCY-WAVENUMBER SPECTRA

A. DESCRIPTION OF EXPERIMENT

A knowledge of the noise structure at the network level is necessary for optimum design of signal detection and extraction procedures for the network. Therefore, an objective of the network noise study is dissection of each station's short-period noise field into frequency and wavenumber components and determination of component sources where possible. The network noise structure may then be interpreted in terms of energy from common sources when seen at each station. The network's capability for locating and tracking energy sources such as tropical storms can also be evaluated.

Such an analysis requires reasonably long simultaneous noise samples from each array station in the network. Practical limitations, including data quality, resulted in a usable data gate length of 6.67 min at each station. Two of the five available noise samples were taken during periods when low-pressure areas were numerous across the northern hemisphere; these samples (16 October 1964 and 29 January 1965) were chosen for analysis. Data for these samples were available from array stations CPO, TFO, OONW, GGGR, and NPNT. Descriptive material pertaining to these stations and the data library is contained in the appendix.

A technique useful for dissection must provide good resolution in both frequency and wavenumber. Therefore, the high-resolution f - \vec{k} spectral technique was employed in conjunction with direct-transform procedures. The use of these techniques for noise analysis was evaluated in a previous special report.⁶

Smoothing across frequency was not performed on the resulting crosspower matrices, so frequency resolution was roughly 0.0025 Hz. Comparisons described in Special Report No. 8 demonstrate that phase relationships between sensors are distorted by smoothing over long time gates, re-



sulting in increased variability in spatial location of peaks with choice of reference sensor. Further comparisons of the unsmoothed spectra with the rather well-documented CPO noise field (in terms of conventional f - \vec{k} analysis) indicate excellent agreement.⁷

Since the high-resolution technique is influenced by reference-sensor choice (due to the finite array geometry), wavenumber responses were computed using each array sensor as reference. These MCF responses are actually the reciprocal of the wavenumber spectral estimate. Prior to the summing across sensors, the reciprocal of each response was taken, yielding additional discrimination between coherent peaks and the overall incoherent level of the plane. Crosspower matrices were normalized to yield unit autopower at each frequency. A signal-to-noise ratio of 0.01 used in the filter design was experimentally determined adequate for resolution in the wavenumber plane.

An incentive for critical analysis of high-resolution spectra computed from unsmoothed direct transforms taken over rather long time gates is the emergence of a mathematical shortcut, facilitating computation of the high-resolution spectral sum. The procedure is valid only for unsmoothed crosspower matrices and eliminates the need to compute and sum individual filter responses for each sensor. Using this shortcut, the summed output was obtained in roughly the time originally required for each individual spectrum. Special Report No. 8 contains a description of the mathematical procedure used.⁶

As a result of summing reciprocals of the individual wavenumber responses, some smoothing in the wavenumber plane appears desirable. This is caused primarily by departures from ideal equalization of coherent energy, especially at the lower frequencies, and is seen in the individual spectra as slight wandering of the coherent peaks in the wavenumber plane. Procedures to smooth in the wavenumber plane require further examination and were not implemented for this study. Instead, a minimum of hand-smoothing was performed during contouring, primarily to enhance the spectral readability.



High-resolution $f\text{-}\vec{k}$ spectra were computed for each station in 0.2-Hz increments from 0.2 Hz to 1.0 Hz (TFO), 1.4 Hz (NPNT, OONW, GGGR), and 2.0 Hz (CPO). Above 2.0 Hz, the seismic validity of the network data is questionable, especially with the compressed FM data. Also, minimum seismometer spacings at the array sites have generally led to space-aliasing of valid low-velocity peaks at the higher frequencies, making interpretation impractical.

B. RESULTS AND CONCLUSIONS

The spatially organized noise observed at the station level appears to be generated primarily by meteorological and cultural sources. The former source type includes regional weather effects (such as nearby low-pressure centers, frontal passages, and wind-generated surf action) and produces the bulk of the coherent energy. The cultural sources appear stationary and highly localized, generating low-velocity (surface-mode) energy that appears random at the network level. Above the microseismic range, these local sources are substantial contributors to the station noise.

Weather-generated energy is a continuous contributor throughout the frequency band (to 2.0 Hz) and dominates in the microseismic range. Table III-1 summarizes coherent energy apparently related to regional storms; subsection C presents and discusses the station high-resolution $f\text{-}\vec{k}$ spectra containing these coherent peaks.

Major coherent peaks at TFO are primarily bodywave energy; CPO and the LRSM stations are dominated by low-velocity energy. Contributing to the sensitivity at TFO are several factors including array aperture (10 km as compared with 3 km at CPO and the LRSM stations), geology (scattering of surface waves at TFO has been noted), relative ambient noise levels, and a lack of localized storm activity in the TFO vicinity.



Table III-1
STORM-GENERATED COHERENT ENERGY

Date	Coherent Peak	Station Observed	Frequencies Observed (kHz)	Mode of Propagation	Velocity Range (km/sec)	Azimuth from Station (°)	Probable Source
29 January 1965	20	CPO	0.2	Surface	3.4	25	Storm center 20 (over Newfoundland)
		TFO	0.8	Bodywave	20.0	30	
		NPNT	0.2, 0.8, 1.0	Surface	2.0-2.7	80-125	
		OONW	0.6	Surface	3.2	280	
			0.8, 1.2	Bodywave	7.0-10.0	275-285	
		GGGR	1.2	Bodywave	15.0	290	
	17	CPO	0.4, 1.6 0.4, 2.0	Surface Bodywave	3.0-3.5 6.0	300-320 315	Storm centers 16, 17, and 18 and frontal passage over Great Plains
		TFO	0.8	Surface	2.8	10	
		NPNT	0.6, 1.0	Surface	2.7-3.5	170-175	
	22	NPNT	0.4, 1.0, 1.4 1.0	Surface Bodywave	2.3-4.5 20.0	305-320 300	Storm center 22 (Kara Sea)
16 October 1964		OONW	0.2	Surface	3.5	15	Possibly storm center 24 (Baltic Sea)
		GGGR	0.2 0.4, 1.0 0.8	Indef. Surface Bodywave	- 2.0-2.5 10.0	~10 10-35 60	
	24	OONW	1.4	Surface	3.3	105	
		GGGR*					Storm center 24 (Baltic Sea)
	25	GGGR	0.8, 1.0	Surface	2.5-5.0	230-270	Storm center 25 (off Portugal)
	23	OONW	0.4	Surface	2.3	330	Storm center 23 (Norwegian Sea)
	26	TFO	0.2, 0.8	Surface	4.0-6.0	265	Storm center 26 (off California)
	19	TFO	0.8, 1.0 0.4	Surface Bodywave	2.5-3.2 14.0	315-330 340	Storm center 19 (Gulf of Alaska)
	1	CPO	0.2, 0.4, 1.0, 1.6, 1.8, 2.0	Surface	2.0-3.7	85-125	Storm center 1 (Atlantic Seaboard)
		NPNT	0.8	Surface	2.0	135	
16 October 1964	14	NPNT	0.4, 1.0 1.4	Surface Bodywave	4.7 10.0	115 120	Storm center 14 (Greenland and Newfoundland coastlines)
		TFO	0.2, 0.4, 1.0 0.4, 0.6, 0.8, 1.0	Bodywave Surface	14.0-24.0 1.9-4.5	15-65 35-50	
	3	NPNT	0.2, 1.0, 1.2	Surface	1.9-2.0	215-220	Storm center 3 (Gulf of Alaska)
	5	NPNT	0.6	Bodywave	20.0	255	Storm center 5 (Pacific Ocean off Japan)
	13	OONW	0.2, 0.6, 0.8, 1.2, 1.4 0.4	Surface Bodywave	2.0-3.6 10.0	170-245 200	Storm center 13 (North Sea)
		GGGR	0.2, 0.8, 1.0	Surface	2.3-3.0	300-345	
	12	OONW	0.8, 1.0	Surface	3.2-6.0	315-320	Storm center 12 (Norwegian Sea)

* Sea coherent peak 22

Nearby storm centers (such as LPC 1 east of CPO and LPC 13 in the North Sea west of OONW) radiate energy over a broad frequency band. However, the coherent peaks generally appear rather narrowband. This is due partly to the high-frequency resolution available — negligible energy is



smearred across frequencies. In addition, the attenuation of energy with both distance and geology is frequency-dependent. The weather-related seismic-energy source functions are not necessarily broadband.

While the more intense low-pressure centers are simultaneously detected at several network stations, this detection is rarely achieved at a common frequency and only once for bodywave energy (LPC 20 seen at both OONW and GGGR for 1.2 Hz). Simultaneous detection of surface-wave energy occurs for LPC 20 (CPO and NPNT at 2.0 Hz), LPC 22 (NPNT and GGGR at 0.4 and 1.0 Hz), LPC 14 (NPNT and TFO at 0.4 and 1.0 Hz), and LPC 13 (OONW and GGGR at 0.2 and 1.0 Hz). This lack of common detection is partly explained by the attenuation of energy with distance to each station as a function of frequency. Also, differences in frequency filtering with azimuth at each station contribute to this effect. Similarly, source-radiation patterns probably are not uniform with azimuth.

The CPO noise spectra are compared with data from a rather comprehensive noise analysis using conventional $f\text{-}\vec{k}$ spectra.⁷ This is done partly to confirm the validity of the data and partly to examine the validity of the high-resolution $f\text{-}\vec{k}$ technique for such noise analysis. Excellent agreement is obtained in terms of general spatial organization and specifically for established stationary sources (e.g., the narrowband coherent peak seen at 1.4 Hz from the north at about 4.5 km/sec). Similarly, general spatial distribution at TFO agrees well with previous analyses.⁸

A few high-velocity peaks which do not appear to be either storm-generated or stationary are detected. Sources for these peaks are not established, although there is the possibility that they represent valid bodywave energy from seismically active areas.

The foregoing analysis, it must be emphasized, is based on a rather limited quantity of network data. Only two noise samples, both highly storm-active, are used. More realistically, several samples covering a range of weather and seasonal conditions should be analyzed. The network of five array stations used actually is not sufficient for comprehensive coverage and should be expanded.



Some preliminary conclusions regarding the character of the network noise field can be made, however, from the foregoing analysis.

The lack of common coherent peaks at the network stations for a given frequency indicates that little or no coherence should be found at the network level. Thus, there appears to be little advantage in using multichannel processing techniques for noise suppression at the network level. The bulk of the station noise appears as low-velocity energy (except at TFO), and no conclusions are drawn regarding the extent of coherence of the bodywave portion of the station noise field. Generally, the station arrays are not adequate to sufficiently suppress the low-velocity component, allowing evaluation of bodywave coherence across the network. Should preprocessing at the station level provide suppression of the low-velocity component, multichannel processing might conceivably be required for directional bodywave noise suppression at the network level.

C. PRESENTATION OF STATION NOISE SPECTRA

High-resolution spectra from the five array stations are analyzed at the same time for each frequency. Data from the 16 October 1964 noise sample are presented first, followed by the 29 January 1965 data. Since a rather large number of spectra are presented, the following format facilitates discussion of both individual and common features: spectra from the five stations are shown together at each frequency, and the discussion pertinent to these spectra is contained on the opposite page. Shown with each set of spectra is a map displaying the relative locations of stations and storm centers for that day.

The wavenumber plane out to an edge velocity of 2.0 km/sec is shown. At the lower frequencies, this region is entirely contained within the unit cell. However, as frequency increases, the available wavenumber



region is reduced by contraction of the unit cell. Dimensions of each unit cell are indicated when they fall within the 2.0-km/sec region displayed. The plots are not contoured outside the unit cell except for a few instances when a low-velocity coherent peak is believed aliased into the cell from outside. Differences in minimum seismometer spacings along the two arms at TFO result in a rectangular unit cell.

Contour levels vary from plot to plot due to variations in dynamic range and complexity. Within each plot, however, the contour increment is held constant. Exceptions occur when relative peak amplitudes are indicated. All plots are oriented conventionally, with north at the top of the page (except CPO, where true north lies 14° west of conventional north) as shown by the arrow at the top of each plot. Coherent spectral peaks occur in the quadrant corresponding to the direction of the source from the station. Shading is used to highlight peaks being discussed. Also, the peaks are assigned numbers corresponding to storm-center designations if believed to be related to that source. Apparently stationary peaks are designated with letters.

The discussion refers to storm centers as low-pressure centers (LPC). Thus, tropical storm Isabel, designated storm center 1, is referred to as LPC 1. Figures III-1 and III-2 show areas of storm activity for the northern hemisphere on 16 October 1964 at 1800 GMT and 29 January 1965 at 0600 GMT, respectively. Investigation of southern-hemisphere weather data indicates no significant storm activity. Isobaric lines of high- and low-pressure areas and frontal lines are shown on each weather map. Figures III-3 and III-4 show sea wind-wave height contours and indicate the location of designated LPC's. Swell-height charts reflect similar sea-state information and are not shown. Figures III-5 through III-19 contain the 2-dimensional wavenumber spectra.

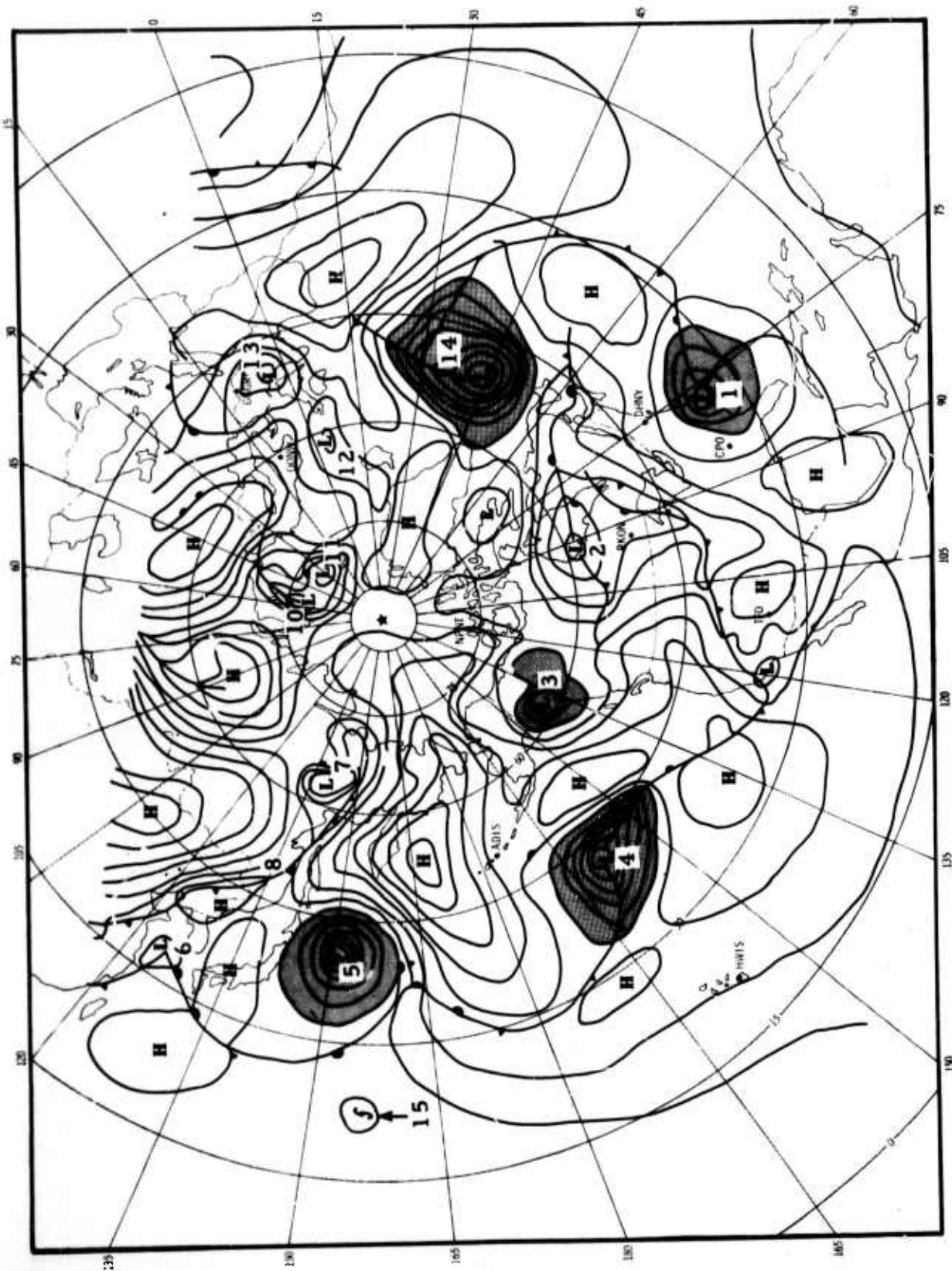


Figure III-1. Surface Weather Map for 16 October 1964 at 1800 GMT

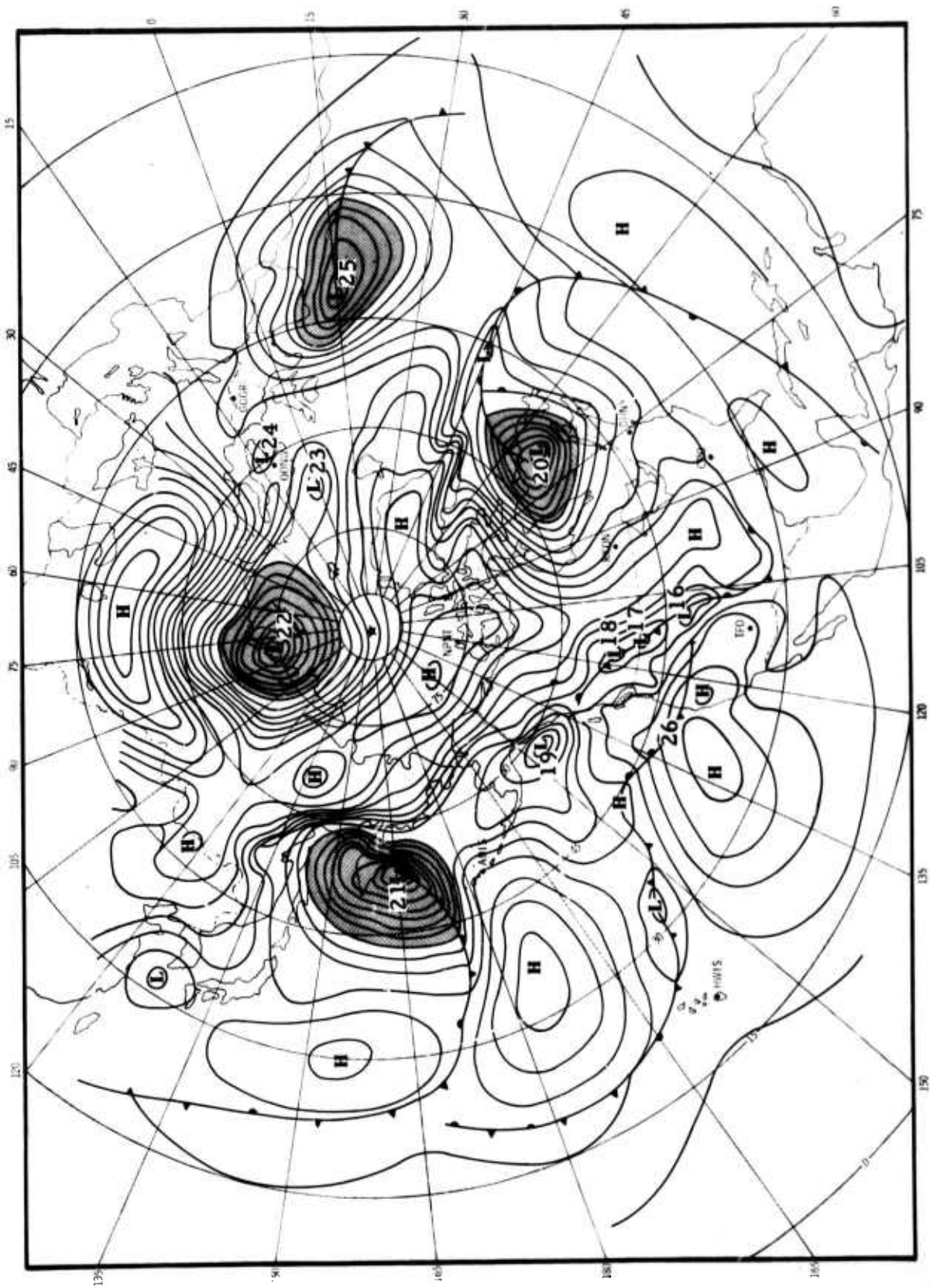


Figure III-2. Surface Weather Map for 29 January 1965 at 0600 GMT

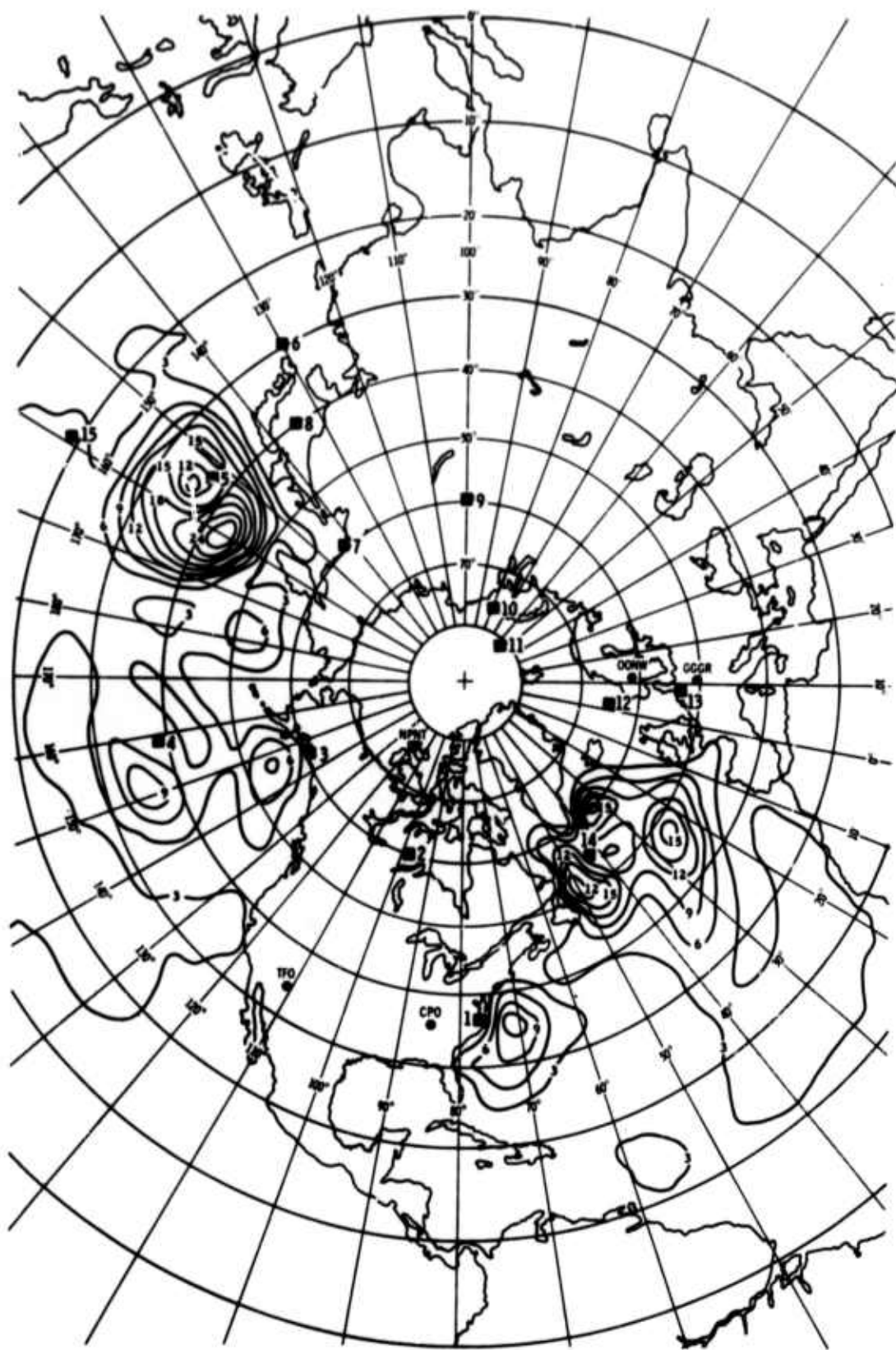


Figure III-3. Sea Wind-Wave Height Chart for 16 October 1964 at 1800 GMT

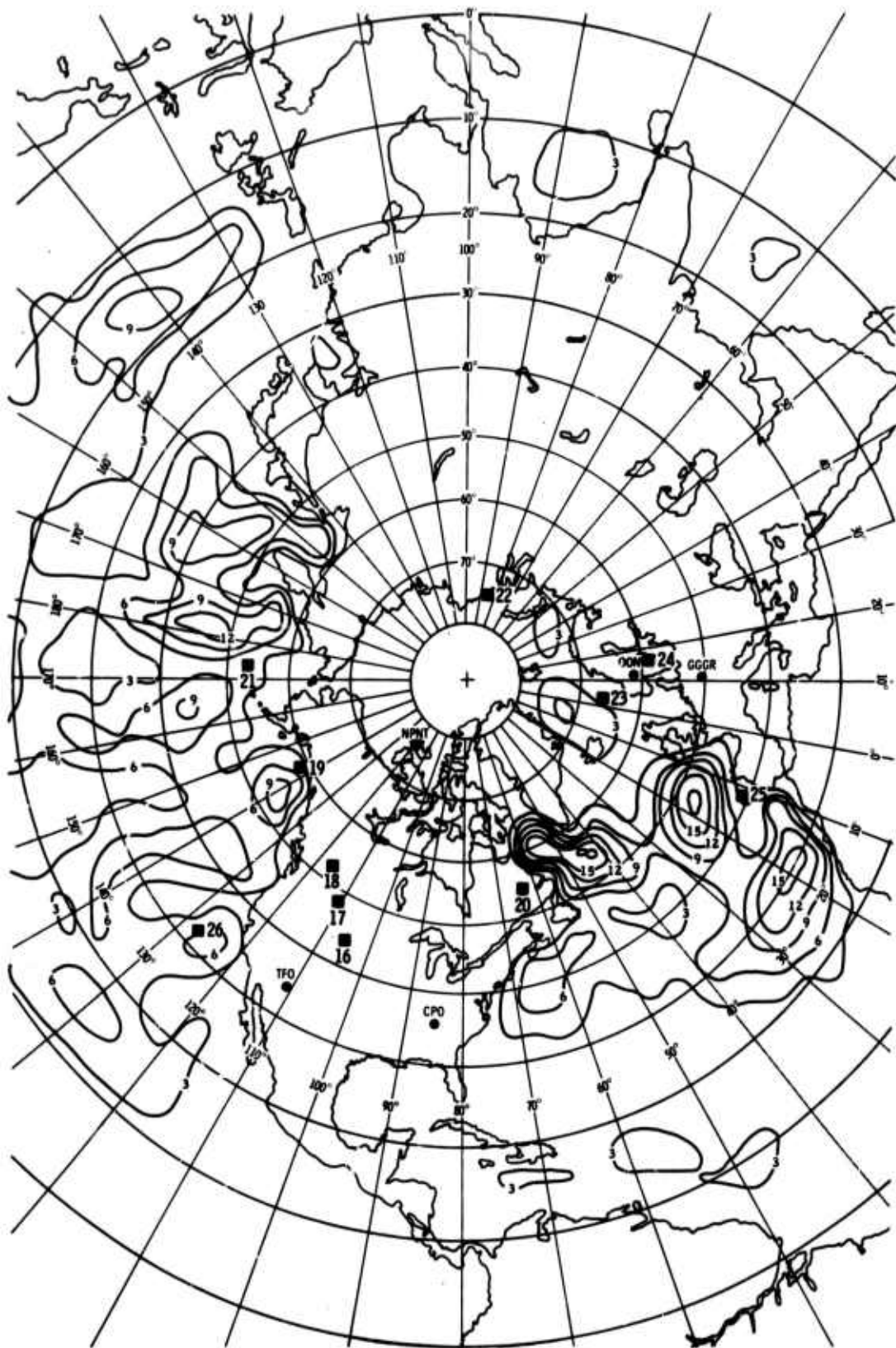


Figure III-4. Sea Wind-Wave Height Chart for 29 January 1965 at 0600 GMT

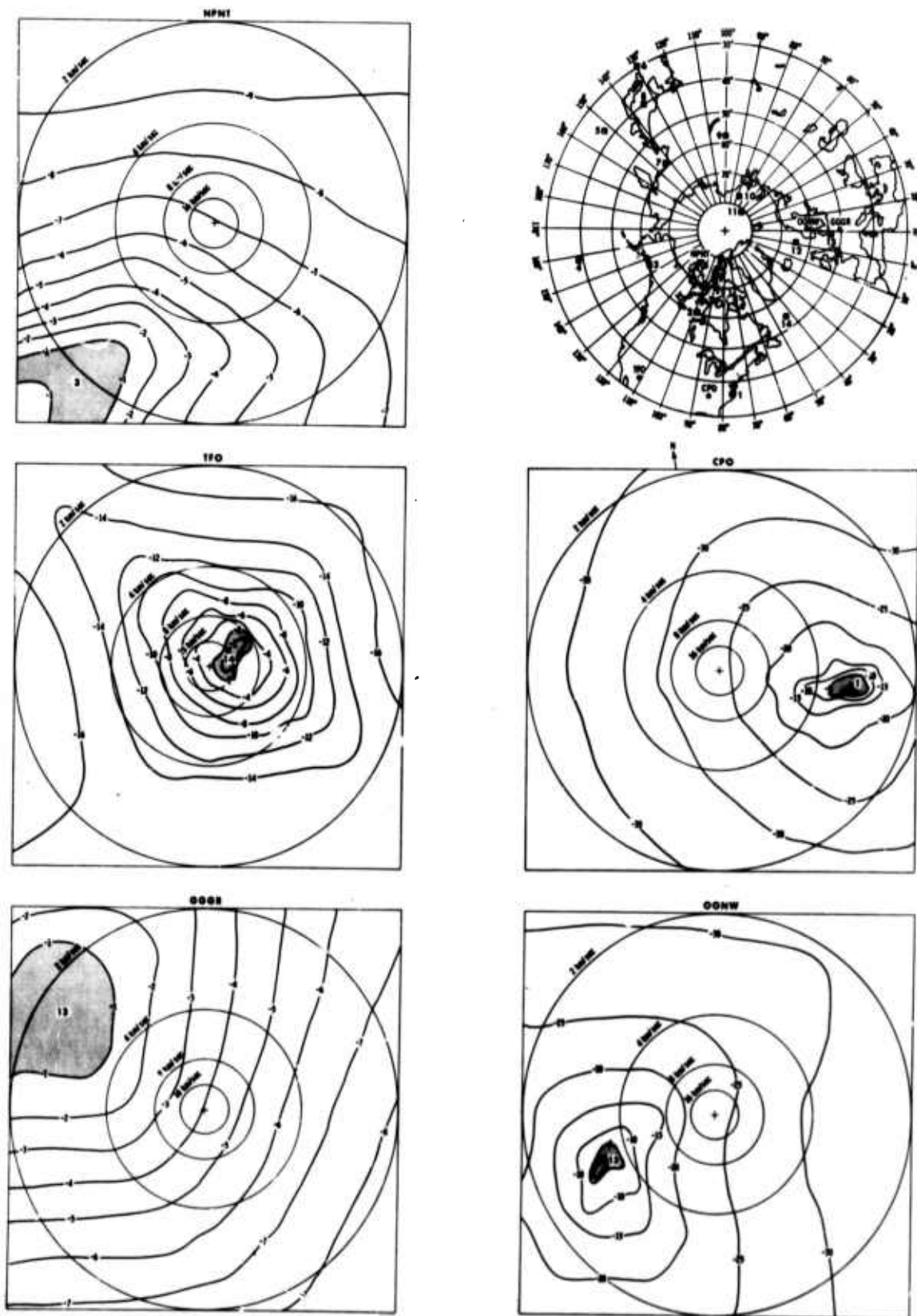


Figure III-5. High-Resolution f - \vec{k} Spectra



Figure III-5, 16 October 1964, $F = 0.2$ Hz

Surface-mode energy generated by regional storm activity dominates the station noise fields at 0.2 Hz during this time period. An exception is TFO, which indicates bodywave energy (15 km/sec) arriving from the northeast (lobe 14), apparently generated by the intense LPC 14 located off the Newfoundland coast.

The surface-mode peak at CPO (lobe 1) is generated by LPC 1 near Cape Hatteras. This energy is observed over a relatively wide frequency band, probably due to the close proximity of the disturbance.

Surface-mode energy indicated at NPNT (lobe 3) is apparently generated by LPC 3 off the southern Alaskan coast. GGGR and OONW indicate surface-mode energy (lobe 13) from LPC 13 located in the North Sea vicinity.

Surface-mode velocities vary from 2.0 to 3.0 km/sec. Spectral-peak definition is generally poor, primarily because of insufficient array resolution at this frequency.

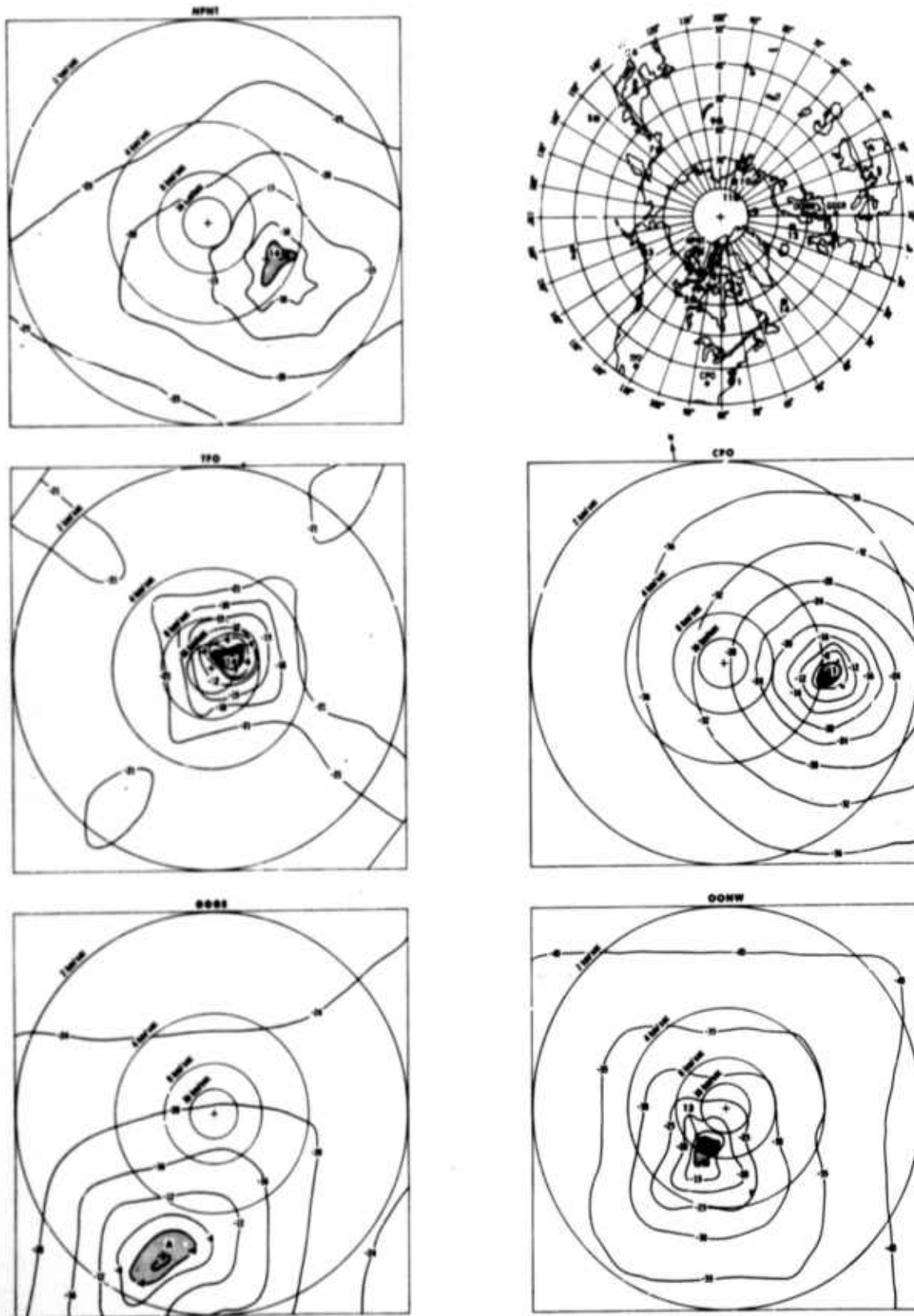


Figure III-6. High-Resolution $f-k$ Spectra



Figure III-6, 16 October 1964, $F = 0.4$ Hz

Regional storms again dominate most spectra at 0.4 Hz, although some seemingly stationary peaks emerge.

Bodywave energy is seen at OONW (lobe 13), with the 8 km/sec peak apparently generated by LPC 13. However, evidence of this source at GGGR is submerged by the strong surface-mode energy from the south (lobe A), which corresponds to the major peak in the station power spectra (Section II). This peak occurs also on 29 January 1965 and is probably related to local cultural activity. The town of Nuremburg, Germany, is 28 km away in this general direction.

Surface-mode energy from LPC 1 still dominates the spectrum at CPO (lobe 1), and bodywave energy from LPC 14 continues at TFO (lobe 14). Both sources are dominant contributors at 0.2 Hz. Surface-mode energy at NPNT (lobe 14) also apparently is related to LPC 14.

Coherent peaks begin to appear relatively narrowband, suggesting the possibility of highly frequency-selective earth filtering.

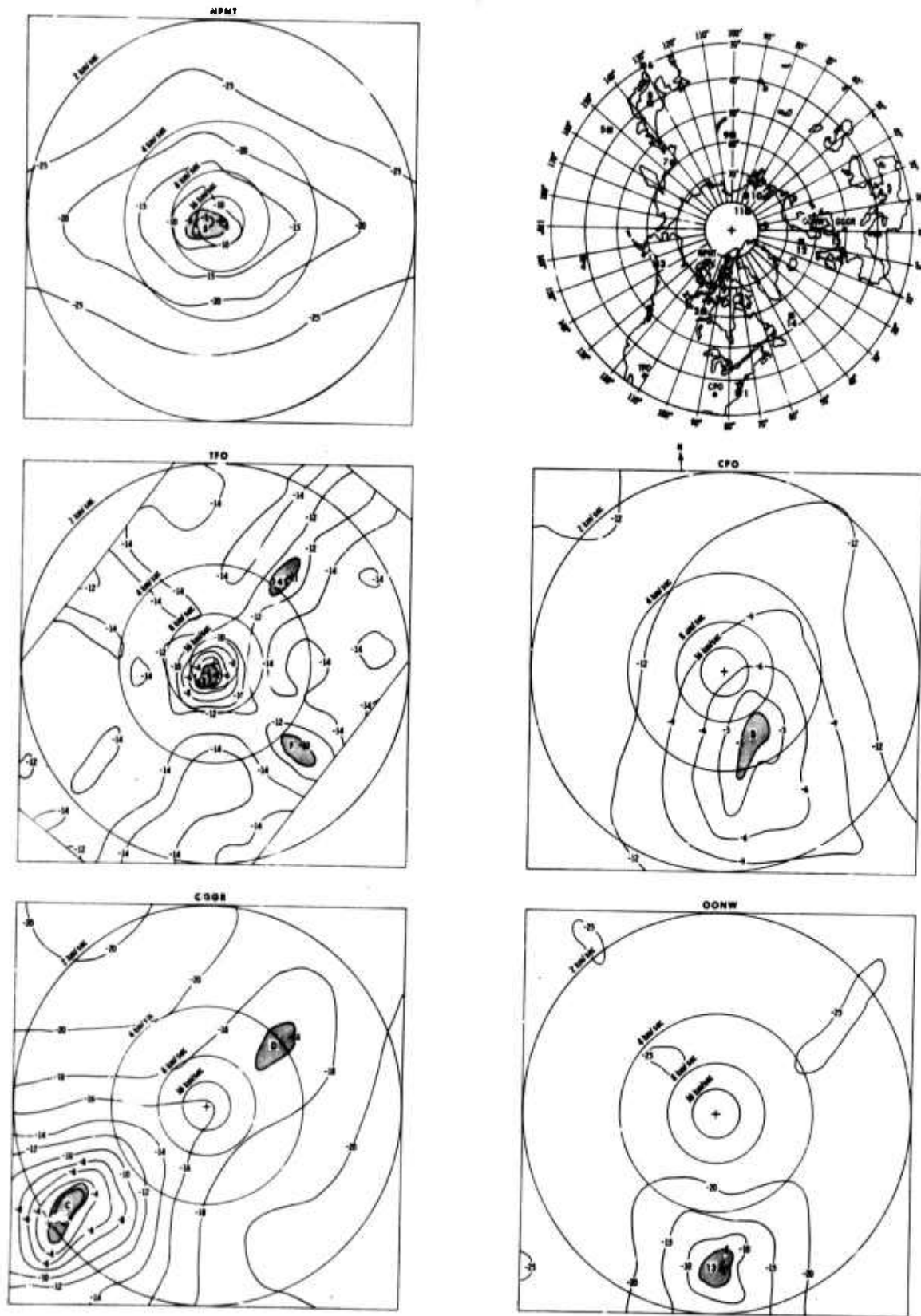


Figure III-7. High-Resolution f - \vec{k} Spectra



Figure III-7, 16 October 1964, $F = 0.6$ Hz

At 0.6 Hz, storm-related energy appears generally less dominant. Coherent energy seems relatively low at all stations, suggesting a transition region in the 0.6- to 0.8-Hz interval. For example, coherent energy from LPC 1 has faded at CPO; a relatively broad, seemingly stationary peak from the southeast (lobe B) appears. The relatively high surface-mode propagation velocity suggests a local cultural source. This peak is slightly better defined in the 29 January 1965 sample.

The bodywave peak seen at OONW at 0.4 Hz is replaced by a surface-mode peak (lobe 13), probably generated by LPC 13. Similarly, the narrowband stationary surface-mode peak seen at GGGR at 0.4 Hz is replaced by a peak from the southwest (lobe C), which also occurs on 29 January 1965 and is probably locally or coastally generated. A weaker peak from the northeast (lobe D) also may be stationary.

Bodywave energy is seen at NPNT (lobe 5), corresponding in wavenumber to the intense LPC 5 off Japan. The bodywave peak at TFO (20 km/sec) from the southwest (lobe E) does not appear to be storm-generated, and its source is not established. Surface-mode energy from the northeast (lobe 14) is apparently related to LPC 14. A surface-mode peak from the southeast (lobe F) is generated either locally or along the Gulf coast.

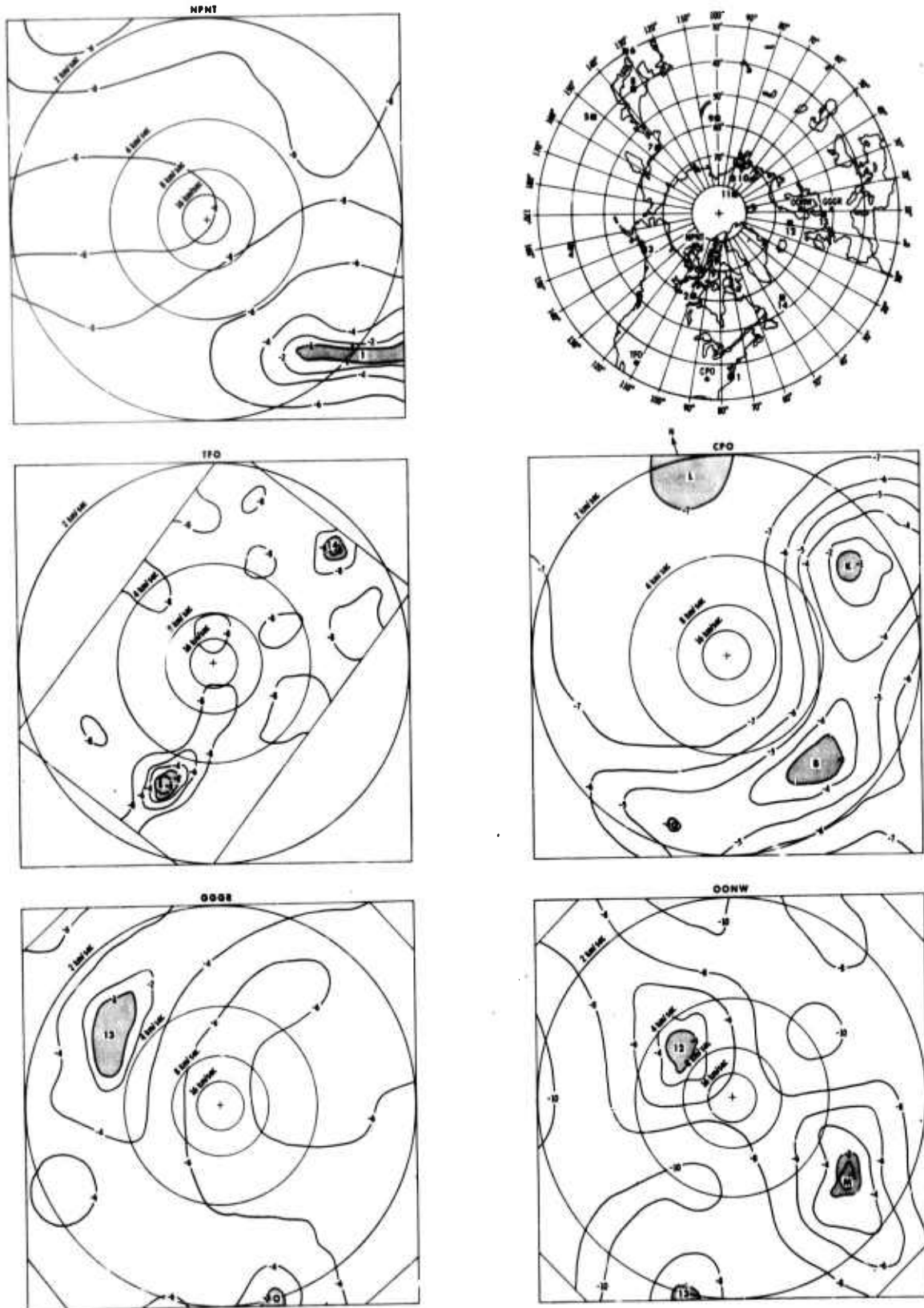


Figure III-8. High-Resolution $f-k$ Spectra



Figure III-8, 16 October 1964, $F = 0.8$ Hz

At 0.8 Hz, surface-mode energy dominates at all stations. Coherent energy levels are still relatively low at this frequency. GGGR indicates a surface-mode peak (lobe 13) from LPC 13 in the North Sea. This energy is indicated at 0.2 Hz and is then replaced by stronger stationary peaks at 0.4 and 0.6 Hz.

Also seen is a weaker peak from the south (lobe 0), apparently neither stationary nor storm-related. OONW indicates an apparently stationary peak from the southeast (lobe M). Lesser peaks from the northwest (lobe 12) and south (lobe 13) likely correspond to surf action from LPC's 12 and 13, respectively.

The CPO spectrum closely resembles that seen for 29 January 1965, with several apparently stationary peaks emerging and forming what appears to be an almost isotropic field. The peaks probably are culturally related. Surface-mode energy at NPNT (lobe 1) appears from the general direction of LPC's 1 and 2 and the Hudson Bay area. TFO has a surface-mode peak from the southwest (lobe E), generated either locally or from the Baja coast. Weak surface-mode energy persists from LPC 14 in the northeast (lobe 14).

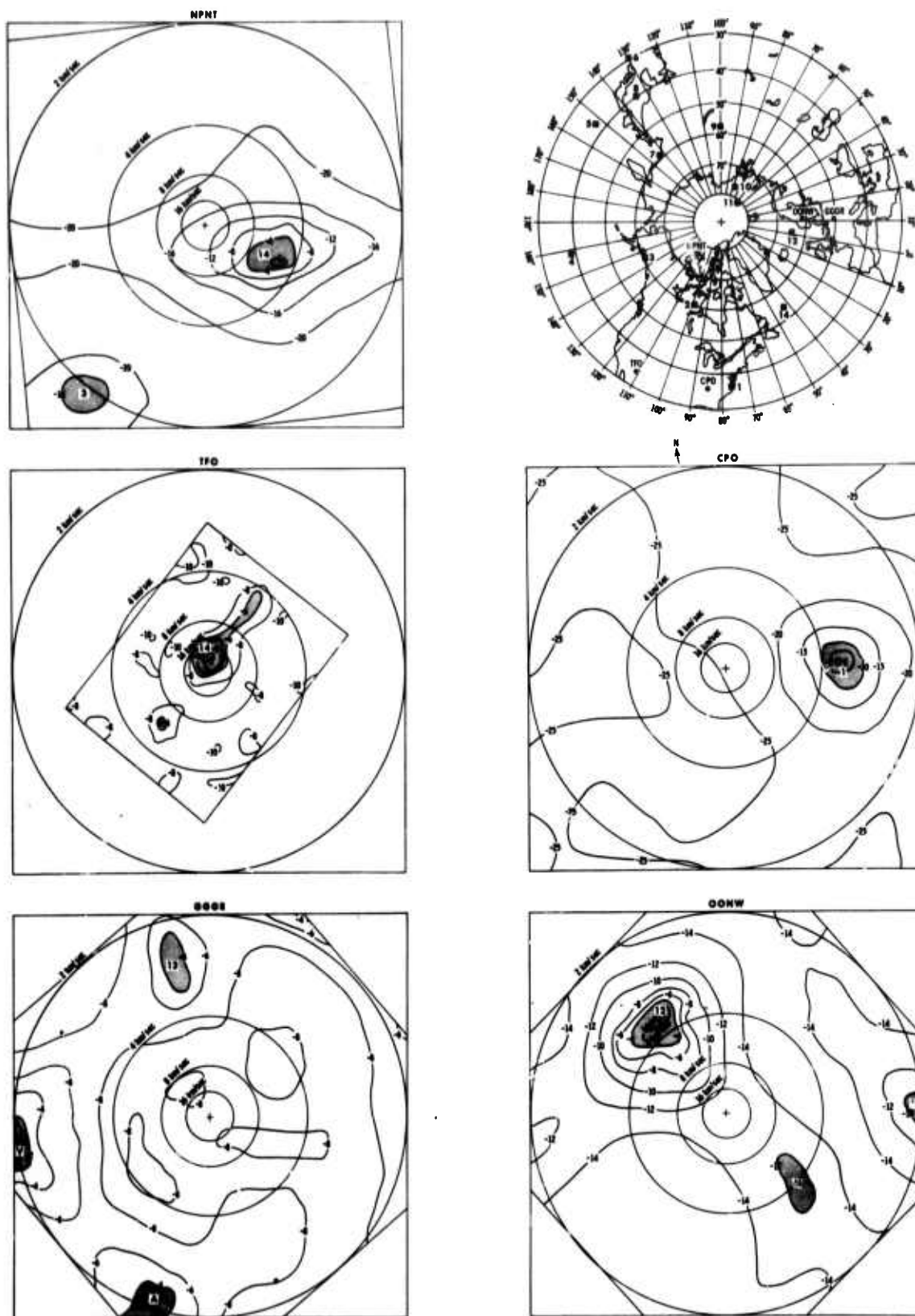


Figure III-9. High-Resolution $f\text{-}\vec{k}$ Spectra



Figure III-9, 16 October 1964, $F = 1.0$ Hz

Regional storm energy again dominates the spectra at 1.0 Hz, generating surface-mode energy at CPO, OONW, NPNT, and GGGR and bodywave energy at TFO. Coherent power levels are generally higher than at 0.6 and 0.8 Hz.

LPC 1 is again a source of coherent energy at CPO (lobe 1). Also, bodywave energy and surface-mode energy appear at TFO (lobe 14) from the complex LPC 14 off Newfoundland. A lesser peak persists from the southwest (lobe E). Surface-mode energy is seen at NPNT from the east (lobe 14) and southwest (lobe 3), corresponding to LPC's 14 and 3, respectively.

LPC 12 is seen as surface-mode energy (lobe 12) at OONW. The seemingly stationary peak from the southeast (lobe M) again appears. The source of the weak surface-mode peak from the east (lobe U) is not established. Three surface-mode peaks appear at GGGR: lobe V appears from the west, possibly the result of surf action along the coast of France; lobe 13 appears from the north, probably generated in the North Sea by LPC's 12 and 13; and lobe A appears from the south, apparently from a stationary source.

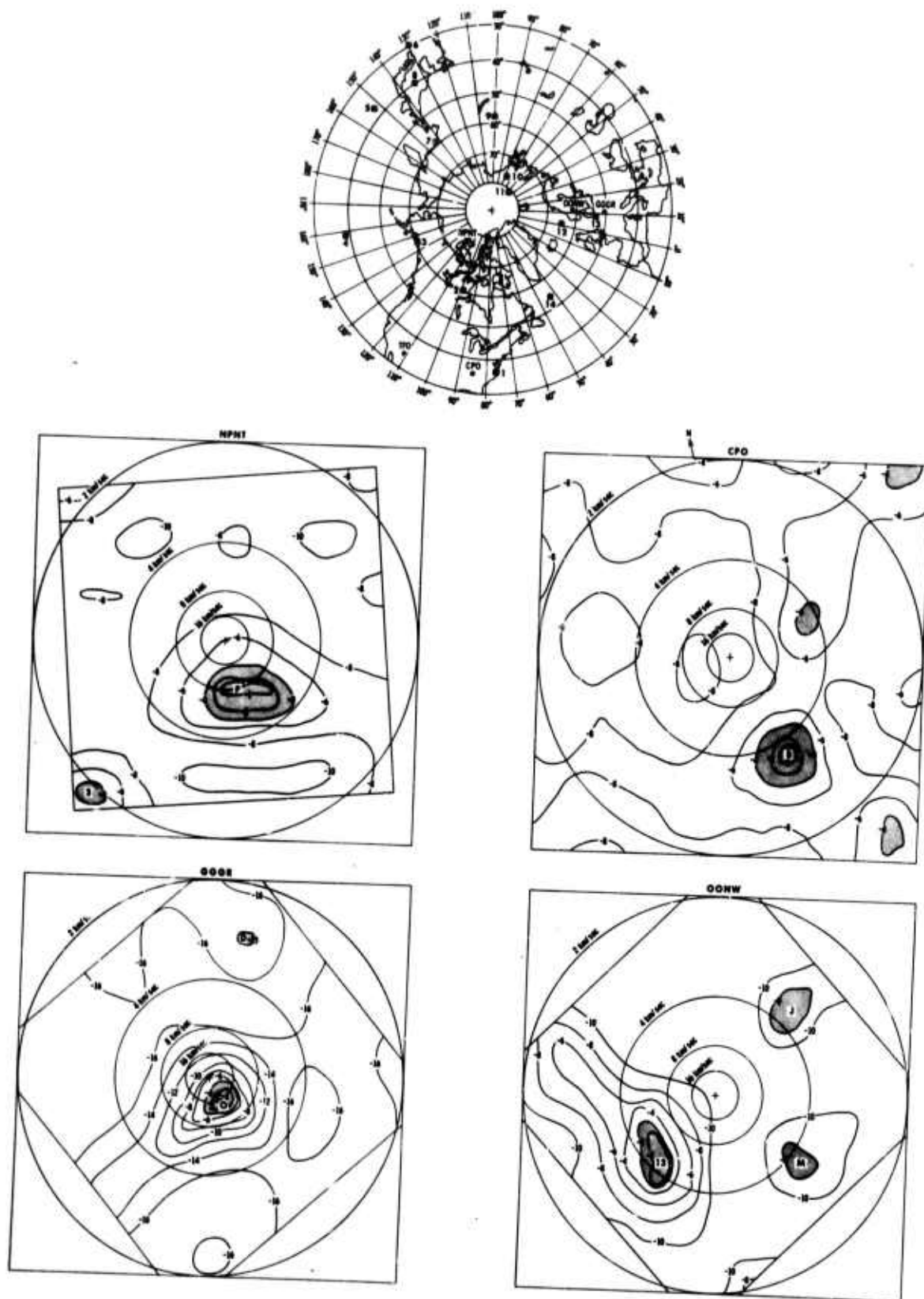




Figure III-10, 16 October 1964, $F = 1.2$ Hz

Coherent energy seen at 1.2 Hz does not appear to be primarily related to regional storm activity during either noise sample. The spectrum for TFO is omitted, as unit cell effects prevent meaningful interpretation.

A surface-mode peak from the southwest (lobe 13) at OONW apparently is related to LPC 13 in the North Sea. Weaker peaks from the northeast (lobe J) and southeast (lobe M), also seen at 0.8 Hz, appear as stationary local sources. The bodywave peak at GGGR (lobe O) appears to be unrelated to meteorological data; its source is undefined. A surface-mode peak from the northeast (lobe D) again appears as an apparently stationary source.

The bodywave peak at NPNT (lobe P) is from the general direction of LPC's 1 and 2. Also seen is surface-mode energy from the southwest (lobe 3) related to LPC 3. Coherent energy at CPO is low, and the dominant coherent energy appears as an apparently stationary surface-mode peak from the southeast (lobe B). Lesser peaks generally from the east correspond to low-level local or coastal sources.

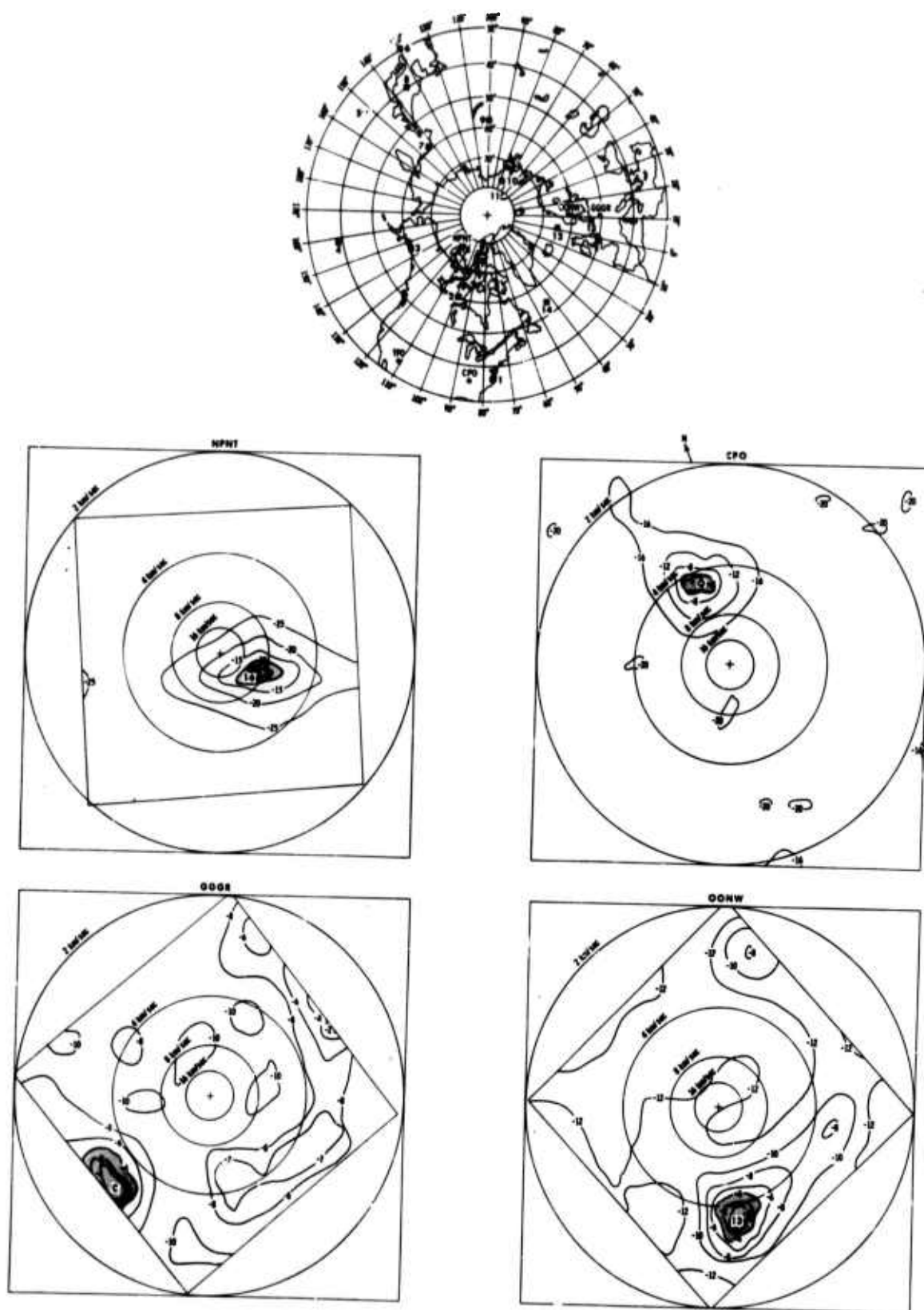


Figure III-11. High-Resolution $f-k$ Spectra



Figure III-11, 16 October 1964, $F = 1.4$ Hz

A strong, very narrowband peak is observed from the north-northwest (lobe Q) in both data samples at CPO. This peak, which has been documented previously,⁷ appears to represent a local stationary source.

Bodywave energy is seen at NPNT from the southeast (lobe 14), related to LPC 14 in the Newfoundland region, with a possible contribution from LPC 1 along the eastern Atlantic coast.

The apparently stationary surface-mode peak from the southwest (lobe C) is the major contribution at GGGR. Surface-mode energy also dominates at OONW (lobe 13), probably from LPC 13.

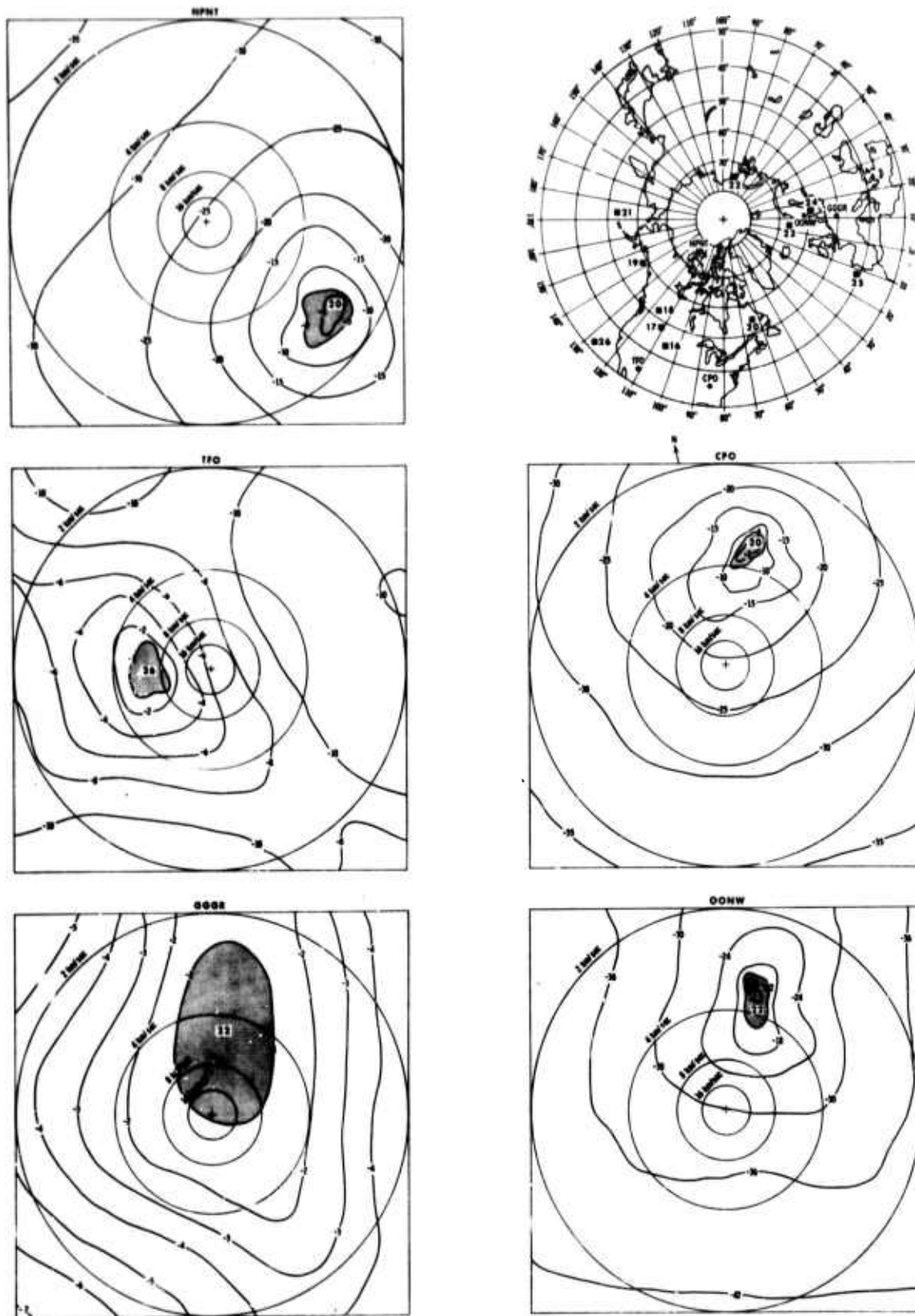


Figure III-12. High-Resolution f - k Spectra



Figure III-12, 29 January 1965, $F = 0.2$ Hz

Storm-generated energy again is dominant at 0.2 Hz on 29 January 1965.

LPC 20 over Newfoundland appears to be generating surface-mode energy at CPO and NPNT (lobe 20). TFO, however, shows only a peak from the west (lobe 26) at an intermediate velocity. This energy may be related to LPC 26 or may be generated locally.

The intense LPC 22 over the Kara Sea is seen at OONW as surface-mode energy from the northeast (lobe 22). The broad, poorly defined peak at GGGR may result either from LPC 22 or from the weaker LPC 24, also located north of Germany.

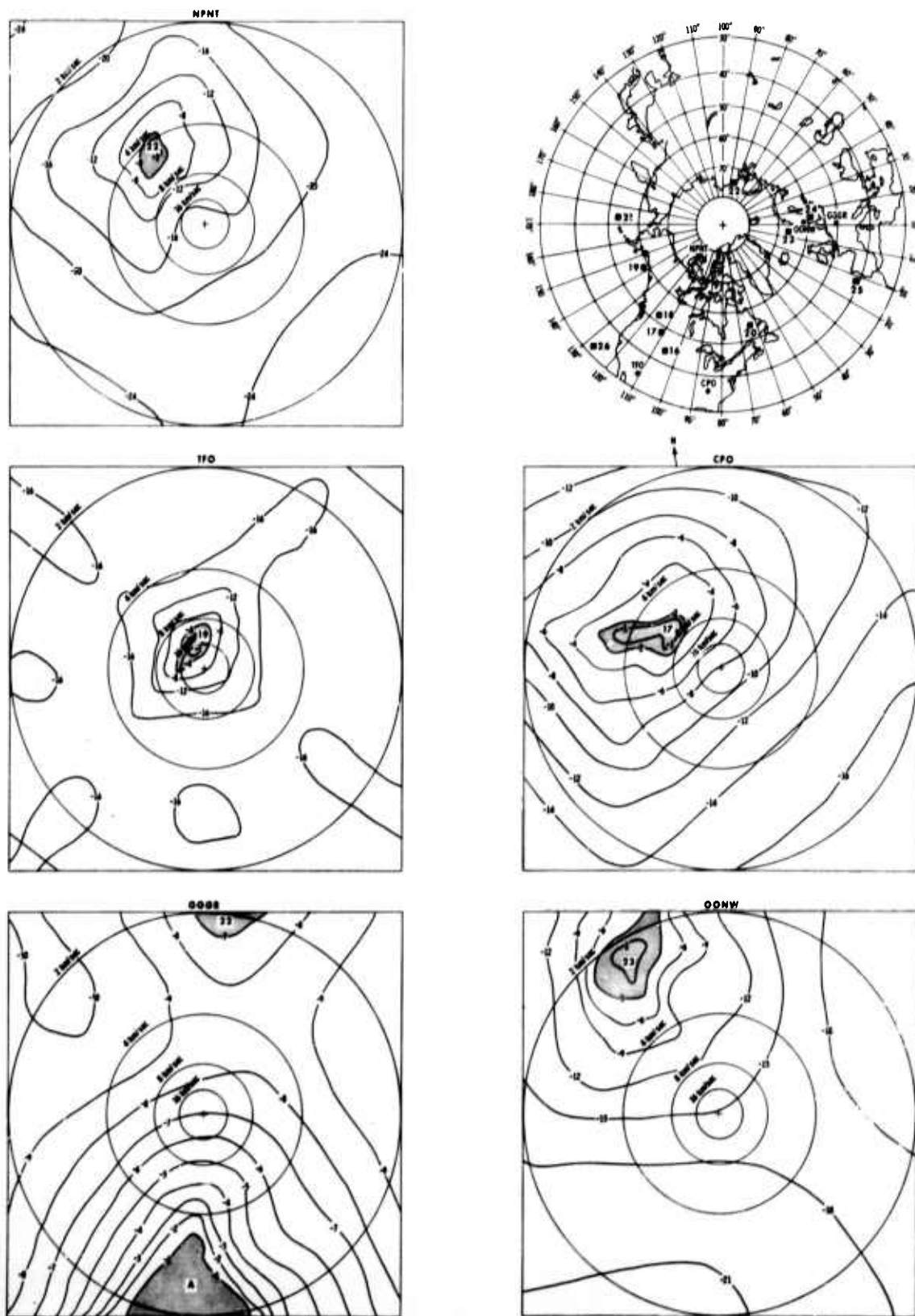


Figure III-13. High-Resolution f - k Spectra



Figure III-13, 29 January 1965, $F = 0.4$ Hz

The narrowband character of the coherent energy is well-illustrated by this 0.4-Hz sample. All stations report coherent energy sources different from those observed at 0.2 Hz. One possible explanation is frequency-dependent earth filtering, since the stronger sources such as LPC's 20 and 22 are at considerable ranges.

At CPO, energy is seen from the northwest (lobe 17), apparently generated by the frontal passage and by LPC's 16, 17, and 18 located over the Plains states. Two peaks are suggested, indicating both surface-mode and intermediate-velocity energy. TFO, however, shows bodywave energy from the north (lobe 19), apparently related to LPC 19. The peak at NPNT (lobe 22) has rather high velocity for surface-mode propagation but is probably due, at least indirectly, to LPC 22.

OONW shows surface-mode energy from the northwest (lobe 23), primarily from LPC 23 in the Norwegian Sea. GGGR exhibits the strong, narrowband, apparently stationary peak from the south (also reported on 16 October 1964). A weaker peak from the north is indicated (lobe 22), probably related to either LPC 22 or 24.

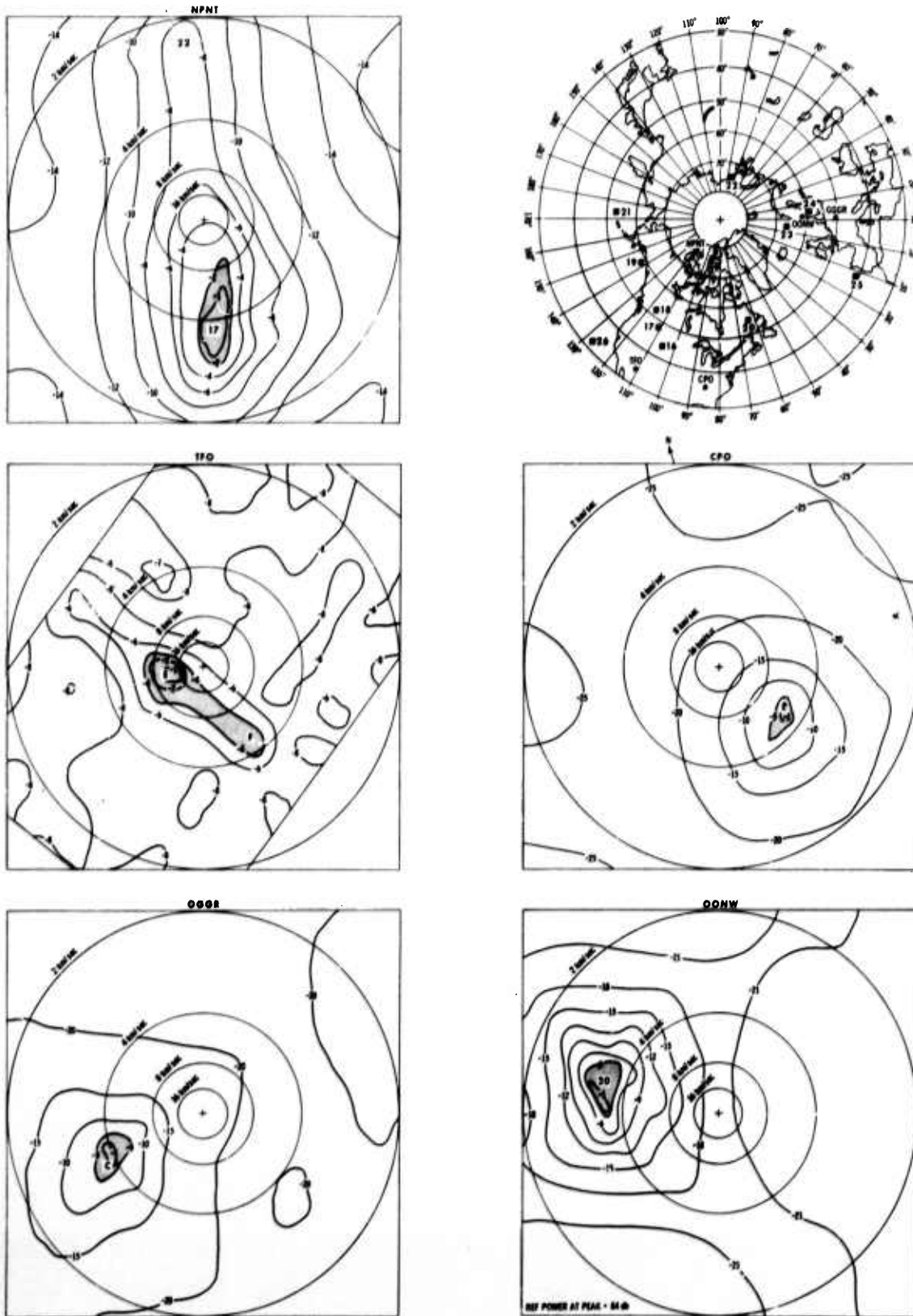


Figure III-14. High-Resolution f - k Spectra



Figure III-14, 29 January 1965, $F = 0.6$ Hz

Again, at 0.6 Hz (and also at 0.8 Hz), regional storm activity ceases to be a dominant contributor, as seemingly stationary peaks emerge at several stations.

A bodywave peak from the southwest (lobe E) at TFO corresponds to the general direction for energy from LPC 26, but the indicated velocity (15 km/sec) suggests a more distant source. Bodywave energy also is seen at this frequency from the southwest on 16 October 1964. This peak apparently is not related to meteorological sources. Also indicated in both samples is a weaker peak from the southeast (lobe F). A surface-mode peak from the southwest at CPO (lobe B) appears stationary.

NPNT shows a strong surface-mode source in the south (lobe 17), generally corresponding to the line of LPC's over the Great Plains. A weaker surface-mode peak from the north (lobe 22) persists from 0.4 Hz and is probably related to LPC 22.

A surface-mode peak from the southwest (lobe C) also is seen on 16 October 1964 at GGGR and is apparently from a stationary source. Surface-mode energy at OONW from the west (lobe 20) may be created either by the intense LPC 20 over Newfoundland or by the nearer LPC 23 off the Norwegian coast.

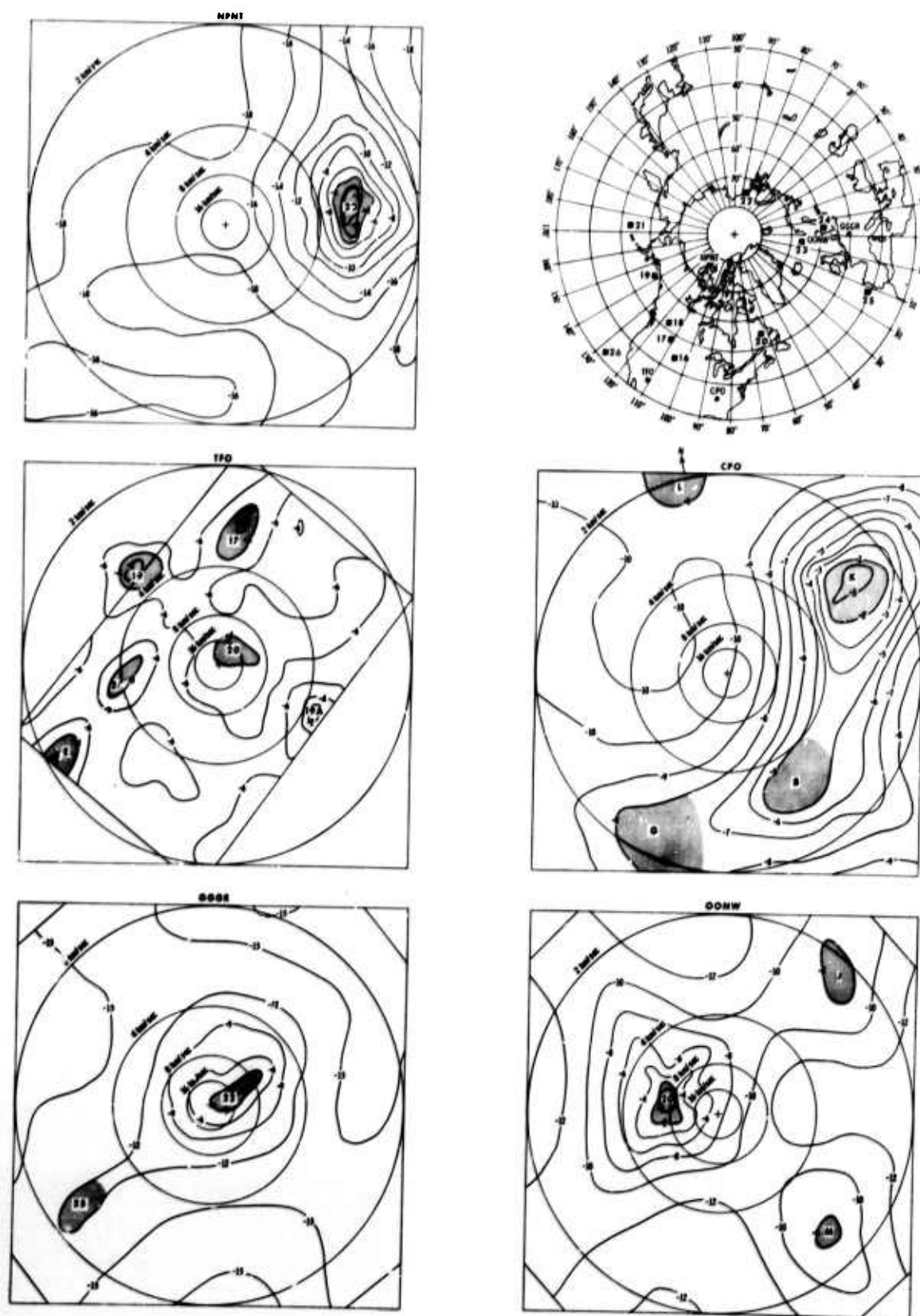


Figure III-15. High-Resolution f - k Spectra



Figure III-15, 29 January 1965, $F = 0.8$ Hz

A relative null in coherent energy level is again generally evident at 0.8 Hz. Bodywave energy appears at TFO, GGGR, and OONW; surface-mode energy is seen at all stations.

The bodywave peak from the northwest (lobe 20) at OONW probably is generated by LPC 20, located over Newfoundland. Smaller peaks from the northeast (lobe J) and southeast (lobe M) occur also on 16 October 1964 and are apparently stationary. Bodywave energy is seen also at GGGR from the northeast (lobe 22), corresponding to LPC 22. A surface-mode peak from the southwest (lobe 25) is seen, representing energy from LPC 25 or the stationary source C.

The CPO spectrum is a virtual repeat of the one shown at this frequency for 16 October 1964, with seemingly stationary peaks from the northeast (lobe K), southeast (lobe B), southwest (lobe G), and north (lobe L). All are probably locally generated or related to coastal surf action. Surface-mode energy is seen from the east at NPNT (lobe 20), related to LPC 20.

A weak bodywave peak is seen at TFO (lobe 20), apparently from LPC 20. Lobe E is generated by the apparently stationary surface-wave source southwest of TFO. Surface-mode peaks from the north (lobe 17) and west (lobe 26) are apparently related to LPC's 17 and 26, respectively. Surface-mode energy also appears from the northwest, apparently generated along the Pacific coast and related to LPC 19. Due to seismometer spacings within the TFO crossarray, the unit cell does not extend to this point in the wavenumber plane at this frequency; therefore, the peak has space-aliased to a point within the unit cell (lobe 19A), creating a pseudo-source from the southwest.

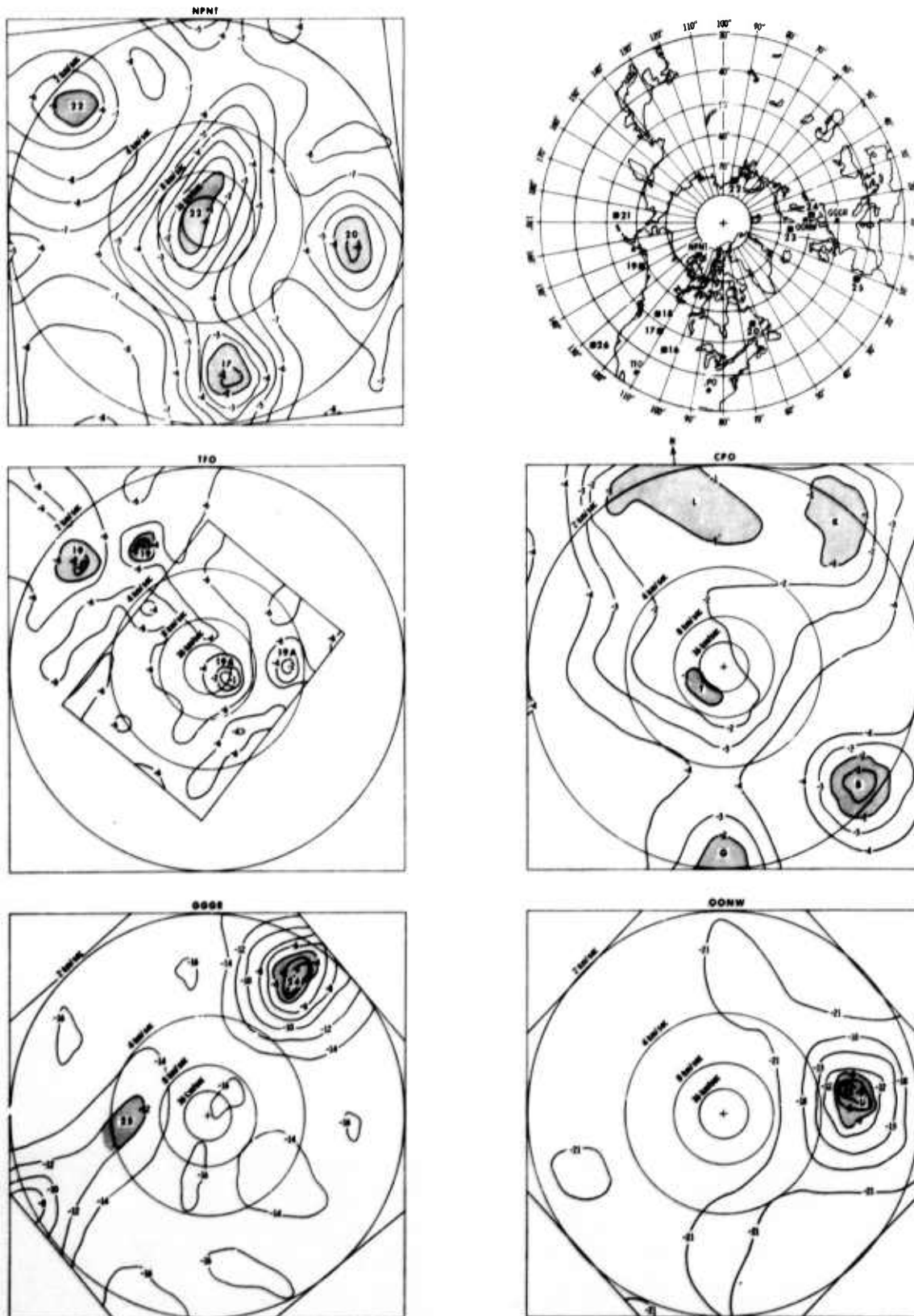


Figure III-16. High-Resolution $f-k$ Spectra



Figure III-16, 29 January 1965, $F = 1.0$ Hz

Unlike the 16 October 1964 sample, regional storm activity does not dominate spectra at 1.0 Hz for this sample. Generally, lower coherent energy levels expose minor structural peaks, and interpretation is correspondingly more complex.

For example, the CPO spectrum resembles that seen at 0.8 Hz, with the appearance of several apparently stationary surface-mode peaks. An additional bodywave peak from the southwest, with unknown source, is seen (lobe T). Two relatively high-velocity peaks at TFO (lobe 19A) are apparently space-aliased into the unit cell from the north and correspond to coastally generated surface-mode energy. Such interpretation is tenuous and is done on the basis of plausible energy sources and propagation velocities.

A broad smear of bodywave energy at NPNT, accompanied by a surface-mode peak (lobe 22), is probably related to Arctic Ocean disturbances created by LPC 22. Low-velocity peaks from the east (lobe 20) and south (lobe 17) correspond to LPC's 20 and 17, respectively.

A surface-mode peak (lobe 24) is seen at GGGR from either LPC 24 or the distant but more intense LPC 22. A much weaker peak from the southeast (lobe 25) is possibly generated by surfaction from LPC 25. The indicated peak at 240° (2.0 km/sec) is apparently energy-aliased into the unit cell from lobe 24. Surface-mode energy is also seen at OONW (lobe U) and is possibly caused by LPC 24.

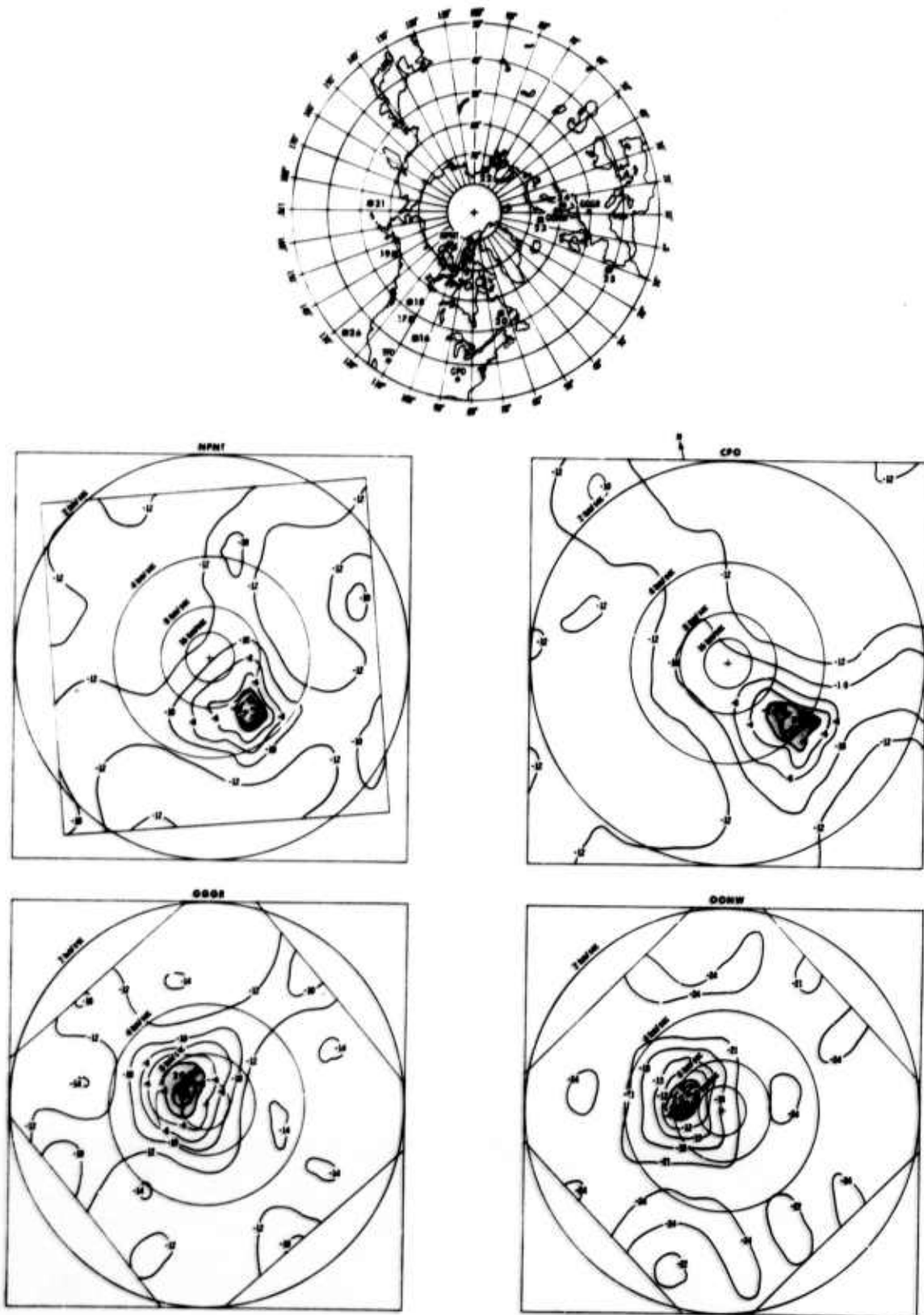


Figure III-17. High-Resolution $f-k$ Spectra



Figure III-17, 29 January 1965, $F = 1.2$ Hz

Bodywave peaks appear at both OONW and GGGR (lobe 20), apparently generated by the intense LPC 20 over Newfoundland.

Surprisingly, the stations located on the same continent as the storm center fail to detect it. Instead, surface-mode energy from the southwest at NPNT (lobe P) appears to be locally generated.

Similarly, an apparently stationary peak (lobe B) southwest of CPO appears as the only coherent structure.

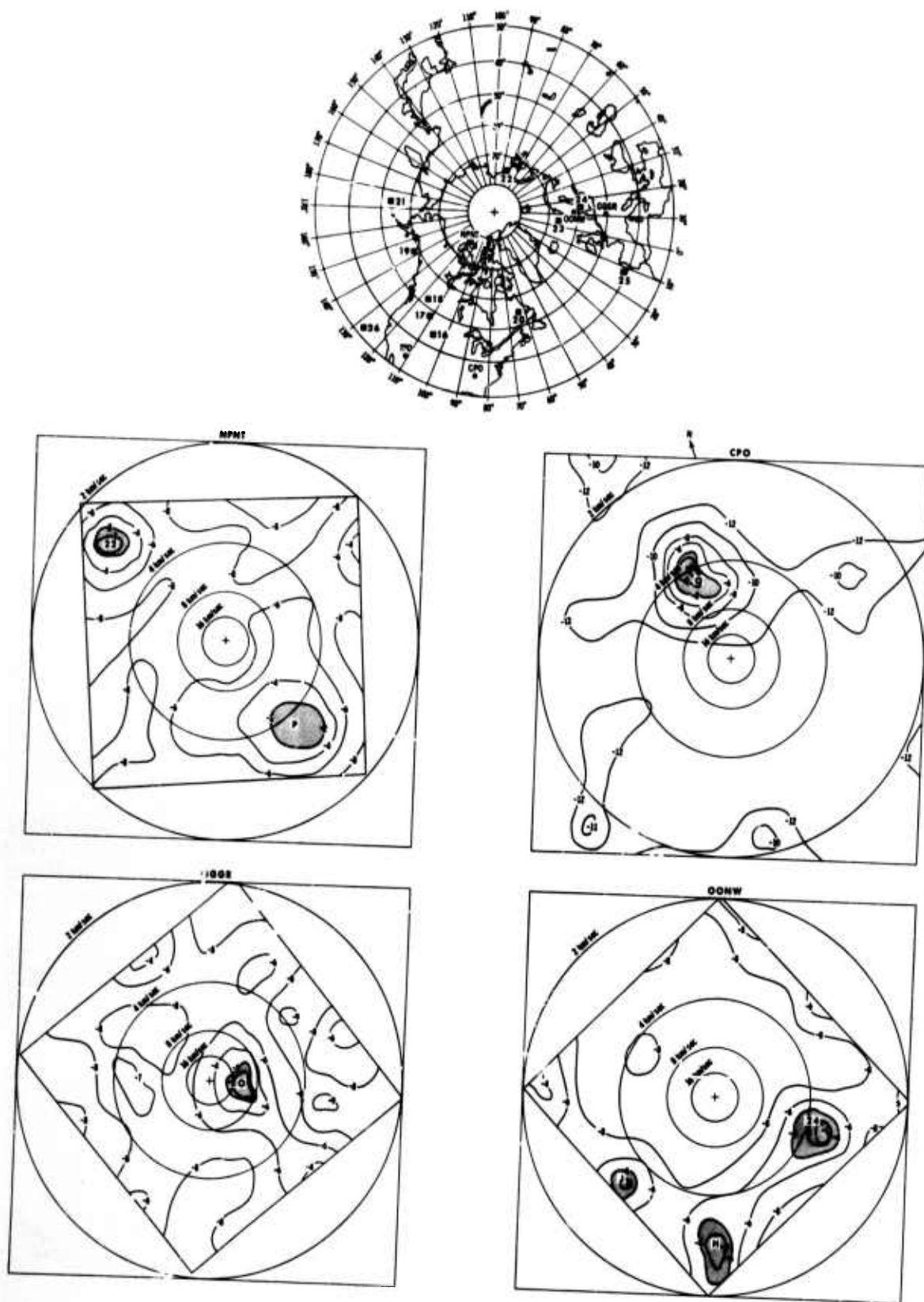


Figure III-18. High-Resolution f - k Spectra

Figure III-18, 29 January 1965, $F = 1.4$ Hz

The apparently stationary narrowband peak (lobe Q) is again evident at CPO for 1.4 Hz.

Two surface-mode peaks appear at NPNT: lobe 22 from the southwest (probably related to storm activity in the Arctic Ocean) and lobe P from the southeast (corresponding to an apparently stationary local source which is possibly surf action).

A surface-mode peak at OONW (lobe 24) is apparently related to LPC 24. Lesser peaks from the south (lobe H) and southwest (lobe J) are probably locally generated, although lobe J is possibly aliased into the unit cell from the northeast.

The source of bodywave energy at GGGR from the east (lobe O) is undetermined. A similar peak is noted at GGGR for 1.2 Hz in the 16 October sample.

Difficulty is experienced in determining the actual direction of the lesser surface-mode peak apparently located on the northwest edge of the unit cell.

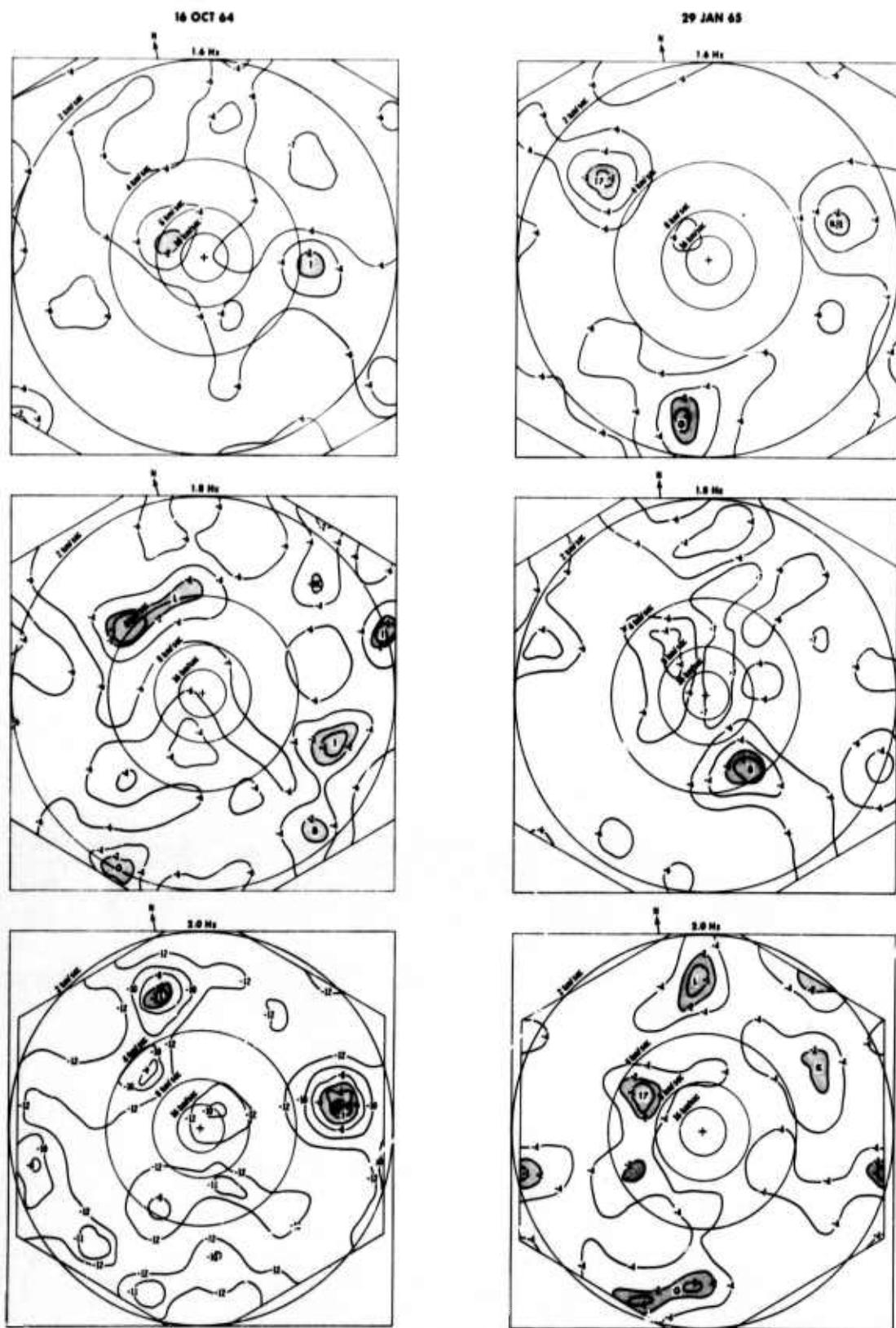


Figure III-19. High-Resolution f - k Spectra

Figure III-19, 16 October 1964 and 29 January 1965, $F = 1.6, 1.8, 2.0$ Hz

Spectra shown in this figure are from CPO for both noise samples and for the frequencies 1.6, 1.8, and 2.0 Hz. Because of space-aliasing effects, CPO is the only network station yielding interpretable $f\text{-}\vec{k}$ spectra at these frequencies.

Several low-level surface-mode peaks appear at each frequency, generally representing a variety of local sources that closely resemble an isotropic field.

The only apparently storm-related peaks are lobe 1 (16 October 1964) and lobe 17 (29 January 1965).

The source of the bodywave peak at 1.6 Hz on 16 October 1964 is not established.

BLANK PAGE



SECTION IV


BODYWAVE NOISE STUDIES

Several approaches to the problem of partitioning the noise have been examined during this study. One approach, which uses high-resolution f - \vec{k} spectra to examine the spatial distribution of the noise, is discussed in Section III. Results of two other approaches — a synthesis method involving solution of simultaneous equations and the computation of 1-dimensional wavenumber spectra (K-line) — are discussed in this section.

The first technique provides an estimate of the relative percentages of high- and low-velocity energy for a given noise sample. This estimate is obtained through an analysis of spectra computed for the average and straight-sum outputs, along with the array straight-sum response. Certain assumptions are made regarding noise isotropy and random-noise content. A set of simultaneous equations is then solved for the relative amounts of high- and low-velocity noise as a function of frequency.

Although the results of such a technique depend heavily on the quality of the assumptions regarding the noise field at a particular station, the assumptions represent educated guesses from available knowledge for that station. Undoubtedly, refinements to the rather elementary approach would yield more exact results; however, general conclusions regarding the extent to which a particular station is bodywave-noise-limited are quite readily made.

CPO and TFO are the two stations investigated in this manner. Results indicate that CPO is primarily dominated by surface-mode energy while TFO is bodywave-noise-limited except at the very low frequencies (below 0.3 Hz). These rather expected results serve primarily to verify the procedure itself; however, the good agreement with previous work is a qualitative check on the assumptions made for each station.



The second technique involves analysis of K-line spectra computed for the crossarray arms at the LRSM stations. The CPO and TFO geometries are unsuitable for K-line analysis. Resolution is somewhat limited at the LRSM stations since each arm contains only four seismometers. However, analysis of the spectra indicates predominantly surface-mode propagation generally correlated with regional storm sources. None of the three LRSM arrays (OONW, NPNT, and GGGR) appear to be bodywave-noise-limited, although high-velocity energy is a greater proportion of the total at NPNT than at the other two stations.

Other approaches to noise partitioning, such as maximum-likelihood adaptive filters and Wiener disk-model MCF's, have been found unsuitable for various reasons. The adaptive approach tends to cause rejection of both bodywave and surface-mode energy. At their present state of development, adaptive disk-model techniques are not economically feasible for this application. LRSM array geometries generally have been inadequate for effective Wiener disk-model design.

An obvious requirement for meaningful future analysis of network bodywave noise is the availability of high-quality seismic-array data. Since the low-velocity energy does not appear coherent at the network level, further work should concentrate on studying the high-velocity component. Station array geometries should be adequate to provide significant reduction in the low-velocity component with station preprocessing. As developmental work continues, adaptive-filtering procedures will conceivably become suitable for bodywave noise extraction at the station level.

A. MULTICHANNEL-FILTER AND STRAIGHT-SUM TECHNIQUES

In the investigation of the relative quantities of high- and low-velocity noise power contained in the CPO and TFO noise fields, the conventional array processing techniques of multichannel filtering and straight

summing have been utilized in a simplified method for partitioning a noise field into high- and low-velocity energy components.

Used in the analysis are noise samples recorded at CPO on 16 October 1964 and 29 January 1965 and at TFO on 29 January 1965. Each noise sample is analyzed, using a 6.67-min time gate. Results of the straight-sum technique are presented for each noise sample; however, results of multi-channel filtering are presented only for CPO on 16 October 1964.

A 0.18-sec disk signal-model MCF has been designed from whitened correlations of CPO measured-noise statistics. The disk signal model has been constrained to have an idealized gain of unity for energy propagating at apparent horizontal velocities of 10 km/sec or greater and of zero for lower-velocity energy. The signal model has been further constrained to have the shape of the 16 October 1964 noise spectrum with an SNR of 4.

Power-density spectral estimates computed from ± 5.0 -sec Parzen-smoothed correlations are presented for each technique in Figure IV-1. Also shown for each noise sample are average power-density spectra formed from all array inputs. The spectral estimates are shown in db relative to $1 \text{ m}\mu^2$ at 1.0 Hz.

In partitioning the noise field, the existence of only three energy components is assumed: low velocity, P_L ; high velocity, P_H ; and random, P_R . P represents power. Low-velocity energy is considered to be concentrated in a 2-km/sec to 6-km/sec apparent horizontal-velocity band and high-velocity energy in a 8-km/sec, or greater, band. Random energy is estimated to be the total energy at 4.0 Hz and is considered to be white across the Nyquist band.

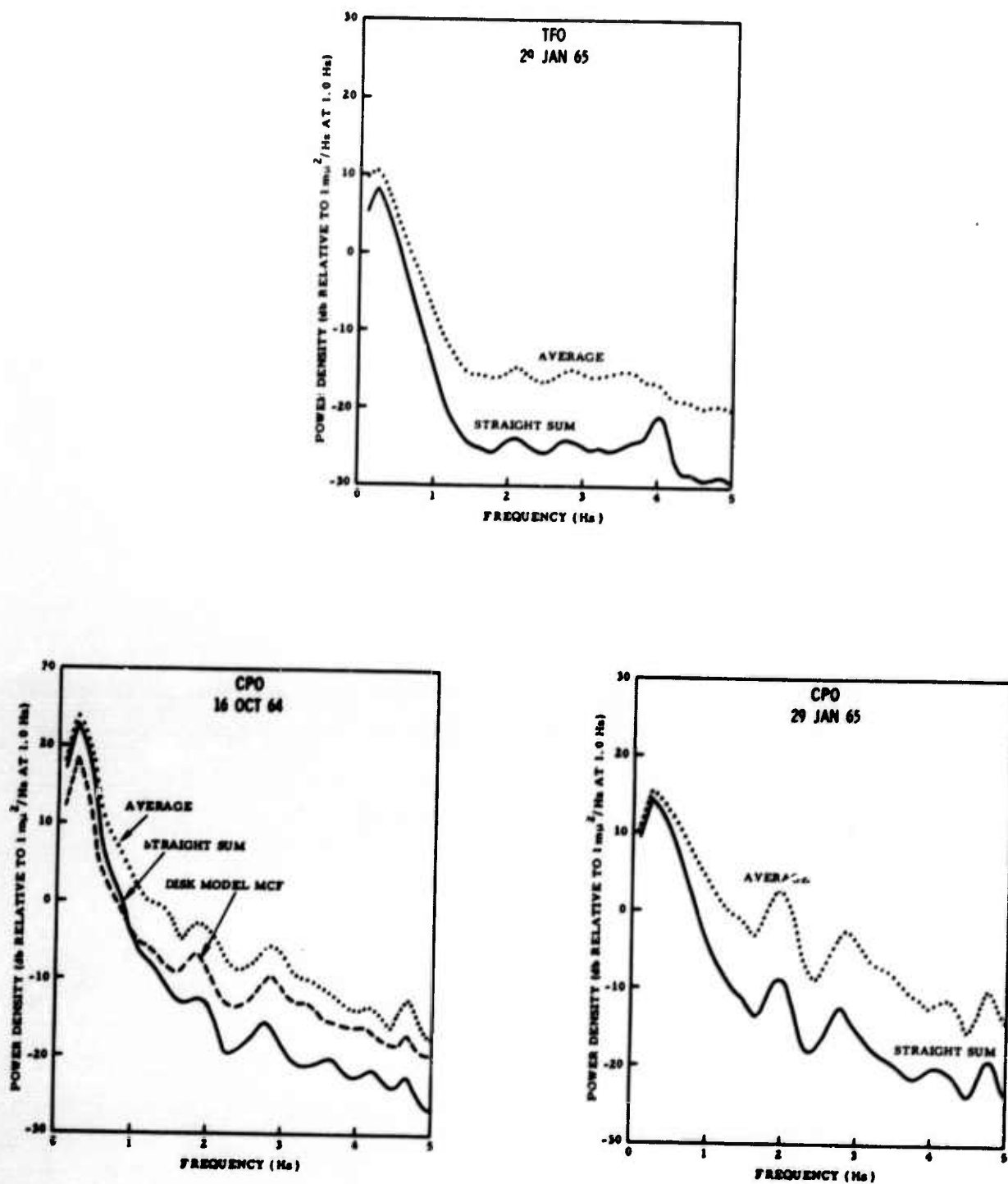


Figure IV-1. Average and Straight-Sum Noise Power-Density Spectral Estimates at CPO and TFO



For the straight sum, average responses of K_L and K_H are computed for the low- and high-velocity regions, respectively, where K represents that portion of each component seen by the straight-sum response. The energy in each region is considered to be uniformly isotropic. The random-noise response is considered to be $1/N$ where N is the number of input sensors.

The average input power spectrum may be expressed as a function of frequency by

$$P_L(f) + P_H(f) + P_R = P_{AVG}(f) \quad (4-1)$$

The straight-sum spectrum may be expressed as

$$K_L(f) P_L(f) + K_H(f) P_H(f) + \frac{1}{N} P_R = P_{SS}(f) \quad (4-2)$$

Solution of simultaneous Equations 4-1 and 4-2 for the relative percentage of low- and high-velocity energy in the average input spectrum yields

$$P'_L(f) = \left[\frac{P_{SS}(f)}{P_{AVG}(f)} - K_H(f) + \frac{P_R}{P_{AVG}(f)} \left(K_H(f) - \frac{1}{N} \right) \right] / [K_L(f) - K_H(f)] \quad (4-3)$$

and

$$P'_H(f) = \left[\frac{P_{SS}(f)}{P_{AVG}(f)} - K_L(f) + \frac{P_R}{P_{AVG}(f)} \left(K_L(f) - \frac{1}{N} \right) \right] / [K_H(f) - K_L(f)] \quad (4-4)$$

Average MCF responses of K'_L and K'_H are computed for the low- and high-velocity regions, respectively. Also computed is the average



random-noise response K_R' of the MCF. The MCF power-density spectrum can then be expressed as

$$K_L'(f) P_L(f) + K_H'(f) P_H(f) + K_R'(f) R = P_{MCF}(f) \quad (4-5)$$

Solution of simultaneous Equations 4-1 and 4-4 for the relative percentage of low- and high-velocity energy in the average input spectrum yields

(4-6)

$$P_L''(f) = \left[\frac{P_{MCF}(f)}{P_{AVG}(f)} - K_H'(f) + \frac{P_R}{P_{AVG}(f)} (K_H'(f) - K_R'(f)) \right] / \left[K_L'(f) - K_H'(f) \right]$$

and

(4-7)

$$P_H''(f) = \left[\frac{P_{MCF}(f)}{P_{AVG}(f)} - K_L'(f) + \frac{P_R}{P_{AVG}(f)} (K_L'(f) - K_R'(f)) \right] / \left[K_H'(f) - K_L'(f) \right]$$

Figure IV-2 shows the results of applying each of the two techniques to the appropriate noise samples. The illustration also presents a composite straight-sum result for CPO on 16 October 1964 and 29 January 1965. Results are evaluated only to 1.5 Hz.

Results obtained for CPO on 16 October 1964 for the straight-sum and MCF techniques agree reasonably well; both indicate an average low-velocity component of 85 percent and a high-velocity component of 15 percent. Previous studies have indicated that the CPO noise field is 90 percent predictable in this frequency range.⁷ The noise field can then be interpreted as consisting of 76-percent coherent low-velocity energy and 14-percent coherent high-velocity energy. The remaining energy, then, is due to seismic noise of random nature.

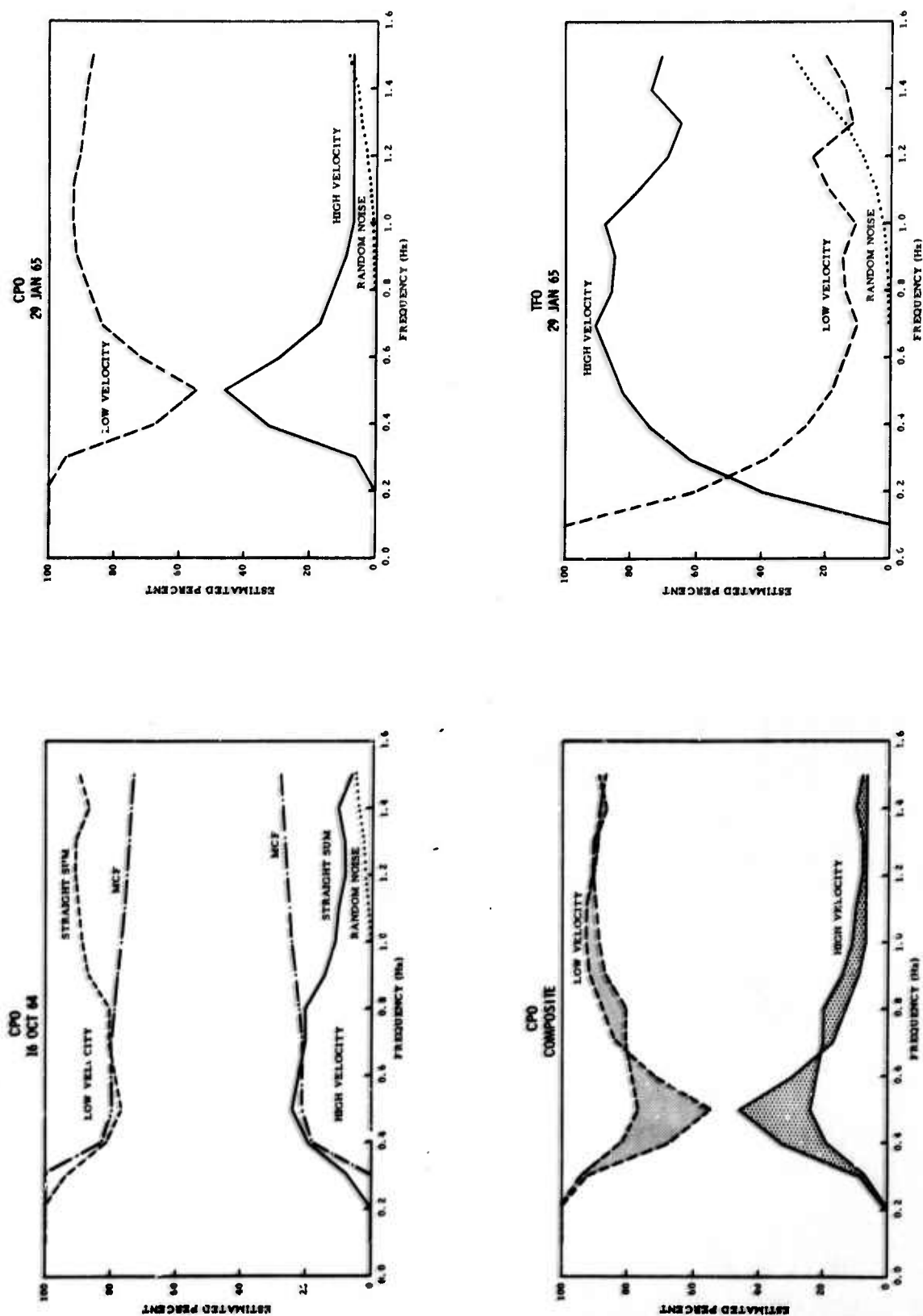


Figure IV-2. Percentage of High- and Low-Velocity Noise Components at CPO and TFO



Results using the straight-sum technique for CPO data recorded on 29 January 1965 indicate a significant minimum in the low-velocity percentage at 0.5 Hz. The composite result indicates good agreement between samples, except in the 0.3- to 0.7-Hz frequency band. The increase in low-velocity energy during 16 October 1964 is believed to be due to intense storm activity east of the station on 16 October (tropical storm Isabel) but could be due to smearing of the 0.25-Hz microseismic peak through smoothing. If such is the case for the differences observed between 0.3 and 0.7 Hz, the overall ratio of high-velocity to low-velocity energy appears relatively constant above 0.3 Hz — even in the presence of increased microseismic activity.

Results using the straight-sum technique for TFO data recorded on 29 January 1965 indicate that the noise field is dominated by high-velocity energy above 0.3 Hz and by low-velocity energy below. This agrees with previous studies of the TFO noise field evaluated by more sophisticated methods.⁸

The 2-dimensional high-resolution frequency-wavenumber ($f-\vec{k}$) spectra (Section III) indicate no high-velocity energy at CPO during the 16 October 1964 or 29 January 1965 samples and indicate both high- and low-velocity energy at TFO. Inherent in the computation of these $f-\vec{k}$ spectra is the assumption of planar-wave propagation. Possibly severe deviations of the high-velocity energy from planar-wave propagation may exist due to scattering and to variations in trapped-mode layer thicknesses, and there is the probability that high-velocity energy will be observed only when it constitutes an appreciable portion of the total energy.



B. ANALYSIS OF K-LINE WAVENUMBER SPECTRA FROM LRSM DATA

The following discusses an analysis of 1-dimensional (K-line) wavenumber spectra obtained from 6.67-min ambient noise samples recorded at LRSM crossarrays OONW, GGGR, and NPNT on 16 October 1964 and 29 January 1965. Analysis objectives include a study of noise-power spatial distribution, comparison with high-resolution 2-dimensional wavenumber spectra computed for the same samples (presented in Section III), and determination of the relative quantities of high- and low-velocity noise power as a function of frequency at each station.

The K-line spectra are physically interpreted as projections of 2-dimensional wavenumber spectra on perpendicular axes which are parallel to the two crossarray arms. Thus, the wavenumber spectra give the power density of the ambient seismic noise as a function of its apparent wavenumber along each of the two arms. The basic input data for calculating these wavenumber spectra are the crosspower matrix values $\left[\Phi_{ij}(f) \right]$ where f is frequency and i and j range over the four seismometers in each array arm.

1. Description of K-Line Spectra

To facilitate presentation, K-line spectra for the two noise samples are shown (for each station) at 0.1-Hz increments from 0.2 to 1.0 Hz, excluding 0.3 Hz which, in all cases, is very similar to the 0.2-Hz plot.

For each frequency, a wavenumber power-density spectrum, superimposed with an integrated wavenumber power-density function, is presented for each arm. For each wavenumber spectrum, the 0-db level indicates the spectrum's average value. The solid vertical line at $K = 0$ represents infinite apparent velocity; i. e., the wave propagation is perpendicular to the direction in which the wavenumber spectrum is measured. Dashed lines on either side of this line show apparent velocities of 8, 3, and 2 km/sec.



The 2-km/sec line falls at the extreme edge of the 1.0-Hz plots. Wavenumber aliasing occurs at 0.5 cycles/km for 1-km spacing between seismometers. (See the appendix for array configurations.) The right halves of the wavenumber spectra show the energy propagating generally from north to south, while the left halves represent energy moving from south to north.

The normalized integrated wavenumber power-density function is

$$\int_{-K}^K P(k) dk, \text{ with } \int_{-K}^K P(k) dk = 1$$

This function is shown plotted in fractional power vs wavenumber in cycles/km. These integrated spectral plots are particularly useful in that they facilitate measurement of the amount of power within any given apparent wavenumber (or velocity) band.

2. Presentation and Analysis of K-Line Wavenumber Spectra

The wavenumber spectra are shown grouped by station. Facing each noise-sample plot is the related discussion.

Some features are common to all plots, however. One such feature is the pronounced drop in power density outside the dashed lines, especially at frequencies below 0.8 Hz. This indicates the seismic validity of the recorded data, since energy traveling at velocities lower than that of the fundamental Rayleigh wave (which is the slowest mode of seismic propagation) is not seismically interpretable. Above 0.8 Hz, an appreciable portion of the power density is apparently either random or nonseismic; this is not particularly surprising, since the dynamic range of the FM-recorded data is virtually exhausted at the lower power densities observed for these frequencies.



The velocity of the Rayleigh-wave energy appears to vary with station and ranges from about 3.1 km/sec at OONW to about 2.7 km/sec and 2.4 km/sec at NPNT and GGGR, respectively. Some dependence of propagation velocity with azimuth is noted at OONW, suggesting a local source. Also, there are indications of surface-wave dispersion at OONW and GGGR.

Another striking feature is the dominance of directional Rayleigh-wave energy at all stations, especially at the lower frequencies. Above 0.4 Hz, there is some evidence of mantle P-wave energy at NPNT. The organized noise appears generally correlated with regional storm activity.

General agreement in spatial organization is seen between the K-line and the 2-dimensional spectra (presented in Section III), especially at the peak power frequency. Observed at other frequencies are some differences caused primarily by two effects. The first is a smearing of spectral power across frequencies, which occurs when the K-line autospectra are boxcar-smoothed to stabilize the spectral estimate; the 2-dimensional spectra are unsmoothed, incurring a somewhat higher variance of spectral estimate but retaining an extremely narrowband look at the noise field. The second effect is a general lack of spatial resolution in the K-line plots, which is due primarily to the availability of only four seismometers along each arm. Burg has shown that interpretation using only four seismometers is practical and has described the effect on spectral resolution as a function of the number of sensors along the arm.⁸



OONW
29 JANUARY 1965

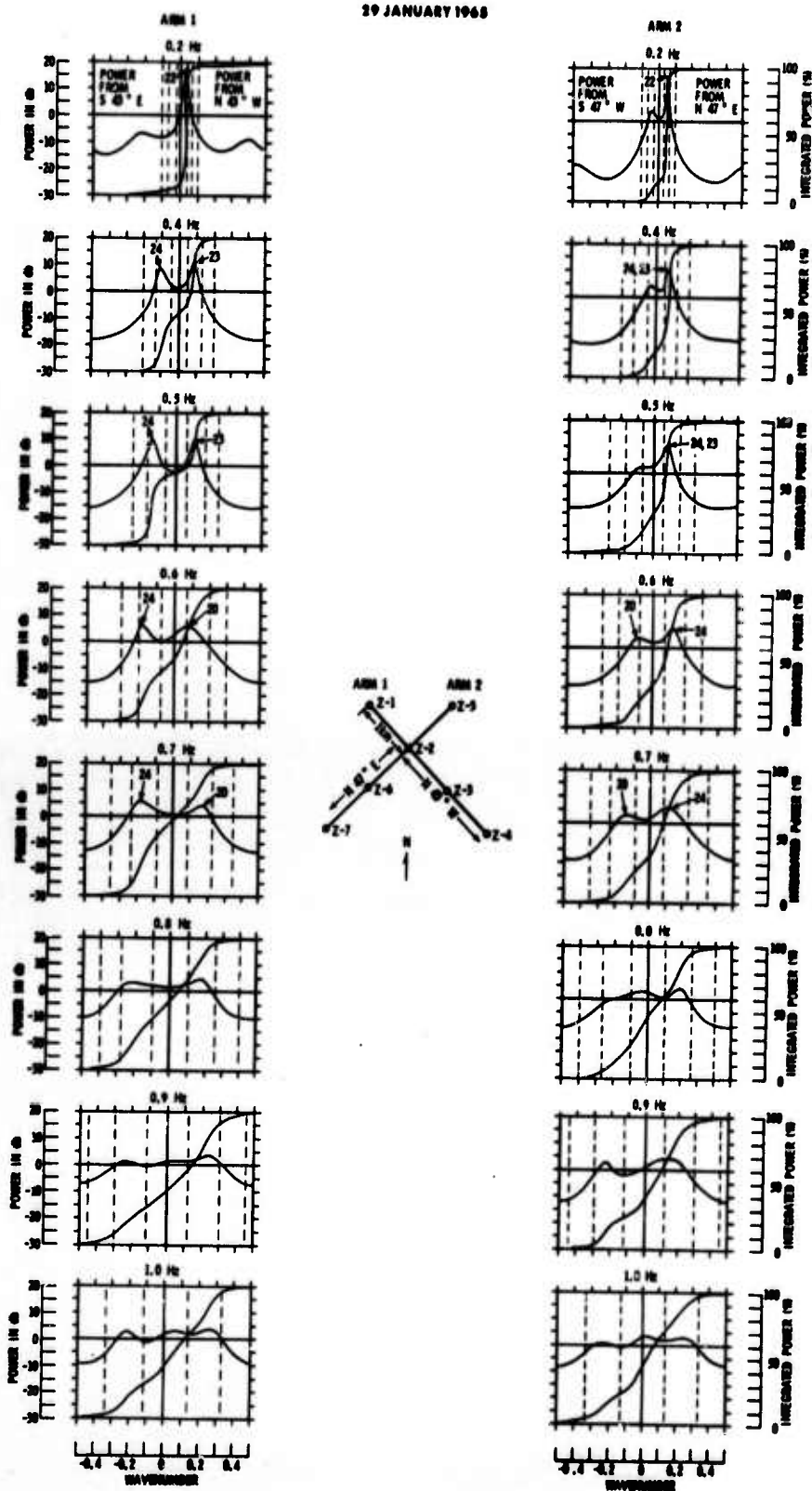


Figure IV-3. Wavenumber and Integrated Spectra from Two Arms at OONW, 29 January 1965



Figure IV-3, OONW, 29 January 1965

Directional surface-mode energy dominates the K-line spectra during this sample.

At the point of peak power, represented by 0.2 Hz (and 0.3 Hz which is not shown), there is excellent agreement with the 2-dimensional spectra. Both show Rayleigh-wave energy (3.3 to 3.5 km/sec), apparently generated by LPC 22 over the Kara Sea northeast of OONW. At 0.4 and 0.5 Hz, a shift in source direction is noted, as the K-line spectra indicate low-velocity (3.1-km/sec) energy from the southeast, probably caused by LPC 24 over the Baltic Sea. Energy at about 5 km/sec from the northwest also appears and may be related to LPC 23 over the Norwegian Sea and to surf action along the northwestern coast of Norway. This latter source is verified by the 2-dimensional spectra at 0.4 Hz, although the observed velocity is much lower (2.0 km/sec).

LPC 24 still appears as a contributor at 0.6 and 0.7 Hz, with an added indication of energy from the west, traveling at about 5 and 3 km/sec, respectively, at these frequencies. Surface-mode energy from this direction (at 3 km/sec) is detected with the 2-dimensional spectra at 0.6 Hz, with a bodywave peak (8 km/sec) at 0.8 Hz from the same azimuth. On the strength of the bodywave peak, LPC 20 (over Labrador) is the likely contributor of this energy. At 0.8, 0.9, and 1.0 Hz, the K-line spectra appear virtually isotropic, and directional source determination is not attempted.

There is indication of possible surface-wave dispersion. Results, while not conclusive, indicate reduction in horizontal propagation velocity with increasing frequency, ranging from about 3.4 km/sec at 0.2 and 0.3 Hz to 3.0 or less above 0.5 Hz.



OONW
16 OCTOBER 1964

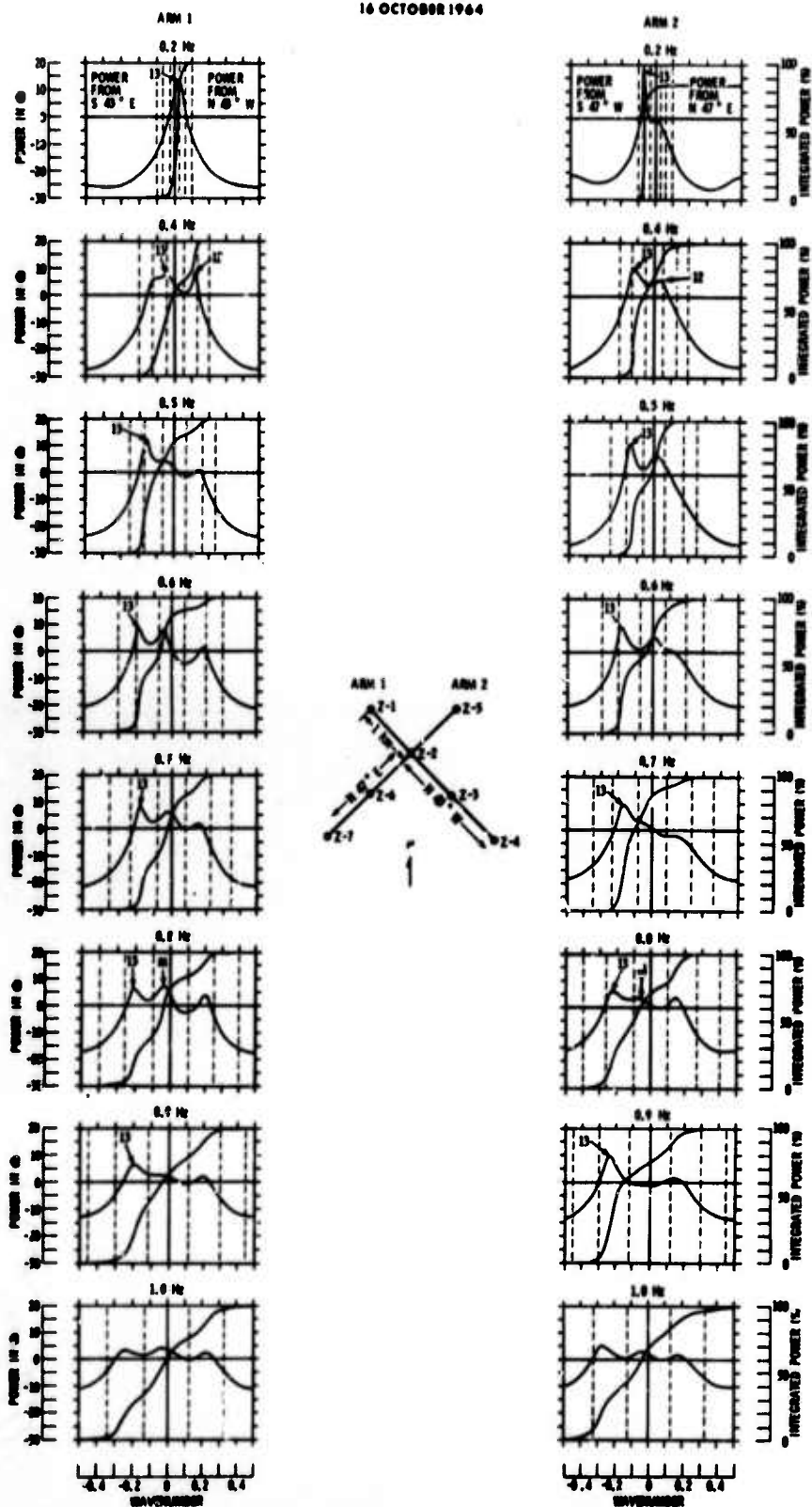


Figure IV-4. Wavenumber and Integrated Spectra from Two Arms at OONW, 16 October 1964



Figure IV-4, OONW, 16 October 1964

Surface-mode energy again appears dominant. Good agreement is seen with the 2-dimensional spectra at 0.2 Hz, with surface-mode energy (3 km/sec) from the southwest and probably related to LPC 13. At 0.4 Hz, the source (still probably related to LPC 13) appears to be located further south, with energy propagating at 3.2 km/sec. The $f-k$ spectra indicate energy from this direction; however, seen in the K-line spectra at 8 km/sec from the northwest is an additional peak possibly caused by LPC 12.

At 0.5, 0.6, and 0.7 Hz, surface-mode energy is seen from due south at 2.4, 2.2, and 2.7 km/sec, respectively, and agrees well with the 2-dimensional spectra at 0.6 Hz. The low velocity suggests a nearby source, such as surf action in the bay south of Oslo, which is likely an indirect result of LPC 13. The energy from LPC 13 appears to persist at 0.8 and 0.9 Hz, with an additional high-velocity source indicated from the southeast (lobe M) which does not appear directly attributable to weather. Both peaks are seen in the 2-dimensional spectra at 0.8 Hz, although lobe M appears as a surface-wave peak. The K-line spectra again appear isotropic at 1.0 Hz.

Slight evidence of dispersion again appears, although it is somewhat obscured by unusually low-velocity energy from the south.



NPNT
29 JANUARY 1965

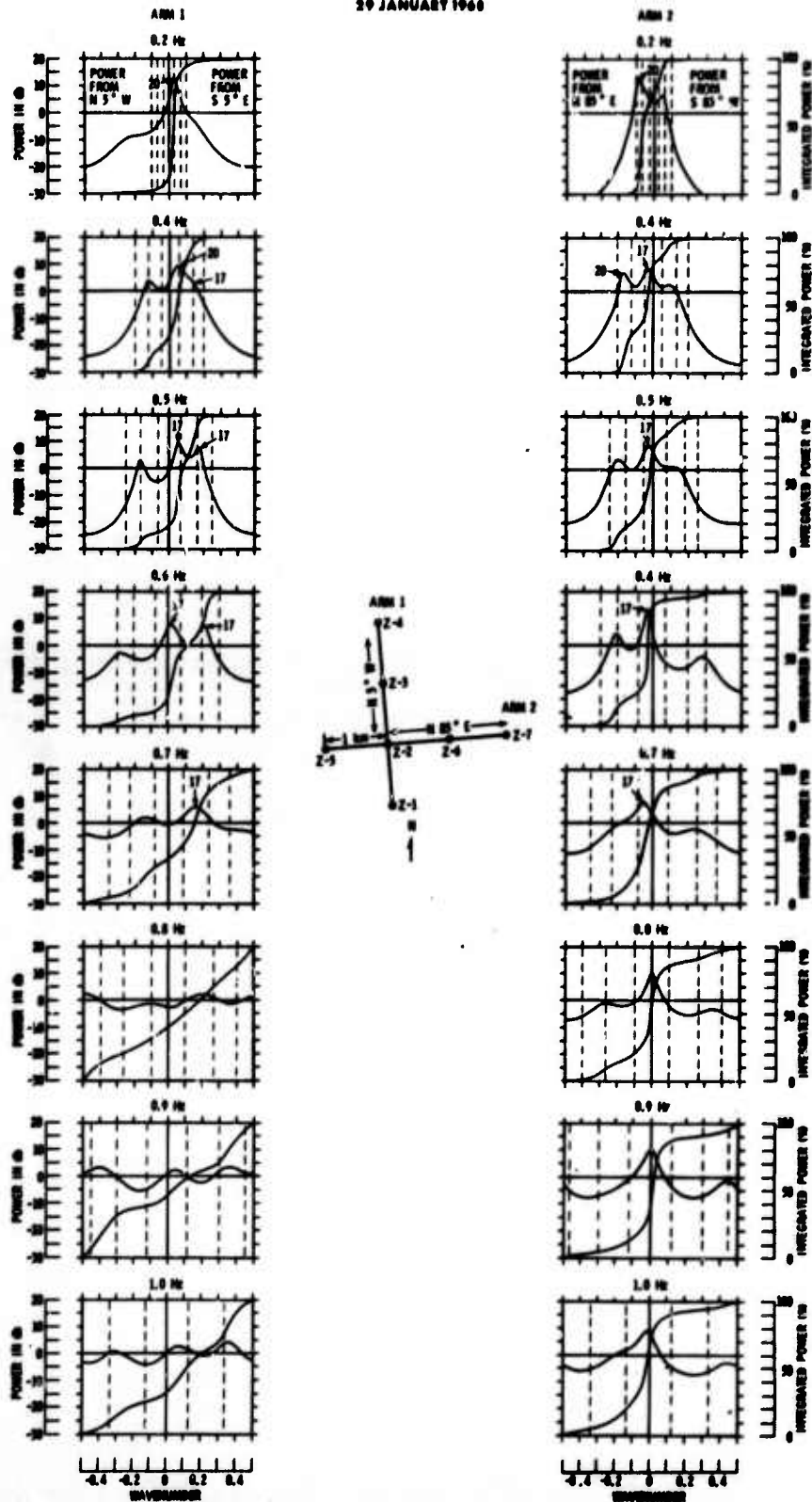


Figure IV-5. Wavenumber and Integrated Spectra from Two Arms at NPNT, 29 January 1965



Figure IV-5, NFNT, 29 January 1965

Excellent agreement between the K-line and 2-dimensional spectra is seen at 0.2 (and 0.3) Hz.

Rayleigh-mode energy from the southwest (at 2.7 km/sec) apparently is related to LPC 20 over Newfoundland. At 0.4 and 0.5 Hz, a new source is indicated; energy from the south-southeast is probably related to the frontal passage over the Great Plains and the associated LPC's 16, 17, and 18.

Both surface-mode (3.1 km/sec at 0.4 and 0.5 Hz) and body-wave (8 km/sec at 0.5 Hz) peaks are observed. The 2-dimensional spectra at 0.4 Hz show only a Rayleigh-mode peak from the northwest, which is possibly related to LPC 22. Additional energy is indicated from LPC 20 in the K-line spectra at 0.4 Hz.

Both spectra indicate surface-mode energy from LPC's 16, 17, and/or 18 at 0.6 Hz. High-velocity energy also is indicated. Surface-mode energy from this source is still apparent at 0.7 Hz in the K-line spectra. From 0.8 to 1.0 Hz, the K-line spectra do not appear seismically interpretable.



NPNT
16 OCTOBER 1964

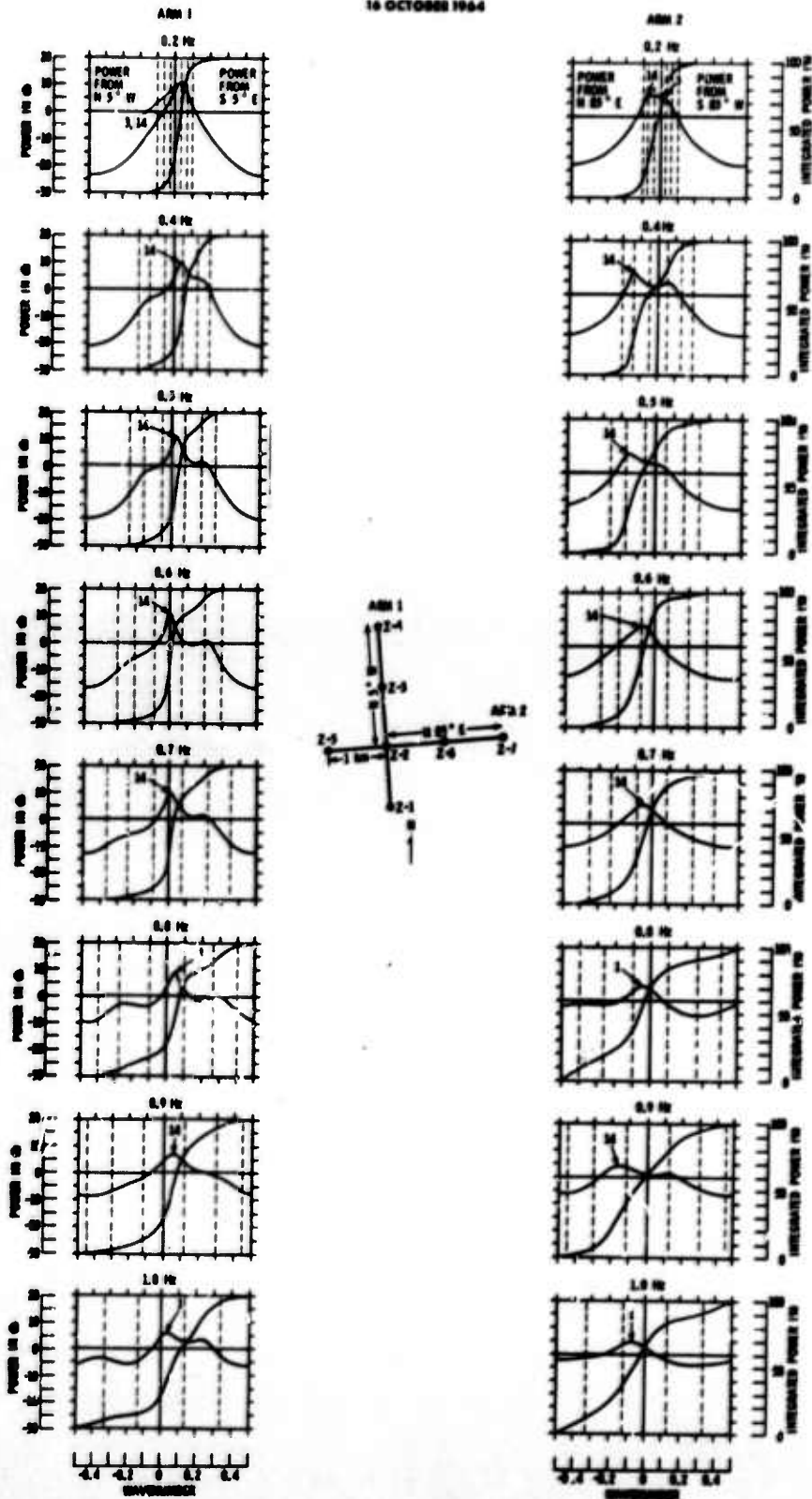


Figure IV-6. Wavenumber and Integrated Spectra from Two Arms of NPNT, 16 October 1964



Figure IV-6, NPNT, 16 October 1964

The K-line spectra for this sample indicate a rather dominant contribution from LPC 14 off Labrador (southeast of NPNT).

At 0.2 Hz, there is indication of surface-mode energy (about 4 km/sec) from the southwest, corresponding roughly to the 2-km/sec peak seen in the 2-dimensional spectra. Surface-mode energy is observed from LPC 14 at 3.3, 3.2, 2.8, and 3.1 km/sec in the K-line spectra for 0.2, 0.3, 0.4, and 0.5 Hz, respectively, and agrees with the 2-dimensional peak seen at 0.4 Hz. However, bodywave peaks are seen at 0.6 and 0.7 Hz in the K-line spectra (also corresponding to LPC 14) with no evidence of the bodywave peak from the west which dominates the 2-dimensional spectra and is apparently related to LPC 5.

From 0.8 to 1.0 Hz, bodywave energy from the southwest, possibly related either to LPC 1 or LPC 14, is indicated in the K-line spectra. The 2-dimensional spectra indicate surface-mode energy from the same directions at 0.8 and 1.0 Hz.

Most notable in this sample are the predominant directionality of the coherent noise and the large amounts of bodywave energy, all apparently storm-generated and traversing the continent across the Canadian Shield.



GGGR
29 JANUARY 1965

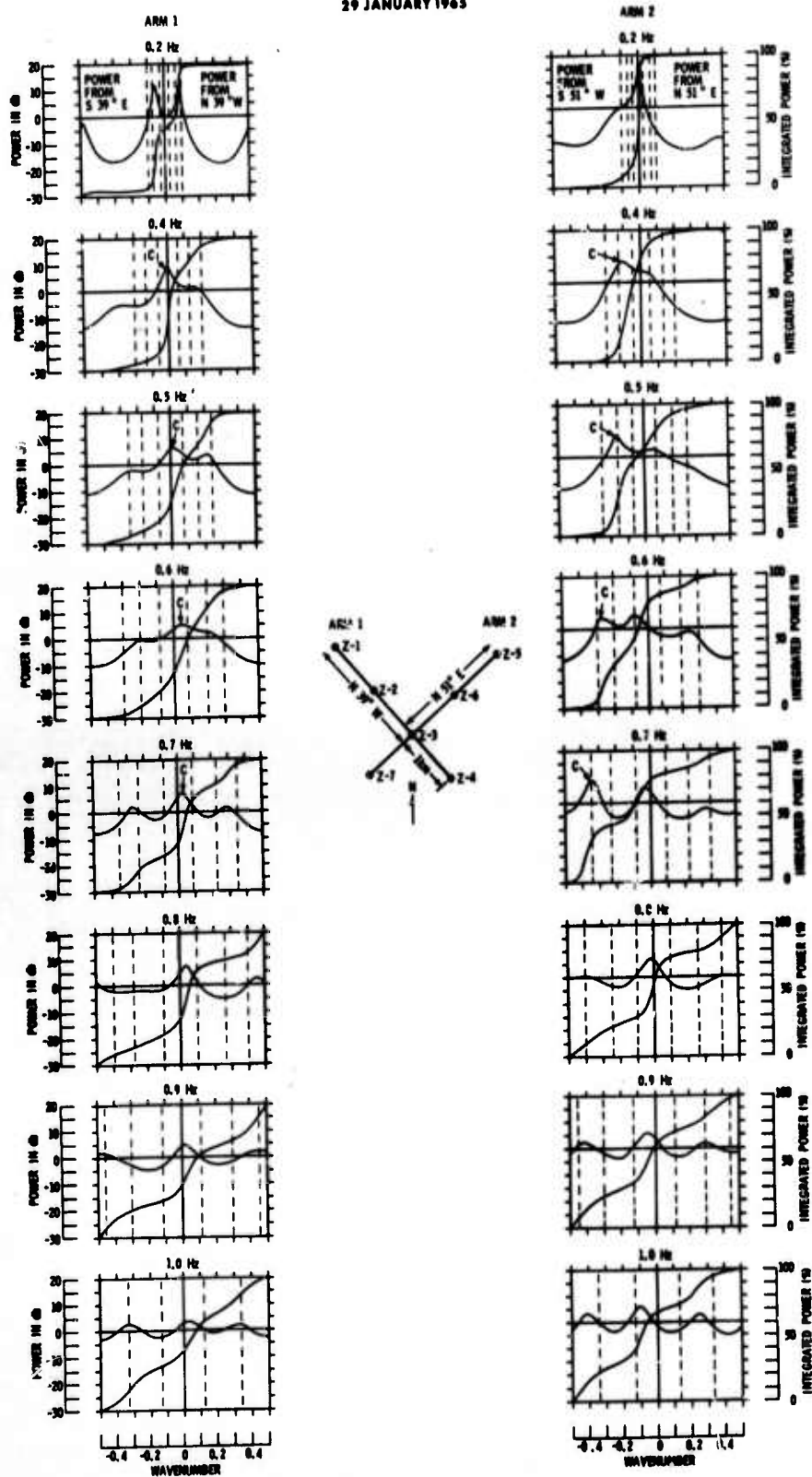


Figure IV-7. Wavenumber and Integrated Spectra from Two Arms at GGGR, 29 January 1965



Figure IV-7, GGGR, 29 January 1965

A poorly defined peak from the north in the 2-dimensional spectra at 0.2 Hz is seen on the K-line spectra as two surface-mode peaks, one traveling northwest and the other southeast. These probably are not seismically valid. The rather peculiar shape of the GGGR spectrum (Section III) should be mentioned.

From 0.3 to 0.7 Hz, the K-line spectra are dominated by Rayleigh-mode energy from the southwest, which is possibly generated by LPC 25 but is more likely from a stationary source since broadband energy is also seen from this direction on 16 October 1964. Above 0.6 Hz, a persistent high-velocity peak is also noted; whether this is instrumental or body-wave energy from LPC 20 (northeast of GGGR) is not established.

The narrowband stationary source in the south (lobe A), indicated in the 2-dimensional spectra at 0.4 Hz, is not seen in the K-line spectra. Energy from LPC 25 is seen in the 2-dimensional spectra at 0.6, 0.8, and 1.0 Hz.

There is some indication of surface-mode dispersion, with the velocity of the Rayleigh wave from the southwest decreasing from about 3.8 km/sec at 0.3 Hz (not shown) to 1.9 km/sec at 0.7 Hz. This effect is established also for the 16 October 1964 sample.



GGGR
16 OCTOBER 1964

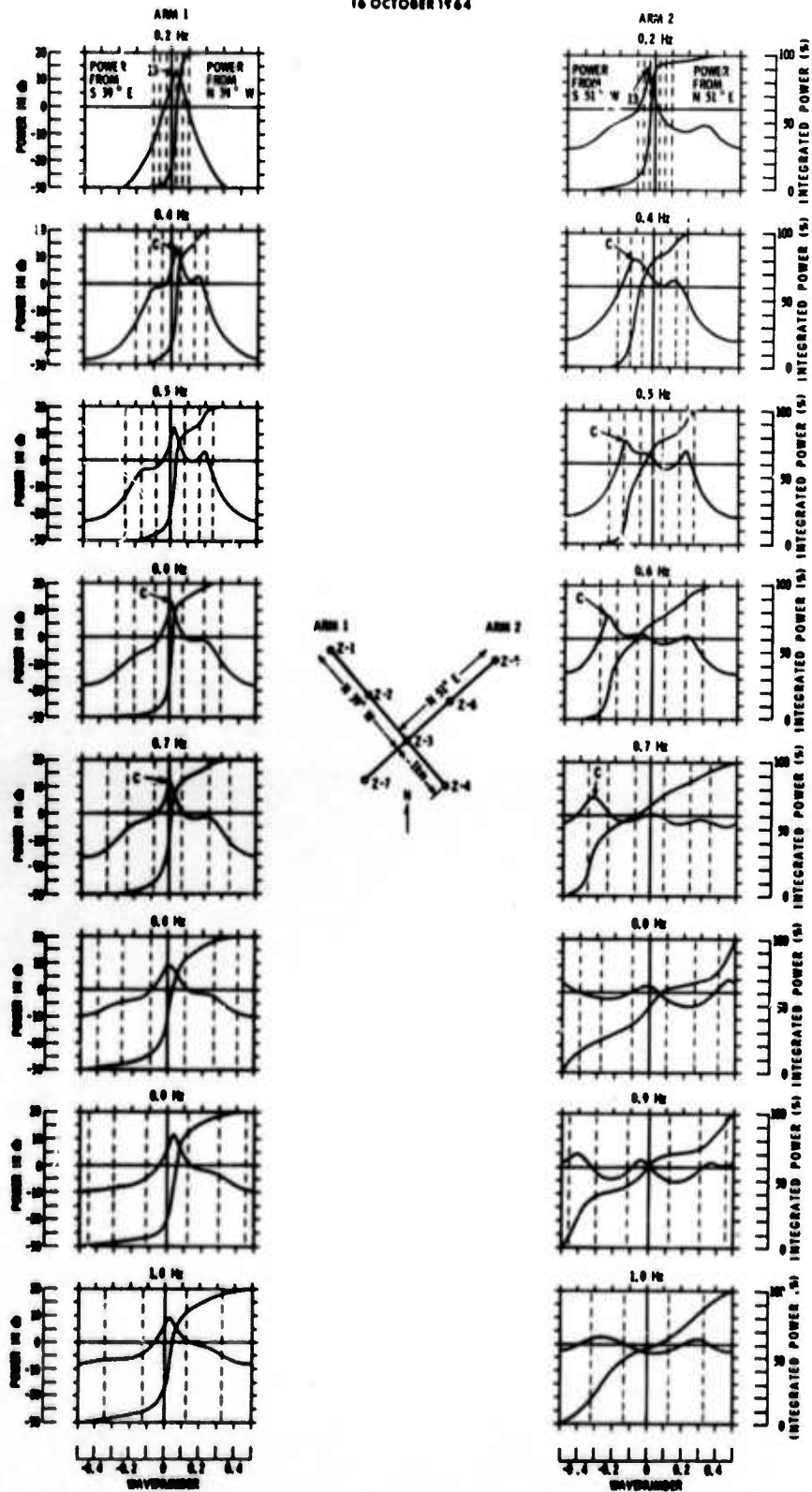


Figure IV-8. Wavenumber and Integrated Spectra from Two Arms at GGGR, 16 October 1964



Figure IV-8, GGGR, 16 October 1964

GGGR again receives broadband surface-mode energy from the southwest.

Little agreement is seen between the K-line and 2-dimensional spectra, except at 0.6 Hz.

At 0.2 and 0.8 Hz, the $f-k$ spectra indicate surface-mode energy from the northwest (LPC 13) and, at 0.4 Hz, from stationary source A.

Above 0.8 Hz, the K-line spectra are not seismically interpretable (in terms of directional noise). From 0.2 to 0.7 Hz, the surface-wave velocity is again observed to decrease as frequency increases.



C. ANALYSIS OF BODYWAVE NOISE POWER DENSITY

Estimates of the bodywave noise levels at the five array stations were made for the 16 October 1964 and 29 January 1965 noise samples (excluding TFO for 16 October 1964). Estimates for OONW, GGGR, and NPNT were made from joint analysis of the 2-dimensional and K-line spectra and, in particular, the integrated fractional power curves for each array arm. Estimates for TFO and CPO were based on the analysis discussed in subsection A of this section.

Figure IV-9 displays short-period absolute power-density spectra (relative to $1 \text{ m}\mu^2/\text{Hz}$ ground motion at 1 Hz for each station) for the two noise samples. Bodywave noise power-density levels also are shown for each station. Instrument responses have been removed to permit comparison of power levels across the network, since different instruments were in use at the various stations.

Stations CPO, OONW, and GGGR appear to be dominated by low-velocity energy, while TFO is apparently bodywave-noise-limited. NPNT appears rather intermediate, with the high-velocity energy being only 3 to 4 db below the total power level at frequencies approaching 1.0 Hz. Bodywave levels vary considerably from sample to sample and actually appear less consistent than the total power noise levels. Such behavior likely reflects, in part, a degree of variability inherent in the analysis approach but also suggests that the bodywave noise is probably not time-stationary.

Figure IV-10 combines the high-velocity noise power-density plots from each station for the two noise samples to permit comparisons of bodywave noise levels across the network. Also shown are the combined total power-density plots.

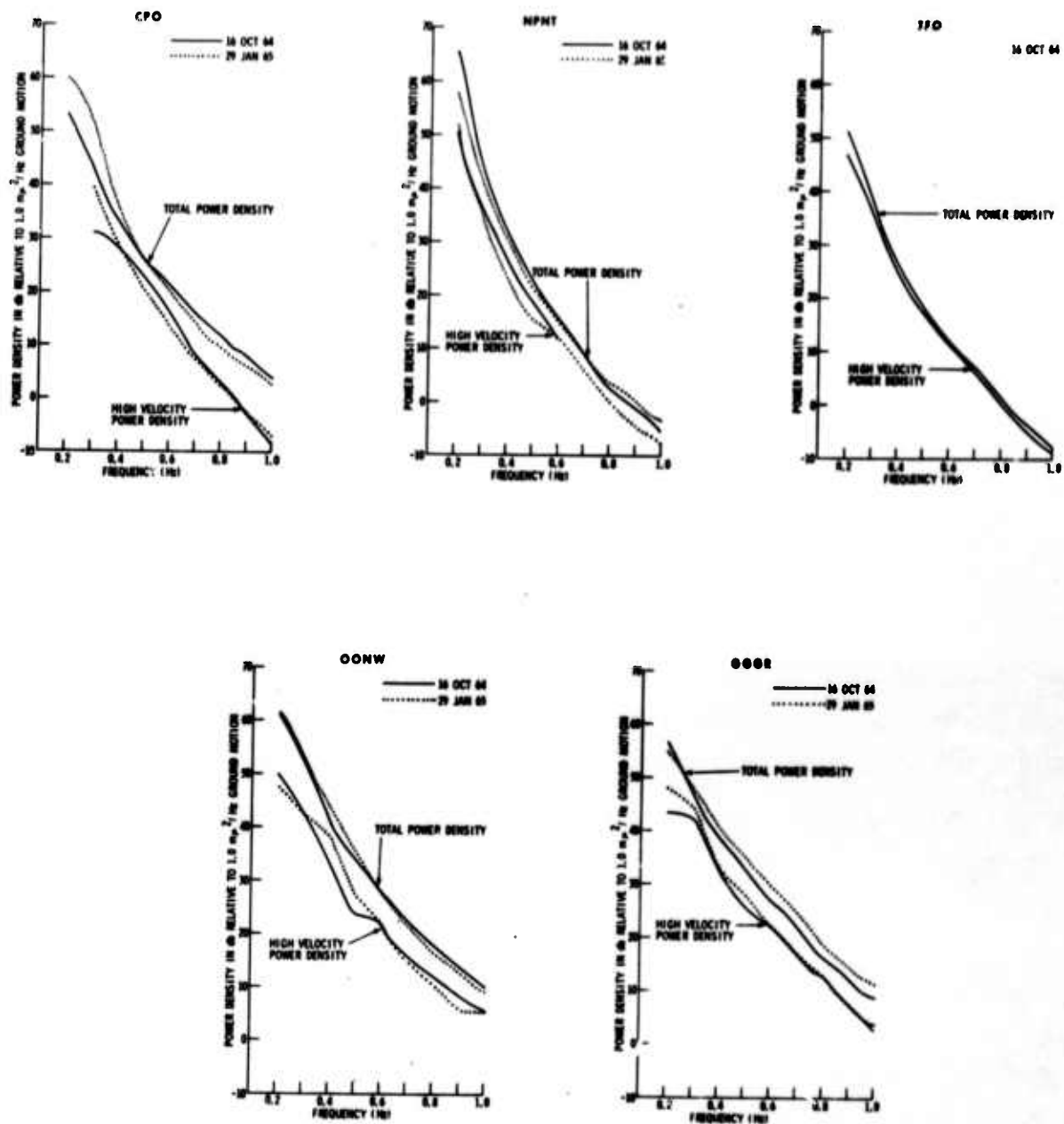
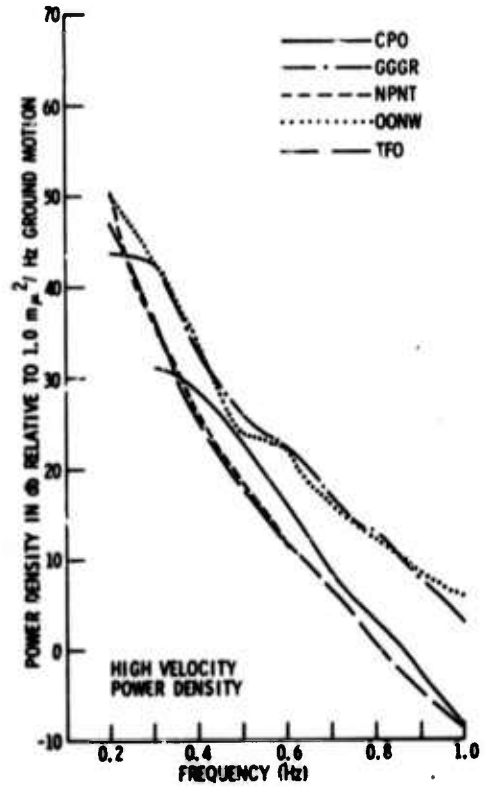
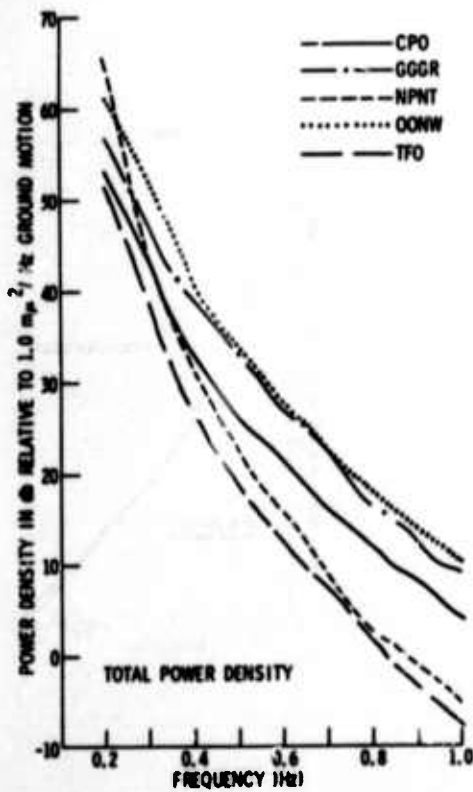


Figure IV-9. Absolute Total and High-Velocity Power-Density Spectra (in db) for CPO NPNT, TFO, OONW, and GGGR



16 OCTOBER 1964



29 JANUARY 1965

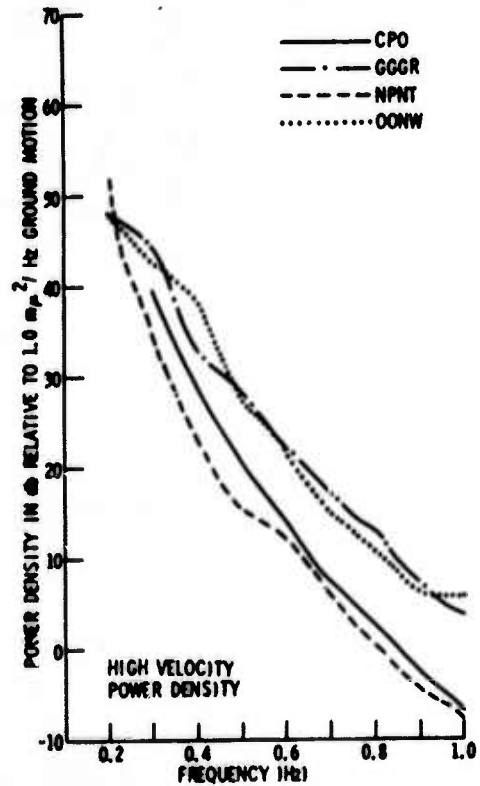
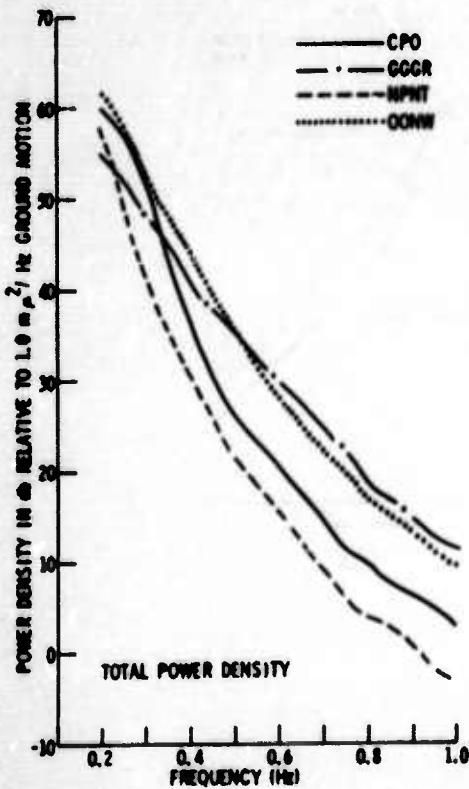


Figure IV-10. Comparison of Station Total and High-Velocity Power-Density Spectra for Each Noise Sample



Two characteristics are noted: first, there appears to be considerable variation in levels among stations, suggesting a lack of space-stationarity; second, significantly different levels are seen for the stations located on the European continent (OONW, GGGR) compared to the levels for the stations on the North American continent (CPO, TFO, NPNT). The variation in bodywave spectral level between continents actually appears to increase with increasing frequency up to 1.0 Hz.

Because of limitations in the procedures for estimating the bodywave noise components, the estimates are probably subject to considerable error, especially at the lower frequencies (near 0.2 Hz). Errors exceeding 3 db seem rather unlikely, however, and will probably not account for the observed differences in continental levels. Several alternative explanations for this effect are possible: e. g., systematic error in procedure including calibration of power spectra and instrument response removal or instrumentally generated (random) noise levels induced by differences in the dynamic ranges of the recordings. More likely, however, the effect is real and is related to differences in area sensitivities to bodywave energy. Such differences may arise from geological structure or relative distances to P-wave sources such as storms and seismically active areas.



SECTION V

REFERENCES

1. Texas Instruments Incorporated, 1966: Wavenumber Analysis of TFO Long-Noise Sample, Array Research, Spec. Rpt. No. 17, Contract AF 33(657)-1274, 15 Sep.
2. Parzen, Emanuel, 1961, Mathematical considerations in the estimation of spectra: Technometrics, v. 3, n. 2, May.
3. Texas Instruments Incorporated, 1964: Noise Study, Spec. Rpt. No. X, Contract AF 19(604)-8517, 15 Nov.
4. Texas Instruments Incorporated, 1967: Analysis of Long-Period Noise, Large-Array Signal and Noise Analysis, Spec. Rpt. No. 12, Contract AF 33(657)-16678, 18 Oct.
5. Amos, D. E. and L. H. Koopmans, 1963: Tables of the Distribution of the Coefficient of Coherence for Stationary Bivariate Gaussian Processes, Sandia Corporation Monograph, Mar.
6. Texas Instruments Incorporated, 1968: An Evaluation of the Use of High-Resolution Wavenumber Spectra for Ambient-Noise Analysis, Advanced Array Research, Spec. Rpt. No. 8, Contract F33657-67-C-0708, 28 Feb.
7. Texas Instruments Incorporated, 1967: CPO Ambient Noise Study, CPO Spec. Rpt. No. 1, Contract AF 33(657)-14648, 27 Jun.
8. Texas Instruments Incorporated, 1967: Analysis of K-Line Wavenumber Spectra from the TFO Long-Noise Sample, Array Research, Spec. Rpt. No. 23, Contract AF 33(657)-12747, 28 Feb.



APPENDIX
DESCRIPTIONS OF WORLDWIDE NETWORK
AND DATA LIBRARY

BLANK PAGE



APPENDIX

DESCRIPTIONS OF WORLDWIDE NETWORK AND DATA LIBRARY

Figure A-1 shows the relative locations of the 10 seismological data recording stations forming the network displayed on a Mercator projection of the world. Nine of the stations are located in the northern hemisphere, and one (LZBV) is in the southern hemisphere. The stations were selected to provide simultaneous data recordings over as extensive an area as possible. Table A-1 presents pertinent information regarding each station; i.e., name, location, elevation, number of short-period instruments, and predominant basement rock.

Table A-1

GENERAL STATION INFORMATION

Station Designator	Station Location	Station Coordinates		Elevation (km)	Instruments		Crustal Composition
		Latitude (°)	Longitude (°)		Type*	No.	
ADIS	Adak, Aleutian Islands	51.87 N	176.67 W	0.06	BEN	1	Basalt
CPO	McMinnville, Tennessee	35.58 N	85.57 W	0.57	JM	10	Limestone
DHNY	Delhi, New York	42.23 N	74.88 W	0.65	BEN	1	Sandstone
GGGR	Grafenburg, West Germany	49.68 N	11.20 E	0.53	BEN	7	Limestone
HWIS	Hawaiian Islands	19.97 N	155.70 W	0.71	BEN	14	Basalt
LZBV	La Paz, Bolivia	16.25 S	68.47 W	3.99	JM	7	Limestone
NPNT	Mould Bay, N. W. Territory	76.25 N	119.37 W	0.06	JM	7	Alluvium
OONW	Oslo, Norway	61.05 N	10.85 E	0.56	BEN	7	Glacial till
RKON	Red Lake, Ontario	50.83 N	93.67 W	0.37	BEN	1	Granite
TFO	Payson, Arizona	34.27 N	111.27 W	1.49	JM	11	Granite

* BEN: Short-period vertical Benioff

JM : Short-period vertical Johnson-Matheson

All stations use 3-component Sprengnether for long-period recording

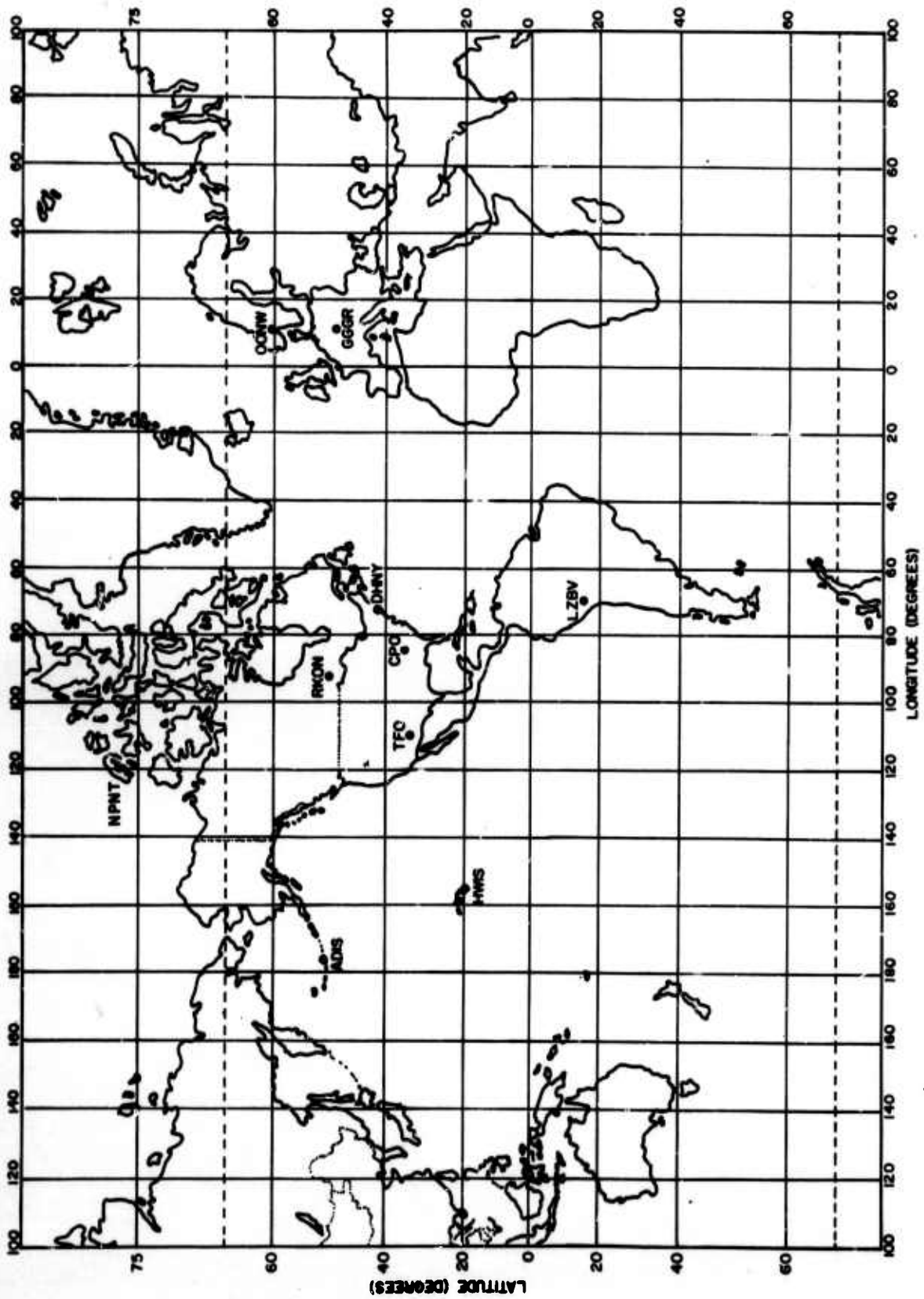


Figure A-1. Relative Locations of Network Stations



Each of the stations, except CPO and TFO which are VELA observatories, are Geotechnical Corporation LRSM mobil installations. Seven of the 10 stations have short-period arrays. Configurations for each of the array stations are shown in Figure A-2.

Three-component short-period and long-period instruments were available at each station; however, only vertical instruments were utilized for the bodywave noise analysis. The short-period vertical recordings at each station were taken from either a Johnson-Matheson or a large Berioff seismometer system (Table A-1), while long-period recordings were made with Sprengnether instruments. Responses for the appropriate seismometer systems are shown in Figure A-3. These response curves represent the normalized magnification of a seismometer system output for a constant current input. Short-period curves are normalized at 1.0 Hz, long-period at 0.04 Hz.

Significant geological and environmental differences exist between stations (Table A-1), as would be expected for a world array. Geological differences result in a variation of crustal filtering effects, scattered energy components, and inherent time residuals for teleseismic energy. Variations in the ambient noise levels at the stations result from environmental changes between stations such as prevailing winds, weather conditions, surf action along nearby coastlines, and local cultural sources.

Field data at each of the network stations were recorded on frequency-modulated (FM) magnetic tapes. The Seismic Data Laboratory (SDL) subsequently digitized and demultiplexed these FM tapes. Figure A-4 is a block diagram showing the sequence of steps involved in the data preprocessing.

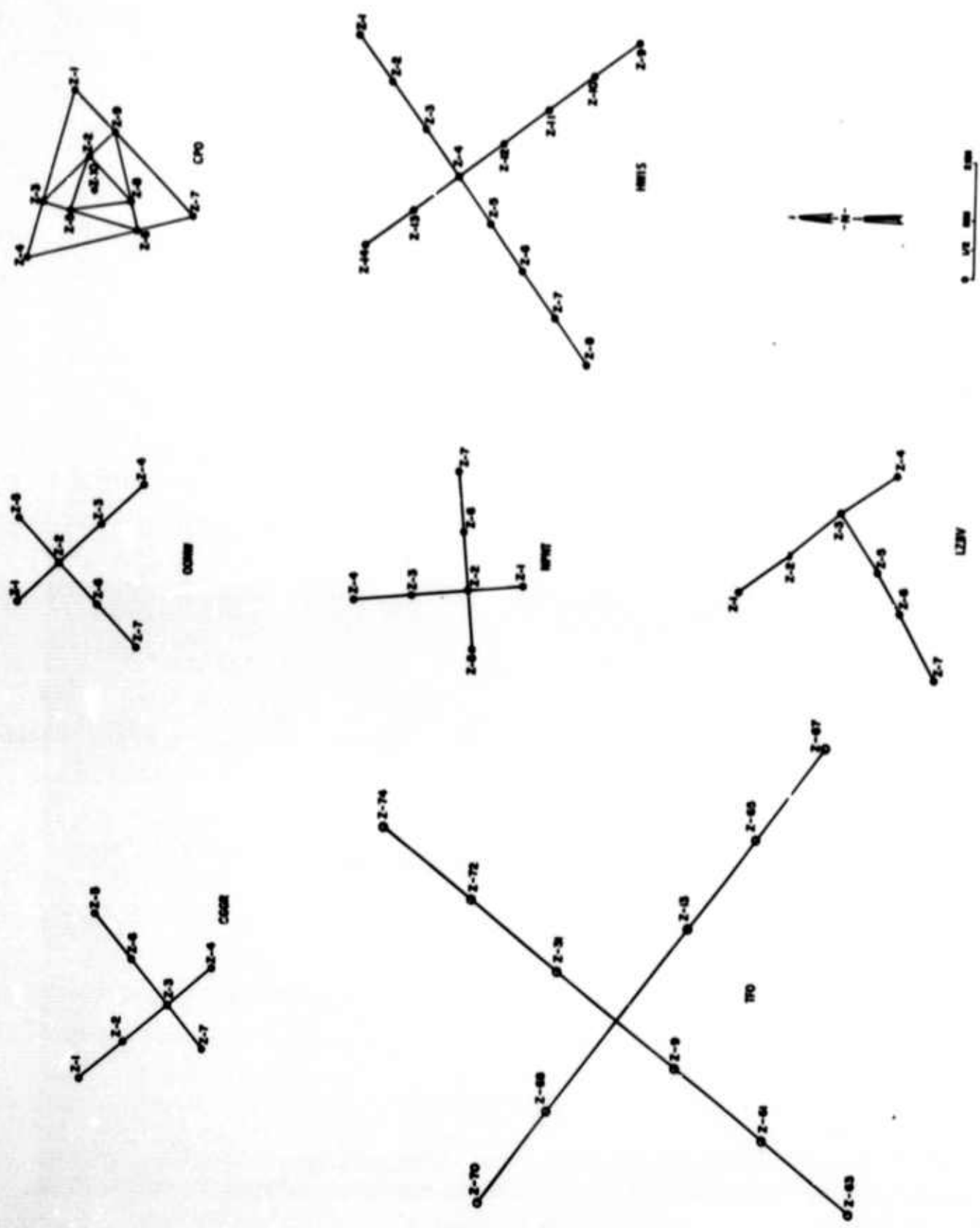


Figure A-2. Network-Station Array Configurations

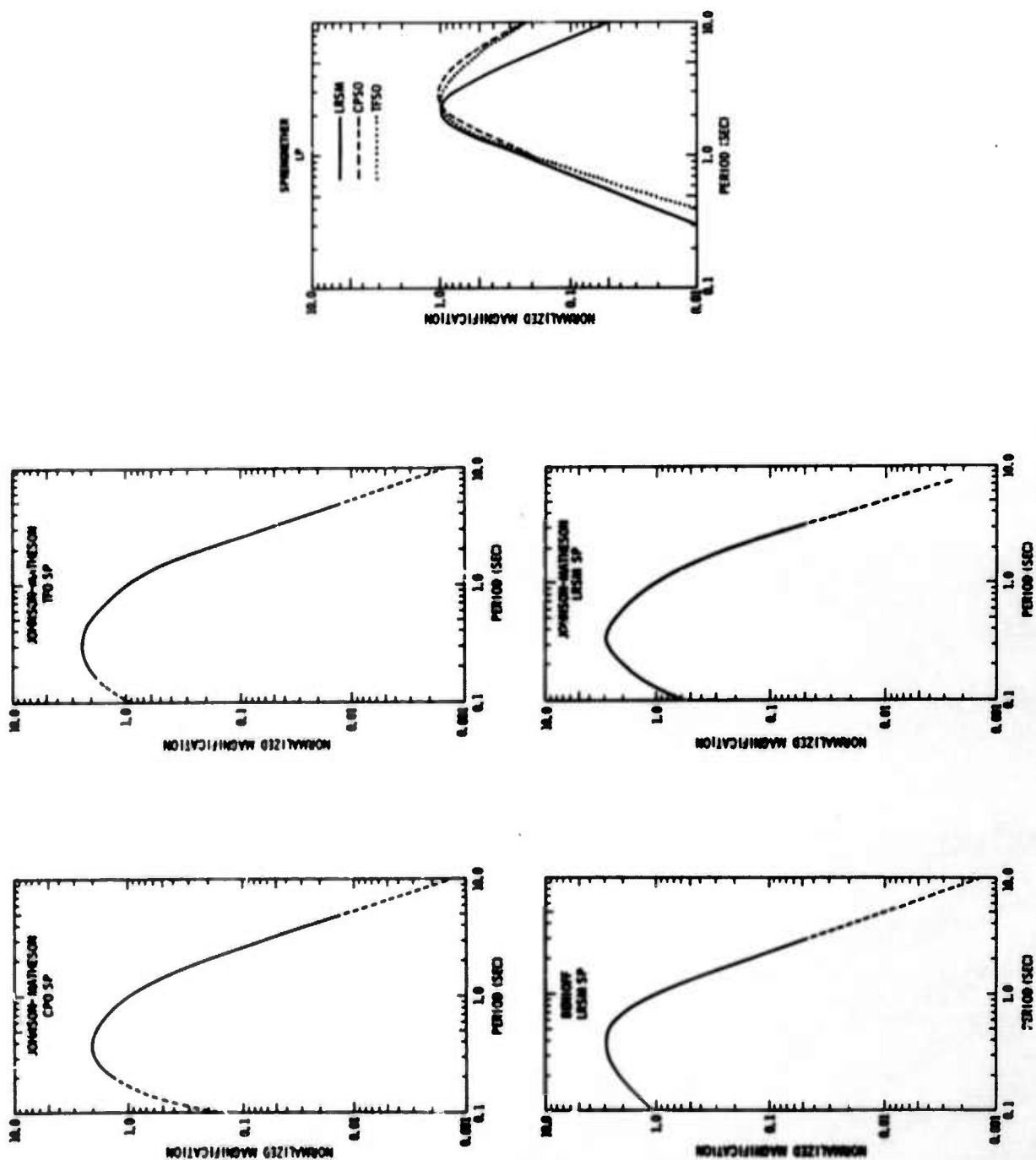


Figure A-3. Normalized Short-Period and Long-Period Instrument Responses

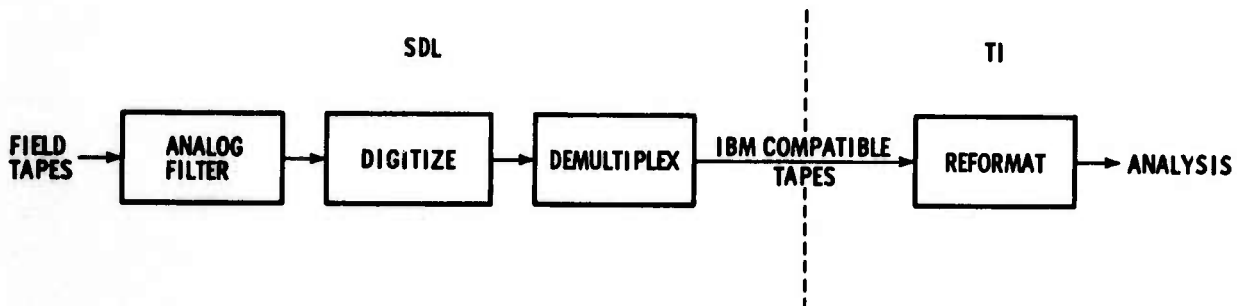


Figure A-4. Flow Diagram of Data Preprocessing Sequence

Data were available at SDL in one of two possible forms: standard FM field tapes or compressed FM tapes (which have been rerecorded in compressed form from standard field tapes to conserve data storage space). The short-period data were digitized at 10 samples/sec in a 12-channel multiplexed form. Due to the multiplexing, an inherent sampling delay between adjacent channels of 1/600 sec and 1/120 sec was introduced from standard and compressed FM tapes, respectively.

Prior to digitization, an analog bandpass filter with half-power points at 0.017 Hz and 5.00 Hz was applied to the short-period data. The filter gain was unity within $\pm 1/2$ db inside the passband, and attenuation was at 24 db/octave outside the passband. The long-period data were digitized at 2 samples/sec subsequent to antialias filtering with a 0.002- to 0.25-Hz bandpass filter. The filter response roll-off rates were again approximately 24 db/octave.

The data after digitization were demultiplexed by SDL into IBM-compatible tapes, which were subsequently reformatted at TI for compatibility with existing software.



Noise samples were selected for the network on the basis of usable seismic data recorded simultaneously at each station over time intervals of approximately 25 min (short-period) and 133 min (long-period). Data were chosen from 35-mm. Develocorder^{*} film, and requests were submitted to SDL for digitization and demultiplexing. Calibration data and station-calibration logs were also obtained for the selected data. Table A-2 describes the noise ensemble received.

Five noise samples were selected for the short-period noise ensemble. Two (16 October 1964 and 29 January 1965) contained significant storm activity and were chosen from the ensemble for use in the bodywave noise analysis. Each was represented at array stations CPO, GGGR, NPNT, OONW, and TFO. All sensors were available at each station with the exception of Z5 at CPO and Z7 at NPNT on 16 October 1964.

Long-period data were obtained for the time periods 1545 to 1758 GMT on 16 October 1964 and 0515 to 0728 GMT on 29 January 1965. Stations ADIS, CPO, RKON, and TFO were represented for both samples, HWIS for the 16 October 1964 sample only, and NPNT for the 29 January 1965 sample only. Data also were received for OONW and NPNT for 16 October 1964; however, difficulty was encountered in reformatting the SDL tape records.

* Geotech Trademark



Table A -2

SHORT-PERIOD NOISE ENSEMBLE

Station	Noise Sample *				
	12 Aug 1964 1544 to 1610 (GMT)	16 Oct 1964 1630 to 1656 (GMT)	6 Nov 1964 2302 to 2328 (GMT)	23 Nov 1964 0600 to 0626 (GMT)	29 Jan 1965 0600 to 0626 (GMT)
ADIS	+	+	+	+	+
CPO	-	+	+	+	+
DHNY	+	+	+	+	+
GGGR	+	+	+	-	+
HWIS	-	-	I	I	I
LZBV	+	-	+	+	+
NPNT	+	+	+	+	+
OONW	+	+	+	+	+
RKON	+	+	+	+	+
TFO	-	+	+	+	+

*
+: Received
-: Not available
I: Inoperative

UNCLASSIFIED

Security Classification

DOCUMENT CONTROL DATA - R&D

(Security classification of title, body of abstract and indexing annotation must be entered when the overall report is classified)

1. ORIGINATING ACTIVITY (Corporate author)

Texas Instruments Incorporated
Science Services Division
P.O. Box 5621, Dallas, Texas 75222

2a. REPORT SECURITY CLASSIFICATION

Unclassified

2b. GROUP

3. REPORT TITLE

NETWORK STUDIES - NOISE ANALYSIS
ADVANCED ARRAY RESEARCH SPECIAL REPORT NO. 6

4. DESCRIPTIVE NOTES (Type of report and inclusive dates)

Special

5. AUTHOR(S) (Last name, first name, initial)

Johnson, William A.
Bonner, James A.

6. REPORT DATE

28 February 1968

7a. TOTAL NO. OF PAGES

106

7b. NO. OF REFS

8

8a. CONTRACT OR GRANT NO.

F33657-67-C-0708-P001

b. PROJECT NO.

VELA T/7701

c.

d.

8a. ORIGINATOR'S REPORT NUMBER(S)

9b. OTHER REPORT NO(S) (Any other numbers that may be assigned this report)

10. AVAILABILITY/LIMITATION NOTICES

This document is subject to special export controls and each transmittal to foreign governments or foreign nationals may be made only with prior approval of Chief, AFTAC.

11. SUPPLEMENTARY NOTES

ARPA Order No. 624

12. SPONSORING MILITARY ACTIVITY

Advanced Research Projects Agency
Department of Defense
The Pentagon, Washington, D. C. 20301

13. ABSTRACT

Network studies are directed toward effective utilization of a collection of seismic stations as a coherent worldwide seismic network to lower the detection threshold for seismic events and improve their classification. This report presents an analysis of ambient seismic noise seen at the network level and is directed toward characterization of the network noise field. Simultaneously recorded noise samples from two VELA stations and eight LRSM stations are investigated through analysis of power-density spectra, coherence, high-resolution frequency-wavenumber spectra, and K-line spectra. The ambient short-period network noise field is found to be highly variable with time and with geographical position. Variations in noise power are directly related to regional storm activity. Dominant noise power at most stations is trapped-mode surface-wave energy that does not exhibit useful interstation coherence.

14.

KEY WORDS

LINK A

LINK B

LINK C

ROLE

WT

RE

T

120

--	--

Advanced Array Research

Network Studies

Noise Analysis

Power-Density Spectral Analysis

Coherency Analysis

High-Resolution Frequency-Wavenumber Spectral Analysis

K-Line Spectral Analysis

Relation to Regional Storm Activity

INSTRUCTIONS

- 1. ORIGINATING ACTIVITY:** Enter the name and address of the contractor, subcontractor, grantee, Department of Defense activity or other organization (corporate author) issuing the report.

- 2a. REPORT SECURITY CLASSIFICATION:** Enter the overall security classification of the report. Indicate whether "Restricted Data" is included. Marking is to be in accordance with appropriate security regulations.

- 2b. GROUP: Automatic downgrading is specified in DoD Directive S200.10 and Armed Forces Industrial Manual. Enter the group number. Also, where applicable, show that optional markings have been used for Group 3 and Group 4 as authorized.

- 3. REPORT TITLE:** Enter the complete report title in all capital letters. Titles in all cases should be unclassified. If a meaningful title cannot be selected without classification, show title classification in all capitals in parentheses immediately following the title.

4. **DESCRIPTIVE NOTES:** If appropriate, enter the type of report, e.g., interim, progress, summary, annual, or final. Give the inclusive dates when a specific reporting period is covered.

- 5. AUTHOR(S):** Enter the name(s) of author(s) as shown on or in the report. Enter last name, first name, middle initial. If military, show rank and branch of service. The name of the principal author is an absolute minimum requirement.

- 6. REPORT DATE:** Enter the date of the report as day, month, year; or month, year. If more than one date appears on the report, use date of publication.

- 7a. TOTAL NUMBER OF PAGES:** The total page count should follow normal pagination procedures, i.e., enter the number of pages containing information.

- 7b. NUMBER OF REFERENCES** Enter the total number of references cited in the report.

- 8a. **CONTRACT OR GRANT NUMBER:** If appropriate, enter the applicable number of the contract or grant under which the report was written.

- 2b, 2c, & 2d. PROJECT NUMBER:** Enter the appropriate military department identification, such as project number, subproject number, system numbers, task number, etc.

- 9a. ORIGINATOR'S REPORT NUMBER(S):** Enter the official report number by which the document will be identified and controlled by the originating activity. This number must be unique to this report.

96. OTHER REPORT NUMBER(S): If the report has been assigned any other report numbers (either by the originator or by the sponsor), also enter this number(s).

10. **AVAILABILITY/LIMITATION NOTICES:** Enter any limitations on further dissemination of the report, other than those

- imposed by security classification, using standard statements such as:

- (1) "Qualified requesters may obtain copies of this report from DDC."
- (2) "Foreign announcement and dissemination of this report by DDC is not authorized."
- (3) "U. S. Government agencies may obtain copies of this report directly from DDC. Other qualified DDC users shall request through _____."
- (4) "U. S. military agencies may obtain copies of this report directly from DDC. Other qualified users shall request through _____."
- (5) "All distribution of this report is controlled. Qualified DDC users shall request through _____."

If the report has been furnished to the Office of Technical Services, Department of Commerce, for sale to the public, indicate this fact and enter the price, if known.

- 11. SUPPLEMENTARY NOTES:** Use for additional explanatory notes.

- 12. SPONSORING MILITARY ACTIVITY:** Enter the name of the departmental project office or laboratory sponsoring (paying for) the research and development. Include address.

13. **ABSTRACT:** Enter an abstract giving a brief and factual summary of the document indicative of the report, even though it may also appear elsewhere in the body of the technical report. If additional space is required, a continuation sheet shall be attached.

It is highly desirable that the abstract of classified reports be unclassified. Each paragraph of the abstract shall end with an indication of the military security classification of the information in the paragraph, represented as (TS), (S), (C), or (U).

There is no limitation on the length of the abstract. However, the suggested length is from 150 to 225 words.

- 14. KEY WORDS:** Key words are technically meaningful terms or short phrases that characterize a report and may be used as index entries for cataloging the report. Key words must be selected so that no security classification is required. Identifiers, such as equipment model designation, trade name, military project code name, geographic location, may be used as key words but will be followed by an indication of technical content. The assignment of links, rules, and weights is optional.